Percolation and Deconfinement in SU(2) Gauge Theory

Santo Fortunato

PhD Thesis

Physics Faculty
University of Bielefeld

Acknowledgements

At the end of a long and intense experience like a PhD in physics, there is normally a long queue of people to thank.

My first thanks go to my supervisor, Prof. Dr. Helmut Satz, for giving me this chance in a delicate moment of my life in which I had started to have doubts on myself. The challenging tasks he gave me and the many discussions we had about the related topics awaked a passion for physics I thought I had lost. I am happy to have the possibility to keep working with him also after the PhD.

A key role in my educational process during these three years has also been played by Prof. Dr. Jürgen Engels, who introduced me into the computational aspects of my research work, providing me most of the tools I needed to get numerical results safely and efficiently. As far as this is concerned, I would also like to thank Dr. Marzia Nardi, Dr. Manfred Oevers and Dr. Piotr Bialas for their patience in assisting me during my early steps in the world of computer programming.

I am particularly indebted to Prof. Dr. Dietrich Stauffer, whom I owe most of what I know about percolation theory and to Prof. Dr. Daniel Gandolfo, who let me become acquainted with analytical results about percolation which turned out to be very useful in my work.

I gratefully acknowledge several interesting discussions with Prof. Dr. Frithjof Karsch, Prof. Dr. Philippe Blanchard, Dr. Sanatan Digal, Dr. Peter Petreczky, Dr. Tereza Mendes, Dr. Attilio Cucchieri. The presence of such a high number of experts in lattice gauge theory and Monte Carlo simulations has allowed me to grow very quickly in this field.

I would like to express all my gratefulness to the whole staff of the Physics Faculty of Bielefeld, for the help and support I received in all circumstances. I thank the secretaries, Gudrun Eickmeyer, Karin Lacey and Susi von Reder, for their sympathy and for facilitating my life especially at the beginning of my stay, when many things had to be properly arranged. I thank the younger members of the staff, undergraduate and PhD students, including some of those who are no longer here, for allowing me to get easily integrated in a reality which is quite different from the Italian one. Without them it wouldn't have been possible for me to learn quickly a complicated language like German, which is of course an essential step towards a cultural integration. I cannot write all names because of the limited space, but I would like to mention the ones with whom I spent most of my time: Ines Wetzorke, Daria Ahrensmeier, Matthias Buse, Peter Schmidt,

Olaf Kaczmarek, Andreas Peikert, Burkhard Sturm, Christian Legeland, Manfred Oevers, Sven Stickan, Olaf Leonhard, Markus Dirks.

Dedico questa tesi alla mia famiglia, che ha sempre avuto un ruolo insostituibile nella mia vita e nella mia carriera. L'amore e la comprensione dei miei cari sono stati essenziali, soprattutto nei momenti difficili che ho dovuto affrontare. Li ringrazio soprattutto per avermi sempre lasciato libero di decidere cosa fare, anche quando ciò comportava dei sacrifici notevoli per me e per loro, come quando ho deciso di continuare i miei studi all'estero. Vorrei chiudere con un ringraziamento speciale per il mio amico e relatore Prof. Antonio Insolia, per l'amicizia e la pazienza che ha dimostrato nel seguire ed assecondare le mie decisioni, pensando solo a ciò che è meglio per me e non ad interessi personali.

Santo Fortunato

Contents

List of Figures

List of Tables

Introduction

The study of critical phenomena has always been one of the most challenging and fascinating topics in physics. One can give many examples of systems which undergo phase transitions, from familiar cases like the boiling of water in a kettle or the paramagnetic-ferromagnetic transition of iron at the Curie temperature, to the more complicated case of the transition from hadronic matter to quark-gluon plasma which is likely to be obtained by high-energy heavy-ion experiments in the coming years. In all cases, one observes big changes of some properties of the system caused by small variations of some parameter (usually the temperature) around a particular value of the parameter (critical point).

In spite of the wide variety of systems in which such phenomena are observed, one has only two main types of phase transitions: first order and continuous (basically second-order) transitions. One of the most attractive features is the fact that whole *classes* of systems, ruled by dynamics which look very different from each other, happen to have the same behaviour at the phase transition. This is particularly striking for second-order phase transitions, as one can define a set of *critical indices* (exponents, amplitudes' ratios), which rule the behaviour of the thermodynamic variables near the critical point: all systems belonging to a class are characterized by the same set of critical indices (*universality*). It is not clear which common elements "unify" different systems so that they have the same critical behaviour; however, it seems that the number of space dimensions plays an important role. This connection to *geometry* is at the basis of our future considerations.

In general, a phase transition corresponds to a change in the *order* of the system. Going from a phase to another, the microscopic constituent particles of the system "choose" a different way of staying together. The interesting thing is the fact that the order is a *macroscopic* feature, while the fundamental interactions which are responsible of the physics of the system, including the phase change, are *microscopic* interactions between the particles. How can parts of the system which are far from each other know about their respective situations, so that they switch all together to the same state of order?

The usual interpretation of this fact is that the interplay of the microscopic interactions all throughout a system at thermal equilibrium gives rise to a *correlation* between the states of the particles. The extent of this correlation depends on the thermal parameters (i.e. the temperature, eventual external fields, etc.) and it is expressed by the so-called *correlation length* χ,

which is the distance over which the fluctuations of the microscopic degrees of freedom (position of the atoms, spin orientation, etc.) are significantly correlated with each other.

The correlation creates thus "ordered" regions which drive the behaviour of the whole system. Because of that, it is natural to consider such regions as the leading characters of the phenomenon and describe phase transitions in terms of the properties of compound objects. The interaction "builds" these objects: the phase transition is related to the *geometry* of the resulting structures.

This picture has, among other things, two big advantages. First, it would justify the connection between critical phenomena and geometry that we have stressed above. Second, if the degrees of freedom relevant for the phase change are the ones of sets of particles, and not of single particles, it is likely that they do not depend on the details of the microscopic interaction, but only on its gross features (e.g. symmetries): this could explain the universality of the critical indices.

On these grounds, it is easy to understand why several attempts have been made to find a geometrical description of phase transitions. The first ideas date back to the end of the 40's, when Onsager [1] proposed an interpretation of the λ-transition in liquid ^4He based on the behaviour of one-dimensional strings, whose size would change dramatically from one phase to the other: whereas in the superfluid phase only finite strings are present, at the critical point infinite strings appear.

This kind of picture is analogous to the well known phenomenon of *percolation* [2, 3], which takes place when geometrical *clusters*, formed by elementary objects of some system, stick to each other giving rise to an infinite network, that spans the whole system. Here, criticality is reached when the *density* of the elementary objects is sufficiently high. The onset of percolation marks a distinction between two different phases of the system, characterized by the presence or the absence of an infinite cluster. The percolation phenomenon turns out to have astonishing analogies with ordinary second order thermal phase transitions. In particular, the behaviour of the percolation variables at criticality is also described by simple power laws, with relative exponents; the values of the exponents, related to each other by simple scaling relations, are fixed only by the number of space dimensions of the system at study, regardless of its structure and of the special type of percolation process one considers.

For these reasons, percolation seems to be an ideal framework for the geometrical description of phase transitions we are looking for. One could try to map the thermal transition into a geometrical percolation transition. In order to do that, one must require that the two critical thresholds coincide, and that the thermal variables can be expressed in terms of corresponding percolation quantities.

The first studies in this direction started at the beginning of the 70's, and concentrated on the Ising model. The main problem was to look for a suitable cluster definition. The first structures which were investigated were the ordinary magnetic domains, i.e. clusters formed by nearest-neighbouring spins of the same sign. In two dimensions such clusters happen indeed to percolate at the thermal critical temperature T_c [4]. Nevertheless, the values of the critical exponents differ from the corresponding Ising values [5]. Besides, in three dimensions, the magnetic domains of

the spins oriented like the magnetization percolate at any temperature; the domains formed by the spins opposite to the magnetization percolate for $T \geq T_p$, with $T_p \neq T_c$ [6].

The problem was solved when it became clear that, to define the 'physical' islands of a thermal system, one must take into account correctly the degree of correlation between the spins. The size of the ordinary magnetic domains, in fact, happens to be too large because of purely geometrical effects, which operate independently of the spins' correlation. In order to get rid of these disturbing effects, Coniglio and Klein introduced a *bond probability* $p = 1 - \exp(-2J/kT)$ (J is the Ising coupling, T the temperature). The new islands are *site-bond* clusters, i.e. clusters formed by nearest neighbouring like-signed spins, which are connected with a probability p, and not always like in the previous definition ($p = 1$). These clusters had actually been introduced some years before by Fortuin and Kasteleyn. They had shown that, by means of such objects, one can reformulate the Ising model as a geometrical model [7]. This result indicates that these apparently artificial structures are strictly related to the Ising dynamics. Coniglio and Klein showed that the new clusters percolate at the thermal threshold and that the percolation exponents coincide with the Ising exponents [8].

So, it is possible to describe the paramagnetic-ferromagnetic transition of the Ising model as a percolation transition of suitably defined clusters. The paramagnetic-ferromagnetic transition is due to the *spontaneous breaking* of the $Z(2)$ symmetry of the Ising Hamiltonian, i.e., the symmetry under inversion of the spins. The spontaneous breaking of the $Z(2)$ symmetry is also responsible of the confinement-deconfinement transition in $SU(2)$ pure gauge theory. Because of that, it was conjectured that $SU(2)$ has the same critical behaviour of the Ising model [9], i.e., it undergoes a second order phase transition with Ising exponents, as it was successively confirmed by lattice simulations [10].

It is then natural to see whether the $SU(2)$ confinement-deconfinement phase transition can be described as a percolation transition like for the Ising model: this is the aim of this work.

The analogue of the spin variable in $SU(2)$ pure gauge theory is the *Polyakov loop* L, a real number which is a well defined function of the gauge fields. The deconfined region is the ordered phase of the system, characterized by a non-vanishing lattice average of the Polyakov loop. In this way, regions of the space where the Polyakov loop has the same sign can be viewed as local "bubbles" of deconfinement. In each of these regions, in fact, the average of the Polyakov loop is necessarily non-zero. If we put a test colour charge into a bubble, it will be free to move within the portion of space occupied by the bubble. But to have a real deconfined phase, the test charge must be able to move freely all throughout the system, so that there must be bubbles whose size is of the same order of the volume of the system. A working percolation picture would support the proposal of such a mechanism for the deconfinement transition.

The question is, again, what clusters to choose. From what we have said, it is simple to deduce that the clusters must be formed by sites at which the Polyakov loops have the same sign. But it is not clear if and how we can extract the other necessary ingredient for the cluster building, namely the bond probability.

The search of the right bond probability is affected by two problems:

- The Polyakov loop is not a two-valued variable like the spin in the Ising model but a continuous one; its values vary in a range that, with the normalization convention we use, is $[-1, 1]$.
- The $SU(2)$ Lagrangian is a function of the gauge fields which cannot in general be expressed only in terms of the Polyakov loop L.

The first point led us to investigate *continuous spin models*, i.e. models where the spin is a continuous variable, to check whether the Coniglio-Klein result can be extended to such more general cases. We began by analyzing the continuous spin Ising model, which is an Ising model with continuous spins. We will see that, in this case, an equivalent percolation picture can be obtained by introducing a bond weight which is similar to the Coniglio-Klein one, with the difference that it contains an explicit dependence on the spins connected by the bond. This *local* bond probability solves the first of the two afore-mentioned problems. Besides, the result can be further extended to models with several spin-spin interactions, if ferromagnetic. We will also show that eventual spin distribution functions and self-interaction terms do not influence the percolation picture. Finally, we will analyze $O(n)$ spin models and find again that their critical behaviour can be easily described by means of cluster percolation.

The second difficulty is hard to overcome. In fact, it seems clear that the percolation picture of a model is strictly related to the *interactions* of the model. In particular, a bond is associated to each spin-spin interaction, with a probability which depends on the value of the coupling strength of the interaction. But, if the $SU(2)$ Lagrangian is not simply a function of L, we cannot exactly specify how the "gauge spins", i. e., the Polyakov loops, interact with each other. It seems then impossible to derive rigorously the corresponding percolation scheme.

However, we can try to solve the problem by using suitable approximations. The best thing to do is to try to approximate $SU(2)$ pure gauge theory by means of an *effective theory*, hoping that the effective model admits a percolation picture.

We shall first exploit a strong coupling expansion derived by Green and Karsch [11], which shows that the partition function of $SU(2)$ can be reduced to the partition function of one of the continuous spin models we have analyzed. This approximation is valid only in the strong coupling limit, more precisely in the cases $N_\tau = 1, 2$ (N_τ=number of lattice spacings in the temperature direction). We will analyze the case $N_\tau = 2$, both in two and in three space dimensions, and show that the percolation picture derived by the effective theory describes well the thermal transition of $SU(2)$.

Next, we will try to find a procedure which can be also applied to the more interesting weak coupling case. This time we shall construct the effective theory starting not from the $SU(2)$ Lagrangian, but from the Polyakov loop configurations. Actually we shall consider the Ising-projected configurations, i.e. the distributions of the *signs* of the Polyakov loops. This is done assuming that the $Z(2)$ symmetry is the only relevant feature at the basis of the critical behaviour.

We will essentially look for a model which can reproduce the Ising-projected Polyakov loop configurations. The effective model must be necessarily chosen inside the group of spin models for which a working percolation picture exists. Our ansatz will be an Ising-like model with just ferromagnetic spin-spin interactions, to which the Coniglio-Klein result can be trivially extended by associating a bond to each coupling. The couplings of the effective theory are calculated following a method used in Monte Carlo renormalization group studies of field theories [12, 13]. We will examine $SU(2)$ in $3+1$ dimensions, for $N_\tau = 2$ and $N_\tau = 4$. The results will be shown to be satisfactory in both cases.

Our results are entirely obtained by means of lattice Monte Carlo simulations of the various models we have studied. We have always used workstations except for some lenghty $SU(2)$ simulations which were performed on a Cray $T3E$ (ZAM, Jülich).

This work is structured as follows. Chapter 1 is devoted to a presentation of the main concepts of percolation theory with a special attention to numerical techniques. In Chapter 2 we focus on the analogies between percolation and thermal phase transitions, which lead to the percolation formulation of the Ising model of Coniglio and Klein. Chapter 3 collects all percolation studies on continuous spin models that we have mentioned above. In Chapter 4 we show the results for $SU(2)$ pure gauge theory. Finally, the conclusions of our investigation are drawn. In Appendix A we present the procedure we have adopted to perform the so-called *cluster labeling*, i.e. the identification of the cluster configurations.

Chapter 1

Introduction to Percolation Theory

1.1 Definition of the problem

Let us suppose to have a piece of some material X which is given by the mixture of two different substances A and B. Substance A is a metal, substance B an insulator. One could ask oneself whether the material X is insulating or conducting. Fig. 1.1 schematizes the situation, assuming for simplicity our system to be two-dimensional. The geometry of the sample X is the one of a regular square lattice, represented by the black points. If we assume that the mixing process is disordered, we can visualize the presence of the metal by distributing randomly resistors between pairs of nearest neighbouring sites. If we set a voltage between the upper and the lower edge of our sample, electric current will flow through the substance if the resistors form a connected structure from top to bottom (red path in the figure). Let p be the concentration of the metal in the substance. Our problem can be reformulated in the following way: what is the minimum value of p which is necessary to have a connected bridge of resistors all through the lattice?

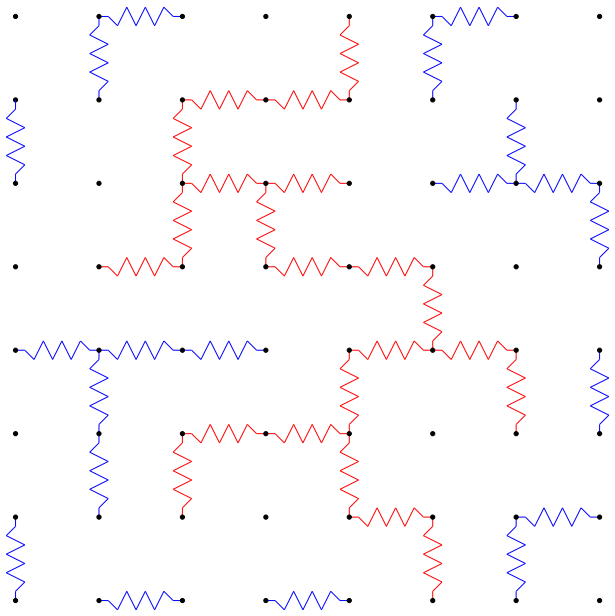

Figure 1.1: Scheme of a two-dimensional random resistor network. The spanning structure formed by the resistors (marked in red) allows electric current to flow all through the material.

The system we have presented here is a *random resistor network*, and represents only one of the many applications of *percolation theory* [2, 3]. The original problem which gave rise to this theory was studied by Flory and Stockmayer [14] during the Second World War. They had a set of small branching molecules and increased the number of chemical bonds between them. In this way larger and larger macromolecules are formed. At some stage it may happen that the chemical bonds form a structure which spans the whole system (*gelation*).

Nowadays the set of problems which can be modelled by using percolation theory is big and various: diffusion in disordered media [15], critical behaviour of systems undergoing second order phase transitions (the topic of this work), fractality [16], spread of epidemics or fires in large orchards [17], stock market fluctuations [18]. In this chapter we want to introduce the percolation problem and illustrate its main features.

Suppose to have some infinite periodic lattice[†] in d dimensions. For simplicity, we consider here a two-dimensional square lattice. We start by distributing randomly objects on the lattice, something like placing pawns on a chessboard. At this stage we have two possibilities: we can place our pawns on the edges of the lattice, or on its vertices. If we work on the edges we have the so-called *bond percolation*: our random resistor network is an example of it. If we instead place our pawns on the sites we are in the *site percolation* case. Other choices are allowed, but they are given by combinations of site and bond percolation (for example one can use edges and sites together). Every bond model may be reformulated as a site model on a different lattice [20], but the converse is false. Therefore site models are more general than bond models and in what follows we will deal essentially with the former ones. We assume that an edge (site) is occupied with some probability p ($0 \leq p \leq 1$), independently of the other edges (sites). To complete the picture we only need to establish a rule to form compound structures (*clusters*) out of our pawns. Percolation theory deals with the properties of the clusters thus formed.

If we increase the probability p, the clusters at the beginning will increase in number and size. Successively most of them will stick to each other to form bigger and bigger clusters until, for some value p_c of the occupation probability, an infinite spanning structure is formed (*percolating cluster*). Further increases of p lead to an increase of the size of the percolating cluster which slowly embodies the remaining ones until, for $p = 1$, it invades every edge (site) of the lattice.

Fig. 1.2 shows three "pictures" of this phenomenon for the so-called pure site percolation case, for which two nearest neighbouring sites always belong to the same cluster. Fig. 1.2a shows a lattice configuration corresponding to a small value of p, in Fig. 1.2b p is higher but below p_c and in Fig. 1.2c p is slightly above p_c.

Particularly interesting is what happens for values of p near p_c. The aspects related to that are called *critical phenomena* and we will focus mainly on that. Indeed, at the percolation threshold p_c a sort of *phase transition* takes place, because our system changes dramatically its behaviour

[†]We remark that the percolation phenomenon does not require a lattice structure, but it can be also studied on continuous manifolds. However, since our work is centered on lattice systems, we will disregard continuum percolation. The interested reader is invited to look at [19].

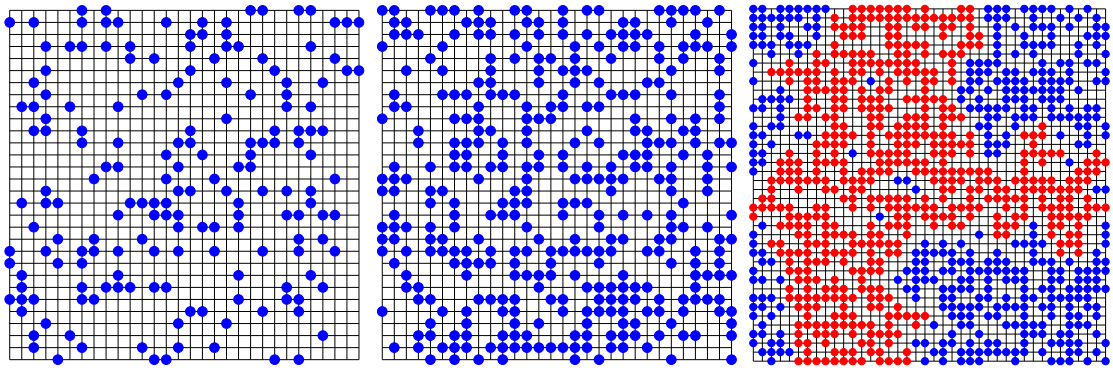

(a) (b) (c)

Figure 1.2: Pure site percolation on a 2-dimensional square lattice. In (a) the density of occupied sites is low and the clusters small. In (b) the density is increased and the corresponding clusters are larger. For a still higher density many clusters stick together to form a spanning structure (red cluster in (c)).

at one particular value of a continuously varying parameter. For an occupation probability $p_c - \epsilon$ (ϵ is an arbitrarily small numer) there is no percolating cluster, for $p_c + \epsilon$ there is (at least) one.

We have defined the percolation process on a regular lattice in d dimensions. It is easy to see that d must be at least 2 in order to have a critical phenomenon. Let us suppose that $d = 1$. Our system can be represented by an infinitely long linear chain, as shown in Fig. 1.3.

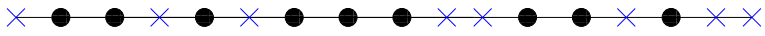

Figure 1.3: Site percolation on a 1-dimensional linear chain. Nearest-neighbouring black circles form the clusters. The crosses indicate vacancies, which separate the clusters from each other. Percolation can take place only if all sites are occupied ($p = 1$).

The black circles in the figure represent the occupied sites. If the occupation probability p is smaller than 1, there will be holes along the chain. But a spanning cluster in this special case must include all sites, therefore there can be percolation only for $p = 1$. There is no separation in two phases, and that makes the one-dimensional case not as interesting as the higher-dimensional ones. We shall thus always assume that $d \geq 2$. The lattice structures on which we can play our percolation game are not restricted to the simple square (cubic) ones: we can use as well triangular, honeycomb lattices (Fig. 1.4). Besides, we can use the same structure in different ways, like in the case of the simple 3-dimensional cubic lattice, from which we can get three lattices: we can consider as sites just the vertices of the cubic cells, the vertices plus the centers of the cubes (*body centered cubic* or *bcc* lattice), or the vertices plus the centers of the six faces of each cube (*face centered cubic* or *fcc* lattice).

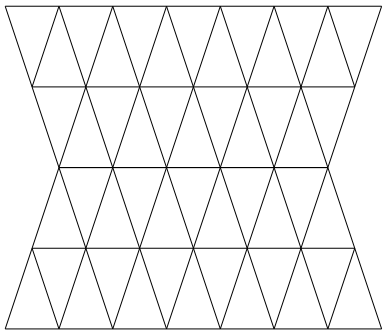

Figure 1.4: Scheme of a triangular lattice. If we consider as sites the centers of the triangles we get the so-called honeycomb lattice.

Because of the different lattice structures, the critical values of the occupation probability p_c will be in general different in each case. In Table 1.1 we have listed the values corresponding to the most studied systems. We notice that, for a fixed lattice structure, p_c gets smaller the higher the dimension d of the lattice.

Lattice	Site	Bond
$d = 2$ honeycomb	0.6962	1-2$sin(\pi/18)$
$d = 2$ square	0.592746	1/2
$d = 2$ triangular	1/2	2$sin(\pi/18)$
$d = 3$ simple cubic	0.31160	0.2488
$d = 3$ bcc	0.246	0.1803
$d = 3$ fcc	0.198	0.119
$d = 4$ hypercubic	0.197	0.1601
$d = 5$ hypercubic	0.141	0.1182
$d = 6$ hypercubic	0.107	0.0942
$d = 7$ hypercubic	0.089	0.0787

Table 1.1: Selected percolation thresholds for various lattices.

1.2 Cluster Size

1.2.1 Cluster Distribution

Once we have defined the problem, we have to see how it is possible to study the percolation phenomenon quantitatively. Percolation is a *random* process, because random is the way in which we occupy the sites (bonds) of the lattice. If we repeat the procedure over and over we will have clusters of different sizes and shapes and therefore it makes sense to study the *averages* of quantities related to the clusters. In order to do that, we must study the *statistics* of these clusters.

In general we define as size s of a cluster the number of sites (bonds) belonging to it. It is interesting to see how the clusters are distributed according to their size. This information is expressed by a function n_s, which depends both on s and on the density p. We define n_s as the *number of clusters of size s per lattice site*, according to the following formula

$$n_s = \lim_{V\to\infty} \frac{N_V(s)}{V}, \tag{1.1}$$

where V is the volume (number of sites) of a finite lattice and $N_V(s)$ the number of clusters of size s on that lattice.

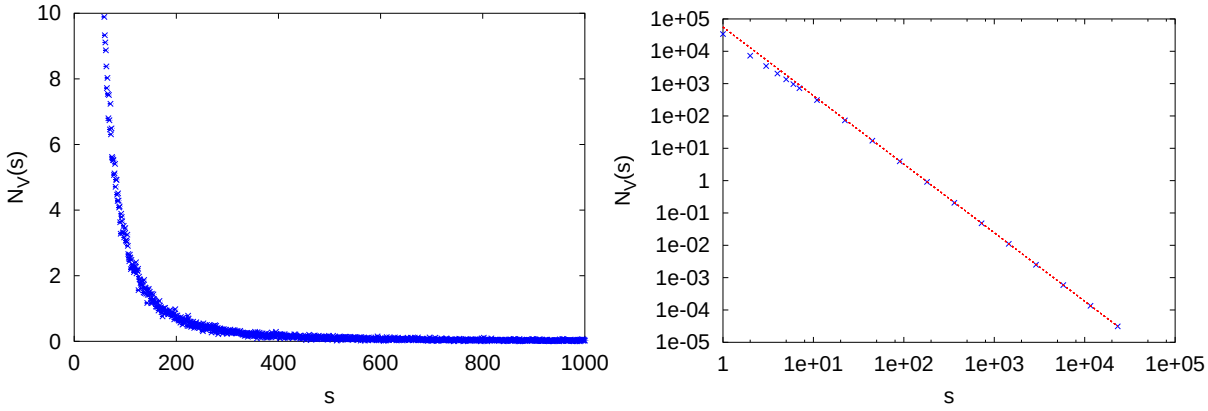

(a) (b)

Figure 1.5: (a) Cluster distribution for site percolation on a 100^3 simple cubic lattice in correspondence of the critical density $p_c = 0.3116$. (b) Log-log plot of the cluster distribution shown in (a). The data are stored in bins to reduce the fluctuations. The slope of the straight line gives an approximated estimate of the critical exponent τ.

It is generally found that, near the critical density p_c and for sufficiently big values of the size s, the distribution n_s has the scaling form:

$$n_s \propto s^{-\tau} f[(p - p_c)\, s^{\sigma}], \tag{1.2}$$

where f is a function to be determined in each specific case and τ, σ are *critical exponents*. The function $f(z)$, however, has some general features: it is basically constant for $|z| \ll 1$ and it decays rapidly for $|z| \gg 1$. That means that, for a fixed value of the density p, n_s will be appreciably different from zero for those values of the size s for which

$$s \; < \; |p - p_c|^{-1/\sigma}. \tag{1.3}$$

For $p = p_c$ the distribution is a simple power law:

$$n_s \propto s^{-\tau}. \tag{1.4}$$

Fig. 1.5a shows the cluster number distribution for pure site percolation on a cubic lattice at the critical threshold $p_c = 0.3116$. The lattice size is 100^3 and we have analyzed 100 samples in order to get a satisfactory statistics. The values on the y axis are the unrenormalized cluster numbers $N_V(s)$. We can see the main features of the cluster distribution, in particular the rapid decrease with the size s. To check whether n_s has really the power law behaviour of Eq. (1.4), we have plotted our distribution in log-log scale. To obtain a good quality of the plot we have tried to reduce the fluctuations which are visible in Fig. 1.5a. An efficient method to do that consists in dividing the s axis in bins and calculating the average of $n_s V$ in each bin. The result can be seen in Fig. 1.5b, where all our data are represented by few points: they look rather stable. Eq. (1.4) is valid only for big values of s, therefore we have excluded the points corresponding to low values of s ($s \leq 20$) and performed a linear best fit on the remaining ones. The straight line we have drawn is in good agreement with the data points, which confirms the correctedness of Eq. (1.4). The slope of the straight line is 2.13, which is a fair approximation of the exponent τ for this system ($\tau = 2.18$).

1.2.2 Average Cluster Size

If we know the cluster distribution function n_s, we may ask ourselves how big on average a cluster is. We must be careful in specifying what we exactly mean by "average" in this case. Let us suppose that we point randomly to a lattice site and want to know how big the cluster to which that site belongs is. If the size of the cluster is s, the number of clusters of that size (per site) is n_s. Therefore, the quantity $n_s s$ is just the probability of picking up a site belonging to one of those clusters. On the other hand the probability that a site of the lattice taken at random belongs to any finite cluster is given by

$$\sum_s n_s s \tag{1.5}$$

(the sum excludes the eventual percolating cluster). So, if we hit some occupied site of the lattice, the probability w_s that it belongs to a cluster of size s is given by

$$w_s \; = \; \frac{n_s s}{\sum_{\bar{s}} n_{\bar{s}} \bar{s}} \tag{1.6}$$

Our procedure will thus lead us to the following definition of *average cluster size* S:

$$S = \sum_s w_s \, s = \frac{\sum_s n_s s^2}{\sum_{\bar{s}} n_{\bar{s}} \bar{s}} \, . \tag{1.7}$$

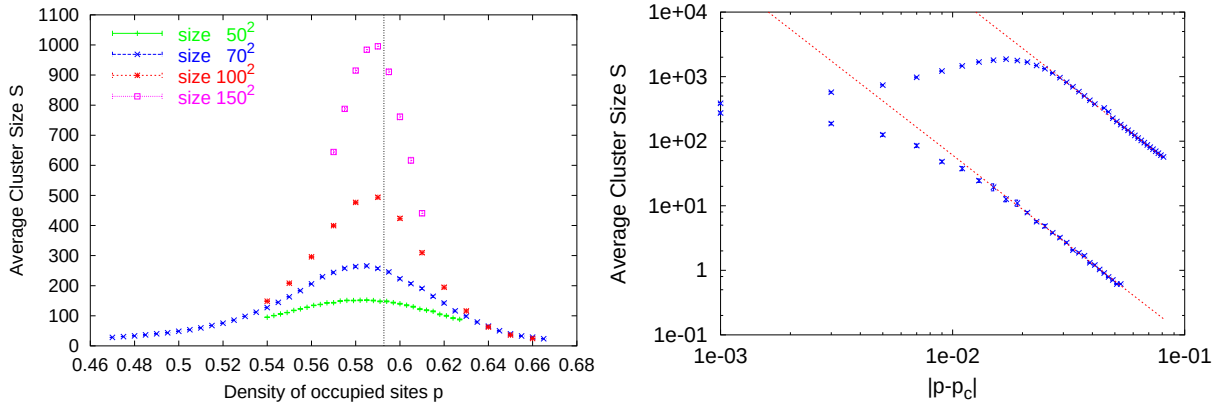

(a) (b)

Figure 1.6: (a) Average cluster size S as a function of the density p for pure site percolation on a 2-dimensional square lattice. The curves correspond to four different lattice sizes and peak near the infinite volume threshold $p_c = 0.592746$, which is represented by the dotted line. (b) Average cluster size S as a function of $|p - p_c|$ for pure site percolation on a 300^2 square lattice. In the logarithmic scale of the plot the scaling behaviour of S is clearly indicated by the two straight lines, which correspond to the different branches of the curve around the peak.

If the sums included the eventual percolating cluster, S would become infinite above the critical threshold. In this way instead the average cluster size is divergent only at the critical density p_c. Besides, its behaviour near p_c is again expressed by a power law:

$$S \propto |p - p_c|^{-\gamma} \tag{1.8}$$

where γ is another critical exponent. The behaviour of S as a function of p is illustrated in Fig. 1.6a, where we present the results of simulations for pure site percolation on a square lattice in correspondence of different lattice sizes. The divergence of S can be seen through the peaks of the curves, which become higher and narrower the larger is the size of the lattice. Besides, increasing the lattice volume, the position of the peaks approaches the critical point of the geometrical transition (dotted line). To check the scaling behaviour of S expressed by Eq. (1.8) we use other data relative to pure site percolation on a square lattice. In general, scaling relations are clearer for big volumes because the effects due to the finite size of the lattice are small (see Section 1.5). In Fig. 1.6b we have plotted S as a function of $|p - p_c|$ for a 300^2 lattice. The branches of the curve to the right and to the left of the peak are represented by the two straight lines in the figure. They are approximately parallel, which confirms the fact that both branches have a power law behaviour with the same exponent γ as in (1.8). Actually the condition of

best parallelism of the two lines is in general obtained for a value of p_c which is slightly different from the infinite volume one also for relatively large lattices: that shows that the infinite volume limit is a condition that is hard to simulate even using modern supercomputers.

1.2.3 Percolation Strength

In introducing the average cluster size S we stressed the fact that to evaluate this variable we don't need any information about the eventual percolating cluster. But such information is of course very important for a thorough understanding of the percolation phenomenon. We thus introduce another variable, the *percolation strength* P, defined as the *probability that an arbitrarily chosen site of the lattice belongs to the spanning cluster*. P is then basically the fraction of the lattice volume which is occupied by the percolating cluster. On an infinite lattice P is zero for any density p below the critical value p_c (no percolation), and a number between zero and one above p_c. P is the *order parameter* of the percolation transition, as its value allows us to distinguish the two phases of the system.

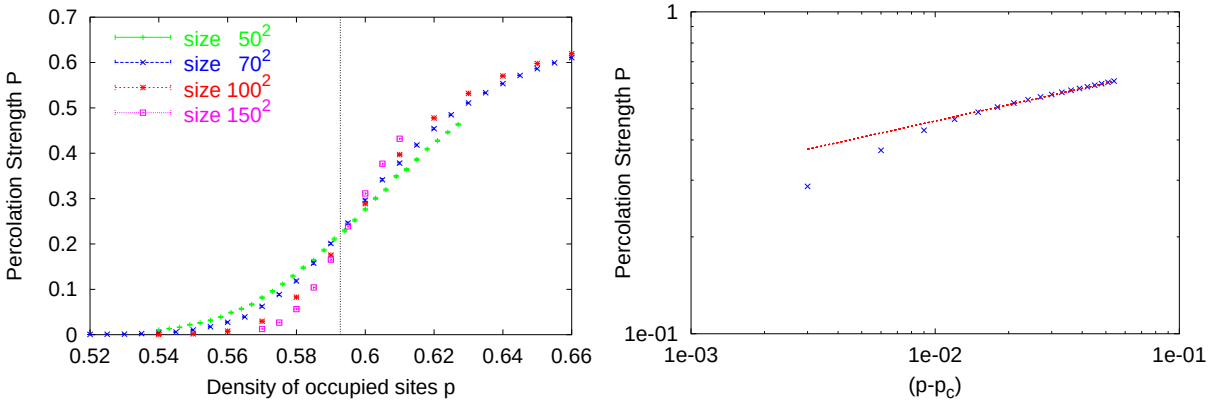

(a) (b)

Figure 1.7: (a) Percolation strength P as a function of the density p for pure site percolation on a square lattice. The lattice sizes are the same as in Fig. 1.6a. The tail of the curves to the left of the critical threshold (dotted line) is smaller the greater the lattice size. (b) Percolation strength P as a function of $(p - p_c)$ for pure site percolation on a 600^2 square lattice. Excluding the closest values of p to p_c, for which the results are strongly affected by the finite size of the lattice, our data points follow approximately a straight line, which confirms the scaling behaviour of Eq. (1.9).

Near the critical density p_c the behaviour of the percolation strength as a function of the density p is again expressed by a power law:

$$P \propto (p - p_c)^{\beta}, \tag{1.9}$$

relation which is obviously valid for $p > p_c$. Fig. 1.7a shows the P curves corresponding to the S curves of Fig. 1.6a. The finite size of our lattices allows percolation to occur also at values of p which are smaller than p_c, but the tails of the P curves to the left of p_c get smaller the bigger the lattice size is. In Fig. 1.7b we show a plot in logarithmic scale of the percolation strength as a function of p for 600^2 lattice. Disregarding the closest points to the threshold, which feel strongly the effects of the finite size of the system (see Section 1.5), the scaling behaviour of Eq. (1.9) is clearly represented by the straight line to the right of the figure.

1.3 Cluster Structure

1.3.1 Perimeter of a Cluster

Most of what we have discussed so far has to do with the *size* of the clusters. But there are also other aspects that can be studied. In particular, we can examine the *cluster structure*, which can let us know the *geometrical properties* of our objects. For example, how can we define the *perimeter* of a cluster? The easiest thing to think of is the number of empty sites neighbouring a cluster. In Fig. 1.8 the crosses around the cluster mark its perimeter according to this definition. If we count the sites of the perimeter of Fig. 1.8 we find that they are approximately as many as the sites of the cluster (15 vs 12). However, from geometry we know that, in a d-dimensional

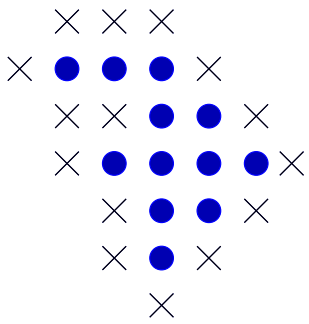

Figure 1.8: Perimeter of a small cluster. We see that the number of sites of the perimeter is of the same order as the size of the cluster. This fact is also valid for large clusters.

space, the perimeter of an object of linear dimension L is proportional to L^{d-1}, while its volume is proportional to L^d: the ratio perimeter/volume goes then like L^{-1}. We might object that this fact is due to the small size of the cluster we have taken in our example, and that going to larger structures we would recover the right behaviour. As strange as it may seem, this objection is not correct. We should not forget that our clusters are *random* structures; because of that, large clusters have in general *holes* in their body (like the holes in a Swiss cheese). The empty sites of these holes contribute to the perimeter as well. We can take as example the big spanning cluster of Fig. 1.2c. There are more than forty holes in it, some of which are so big that other

clusters are contained in them. On these grounds it isn't surprising that even the perimeter of large clusters is proportional to their size. One could still say that the real perimeter is only the external one, i.e., it is given by the empty sites surrounding the cluster, excluding the contribution of eventual inner holes. But even in this case, the result remains valid. We can easily convince ourselves in the case of site percolation on a simple cubic lattice. If we take a density p between 0.4 and 0.6, we have percolation both for the occupied and for the empty sites of the cube. In fact, both the density of occupied sites p and the one of empty sites $1-p$ are above the critical threshold ($p_c = 0.3116$). Nearly every occupied (empty) site belongs to the infinite network of occupied (empty) sites. Thus everywhere in the lattice, each occupied site has with high probability at least one neighbour belonging to the infinite cluster of empty sites. Such empty site contributes to the external perimeter, since inner holes are, of course, disconnected from the infinite network. This simple example shows clearly that the perimeter of a cluster is proportional to its size s and not to $s^{(d-1)/d}$.

1.3.2 Cluster Radius and Fractal Dimension

To examine the cluster structure it is also important to define the linear dimension of the cluster, i.e., its *radius*. To define the radius of such complicated objects may not be that easy. The need to focus on some features of the cluster geometry instead of others may lead to different definitions. We will define the radius R_s of a cluster of size s through

$$R_s{}^2 = \sum_{\mathbf{i}=\mathbf{1}}^{s} \frac{|\mathbf{r_i} - \mathbf{r_0}|^2}{s}, \tag{1.10}$$

where

$$\mathbf{r_0} = \sum_{\mathbf{i}=\mathbf{1}}^{s} \frac{\mathbf{r_i}}{s}, \tag{1.11}$$

is the position of the *center of mass* of the cluster and $\mathbf{r_i}$ the coordinates of the site $\mathbf{i}$. If we relate R_s to the average distance between two cluster sites we get the formula:

$$R_s{}^2 = \sum_{\mathbf{i},\mathbf{j}} \frac{|\mathbf{r_i} - \mathbf{r_j}|^2}{2s^2}. \tag{1.12}$$

(We put the origin of the coordinates at the cluster centre-of-mass.) It is interesting to check whether the radius R_s of a cluster is related in some simple way to the cluster size s. One finds that for large values of s the following simple power law is valid

$$R_s \propto s^{1/D}. \tag{1.13}$$

The number D is called *fractal dimension*. An interesting feature of Eq. (1.13) is the fact that D varies with the density p. In particular, it may take non integer values. To evaluate the fractal dimension D in correspondence of some density p we just need to test the scaling relation (1.13). However, there is a special case in which D is relatively easy to determine.

In fact, at the critical density p_c, the radius of the largest clusters on a lattice of linear dimension L is with good approximation just L. On big lattices one can thus write

$$s \propto L^D, \tag{1.14}$$

being s the size of the largest cluster. Fig. 1.9 illustrates a numerical test of Eq. (1.14). The

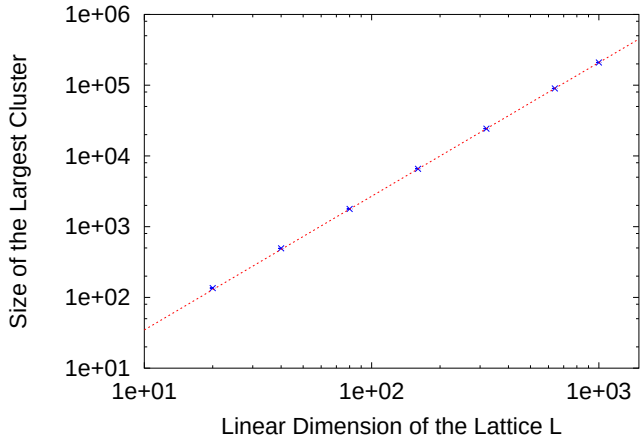

Figure 1.9: Test of the scaling relation (1.14) for 2-dimensional site percolation on a square lattice. Except the points corresponding to the smaller lattice sizes, our data points fall remarkably well on a straight line. The slope is the fractal dimension D at p_c.

clusters are again the ones of pure site percolation on a square lattice. We have drawn our data points on a log-log plot, and it is clear that, apart from little deviations for the smaller lattices, the behaviour expressed by Eq. (1.14) is correct. The slope of the straight line is 1.89(1), in good agreement with the exact value $91/48 = 1.896$. Since D is smaller than the space dimension d of the system, we say that large clusters at criticality are *fractal objects*. This is not true at higher densities. One can easily argue that, for $p \approx 1$, large clusters do not present holes in their body and therefore they are 'real' objects, i.e., $s \propto {R_s}^d$. One finds that this result is more general, namely

$$D(p > p_c) = d \tag{1.15}$$

So, there is a jump in the value of the fractal dimension when one goes from p_c to $p > p_c$. Large clusters have again the same fractal dimension at any $p < p_c$. In general

$$D(p < p_c) < D(p = p_c) < D(p > p_c) = d. \tag{1.16}$$

What we have just said about the fractal dimension allows us to illustrate an important point that we have on purpose neglected till now. We have so far spoken of "percolating cluster", assuming that, at $p \geq p_c$, only one spanning network can be formed. This fact is not at all trivial, and it has been a source of hot debates inside the percolation community. Nowadays the situation seems to be clear and we present it here, without going into the details. One has to distinguish two cases:

- $p > p_c$. The fractal dimension of a percolating cluster is, from Eq. (1.15), equal to the number of space dimensions of the lattice. That means that their density inside the lattice is *finite*, no matter how small, i.e. the clusters cover a finite fraction of the whole lattice. Starting from this, it was proved rigorously that there can be *only one* percolating cluster [21].
- $p = p_c$. In this case, as we have seen, the fractal dimension of a percolating cluster is smaller than d. The relative density of such a cluster inside the lattice is *zero*, like the density of a straight line on a plane. This would allow, in principle, the existence of several percolating clusters at p_c. Aizenman proved that there is indeed a small but finite probability to have more that one spanning cluster, even in two and three space dimensions [22].

On the grounds of these results, we shall keep assuming that there is a single percolating cluster, meaning a spanning cluster with a finite density.

1.3.3 Correlation Length

If we take a site of a cluster, the probability that an occupied site put at some distance r from the first one belongs to the same cluster is non-negligeable as long as r is of the same order of the cluster radius R_s. The average value of this probability is the *correlation function* $g(r)$. If we sum $g(r)$ over all distances r, we get the average number of sites connected to some occupied site of the lattice. The equivalence of $\sum_r g(r)$ and the average cluster size S is clear. So, in general:

$$pS = \sum_s n_s s^2 = p \sum_r g(r), \tag{1.17}$$

relation that is valid for $p < p_c$ because, above p_c, $g(r)$ would take into account the spanning cluster as well, whereas S excludes it. Eq. (1.17) can, however, be extended also to the region $p > p_c$. For that it is enough to subtract the contribution of the spanning cluster from the definition of the correlation function $g(r)$. The probability p_{inf} that an occupied site s_0 taken at random belongs to the infinite cluster is given by P/p, where P is the percolation strength P. In fact, let S_p be the size of the infinite cluster, N the number of occupied sites and V the lattice volume. The probability p_{inf} is given by

$$p_{inf} = \frac{S_p}{N} = \frac{S_p}{V}\frac{V}{N} \equiv P\frac{1}{p}. \tag{1.18}$$

Now, the probability that another randomly selected site s_r (occupied or not), distant r from s_0, belongs as well to the infinite cluster is simply given by $p_{inf}\, P = P^2/p$. The contribution of the spanning cluster to the correlation function is thus P^2/p. In this way, if we replace $g(r)$ by $g(r) - P^2/p$, we get

$$p\sum_r [g(r) - P^2/p] = p\sum_r g(r) - p\sum_r P^2/p = \sum_s n_s s^2 - P^2 V = \sum_{s'} n_{s'} s'^2 = pS \tag{1.19}$$

(the sum over s' runs over non-percolating clusters), which is the generalization of Eq. (1.17) for any value of the occupation probability p.

We define the *correlation* or *connectivity length* ξ as some average distance of two sites belonging to the same cluster:

$$\xi^2 = \frac{\sum_r r^2 g(r)}{\sum_r g(r)}, \tag{1.20}$$

The sum over r can be written as a sum over the cluster size s following this reasoning. If we point to an occupied site of the lattice, the probability $g(r)$ will be zero for all sites which do not belong to the same cluster. So, we have basically to perform a sum only within each cluster and average over all clusters of the lattice. Now we have to express Eq. (1.20) in terms of s-quantities. Let us take at random a site i of the lattice. Supposing it belongs to a cluster of size s, we have

$$\sum_r g(r) = p \sum_s \frac{1}{s} \sum_i \sum_j |\mathbf{r_i} - \mathbf{r_j}|^2 n_s s \tag{1.21}$$

where the indices i and j run over all sites of the cluster. The probability that any site belongs to a cluster of size s is $n_s s$, and that weighs the distance $|\mathbf{r_i} - \mathbf{r_j}|^2$ in our equation. The second sum (divided by s) corresponds to averaging over the site i picked up at the beginning. From Eq. (1.12) we get

$$\sum_{\mathbf{i},\mathbf{j}} |\mathbf{r_i} - \mathbf{r_j}|^2 = 2{R_s}^2 s^2. \tag{1.22}$$

by which we can write

$$\sum_r g(r) = p \sum_s 2{R_s}^2 n_s s^2 \ . \tag{1.23}$$

The denominator of Eq. (1.20) can be easily rewritten using Eq. (1.17), so that we finally obtain

$$\xi^2 = \frac{\sum_s 2{R_s}^2 n_s s^2}{\sum_s n_s s^2}. \tag{1.24}$$

Eq. (1.24) shows that the correlation length is basically determined by those clusters which give the main contribution to the average size S: ξ is essentially the average radius of those clusters. Approaching the critical density, the correlation length as well as S are thus divergent at p_c. From what we have said it is not surprising that, for $p \approx p_c$, also ξ has a power law behaviour,

$$\xi \propto |p - p_c|^{-\nu} \tag{1.25}$$

with ν as critical exponent. There is, however, much more than that. It is rather easy to argue that all divergencies we have encountered so far are also due to the clusters which are responsible for the divergencies of the average size S and the correlation length ξ. For all variables, indeed, a key role is played by the cluster number distribution n_s, which is explicitly or implicitly present

in all our definitions. We have actually seen above (Eq. (1.3)) that there is a sort of *cutoff* for the size of the clusters for which n_s is non negligible: the properties of these clusters *determine the critical behaviour of the percolation phenomenon*. In particular, the divergence of the correlation length is at the basis of the scaling laws we have met up to now, as we will explain more in detail in the next section. If the behaviour of all variables we have introduced is determined by the few properties of some special clusters, it is easy to deduce that the corresponding critical exponents, which fix the functional dependence on p of the variables at criticality, are somehow related to each other. The distribution n_s at criticality is ruled by the two critical exponents τ and σ (see Eq. (1.2)), so that we expect that all other exponents are simple combinations of τ and σ. That turns out to be true: below we show how one can calculate all exponents starting from the two fundamental ones

$$\alpha = 2 - \frac{\tau - 1}{\sigma}, \qquad \beta = \frac{\tau - 2}{\sigma}, \qquad \gamma = \frac{3 - \tau}{\sigma}, \qquad \nu = \frac{\tau - 1}{\sigma d}, \qquad D(p = p_c) = \frac{1}{\sigma \nu} = \frac{d}{\tau - 1}. \tag{1.26}$$

(We indicate with d the space dimension of the lattice.) If we play a bit with Eqs. (1.26) we can derive other useful relations: particularly important is

$$2\,\frac{\beta}{\nu} + \frac{\gamma}{\nu} = d. \tag{1.27}$$

The relations containing the dimension d are called *hyperscaling relations*. It is believed that the hyperscaling relations are valid only for values of d satisfying $d \leq d_u$, for some d_u called the *upper critical dimension*. When $d \geq d_u$, one finds that the percolation process behaves roughly in the same manner as percolation on an infinite regular tree, like the *Bethe lattice*. The values of the critical exponents for this problem are analytically known: $\tau = 5/2$, $\sigma = 1/2$, $\nu = 1/2$. We can ask ourselves for which value of d the hyperscaling relation

$$\nu = \frac{\tau - 1}{\sigma d} \tag{1.28}$$

is satisfied by such exponents. According to what we have said, the solution is just the upper critical dimension d_u. From Eq. (1.28) one obtains $d_u = 6$.

The fact that the space dimension d of the lattice is present in Eqs. (1.26) means that the scaling relations are well-defined once we fix the value of d, independently of the type of percolation (site, bond) and (or) the lattice structure we are studying. It is actually remarkable that the dimension d seems to fix not only the scaling relations (1.26) but even the values of the single exponents. This property is called *universality* and so far all tests which have been performed, both analytically and numerically, haven't found exceptions to it. In Table 1.2 we have reported the values of the critical exponents for several values of the space dimension d.

Exponent	d=2	d=3[‡]	d=4	d=5
α	-2/3	-0.6295(53)	-0.72	-0.86
β	5/36	0.4181(8)	0.64	0.84
γ	43/18	1.793(4)	1.44	1.18
ν	4/3	0.8765(17)	0.68	0.57
σ	36/91	0.4522(9)	0.48	0.49
τ	187/91	2.18906(8)	2.31	2.41
$D(p = p_c)$	91/48	2.5230(2)	3.06	3.54
$D(p < p_c)$	1.56[§]	2	12/5	2.8
$D(p > p_c)$	2	3	4	5

Table 1.2: Percolation critical exponents in d dimensions.

1.4 Real Space Renormalization

As we have seen up to now, the behaviour of all percolation variables at criticality is described by simple power laws. Apart from the simplicity of their form, power laws have a remarkable property: they are *scale free*. To understand this feature, we take the simple function $f(x) = x^{1/2}$, and focus on two intervals of the x-axis, namely $[1, 2]$ and $[10, 20]$. The ratio of the extremes of the intervals is the same ($2 : 1 = 20 : 10 = 2$) in both cases: the corresponding ratios of the values of the function is also the same ($2^{1/2} : 1 = 20^{1/2} : 10^{1/2} = 2^{1/2}$). That means that if we perform a change of scale, from x to $x' = ax$, the y-axis will be correspondingly rescaled, and the curve will look identical after the transformation. That does not happen if we use, for example, an exponential function. In fact, taking $g(x) = e^x$ and the same intervals of our example, we would find two different ratios for the values of the function at the extremes of the ranges ($e^2 : e^1 = e \neq e^{20} : e^{10} = e^{10}$): if we go from a range to another through a scale change, the function will look different after the transformation. In this sense we say that there is no characteristic length for a phenomenon described by a power law: it will look identical in each scale.

[‡]The values of the critical indices for $d = 3$ are taken from a recent study of random percolation on a simple cubic lattice [23].

[§]One could wonder why we have given a numerical estimate of $D(p < p_c)$ in two dimensions, whereas for $d = 3, 4$ analytical results are known. The percolation clusters below p_c belong to the universality class of *lattice animals*. In 1980 Parisi and Sourlas showed that the d-dimensional lattice animal problem corresponds to a $(d - 2)$-dimensional different problem, solvable in one and two dimensions: that is why exact results are known for $d = 3$ and $d = 4$.

We have stressed in the previous section that the correlation length ξ is the characteristic length of the percolation phenomenon, expressing the average radius of those clusters which give the greatest contribution to the percolation variables. So, at some density p, the value of ξ fixes the scale of the phenomenon: the (large) clusters of radius R_s smaller than ξ determine the percolation variables. The correlation length thus divides all clusters in two distinct categories. At the critical density p_c, ξ becomes infinite. Therefore, in a sense, there are no longer fundamental distinctions between two large clusters A and B at criticality, even if A is much bigger/smaller in size than B. If we take out a medium size piece of a big lattice, the linear dimensions of the lattice and of the piece are both much smaller than ξ at p_c. The original lattice and its part will then be similar as far as their average properties are concerned. A nice example of this is represented by Fig. 1.9: the average size of the largest cluster for all lattice sizes above 100^2 scales clearly with the linear dimension L, which means that all lattices are basically equivalent to each other. In this respect, the lattice 100^2 contains all the information that can be extracted by 1000^2, 10000^2, etc. Going from a lattice size A to B we just need to rescale properly the values of the variables in A to obtain the values we would measure in B. This feature is called *self-similarity* at the critical point and, according to what we have said at the beginning of this section, it naturally leads to the power law behaviour of the percolation variables.

Self-similarity is the basis of the *renormalization group* treatment of percolation. This approach was historically first applied to thermal phase transitions by K. G. Wilson [24] to justify the scaling assumptions and to calculate the critical exponents. We will briefly present the extension to percolation, introduced by Reynolds et al. [25, 26]. It is based on the so-called *real space renormalization*, by which one performs transformations on the position coordinates in ordinary space. The first step consists in *blocking* the lattice, i.e. dividing the sites of the lattice into groups or *blocks*, and then replacing each block by just one single site.

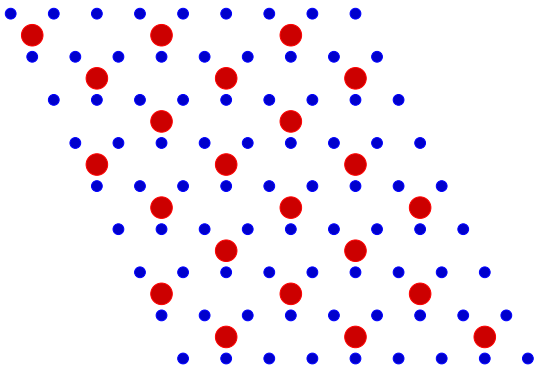

Figure 1.10: Real space renormalization on a triangular lattice (blue structure). The new sites, marked in red, replace the triangles which surround them. The new lattice, which is still triangular, has therefore one third of the sites of the original one.

Fig. 1.10 shows an example of this operation on the 2-dimensional triangular lattice. We block the sites in triangles and replace them by the red sites put in the center of each triangle. One of the requirements of the blocking procedure is that one must get the same lattice structure after any transformation. In our case we clearly see that the new structure we have formed is again a triangular lattice, and it contains one third of the sites there were at the beginning. In order to complete the transformation, we must decide which of the new sites are occupied and which are not. We need that the renormalized lattice keeps some essential features of the old one, because the latter is the system we want to analyze. That means that the status of each new site (occupied, free) must be related to the status of the three sites it replaces. There is no unique way of doing that. If we take a group of

three sites, we can get four possible configurations, since we may have zero, one, two or three occupied sites (Fig. 1.11). What we want to keep is the essential physics of percolation of the initial configuration. Since percolation involves the formation of an infinite connected network, by which one gets across the whole lattice, a sensible choice could be to define a cell as occupied if and only if it contains a set of sites such that the cell 'percolates'.

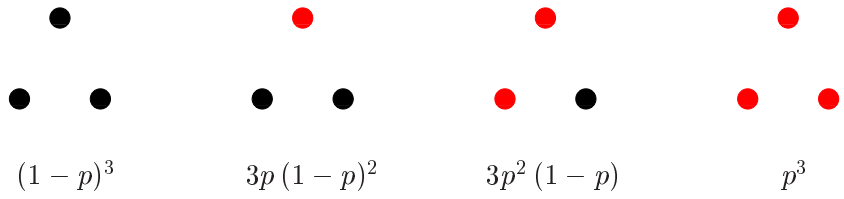

Figure 1.11: Possible states of a group of three sites. In black we mark the free sites, in red the occupied ones. Apart from irrelevant permutations, there are only four different combinations. Under each scheme we have written the corresponding probability.

As we can see in Fig. 1.11, the first and the second schemes are not percolating, and the relative super-site will be set free, the last two are percolating and the relative super-site will be occupied. Since the occurrence of the four triangular schemes of Fig. 1.11 is a different function of p in each case, the density of the blocked configuration will be in general some $p' \neq p$. In our example it is easy to calculate p': it is just the probability for a triangular block of the unblocked lattice to be either the third or the fourth triangle of Fig. 1.11. The probability for a triangle to have two occupied sites is $3p^2\,(1-p)$, to have three p^3. Then

$$p' \;=\; 3p^2\,(1-p) + p^3 \tag{1.29}$$

At $p = p_c$ we expect our operation to be basically equivalent to a rescaling of the structures of the original lattice and, because of self-similarity,

$$p' \;=\; 3p^2\,(1-p) + p^3 \;=\; p \;=\; p_c \tag{1.30}$$

The equation $p' = p$ has three solutions: 0, 1/2, 1. Discarding the trivial 0 and 1, we find $p_c = 1/2$, which is indeed the exact value of the percolation threshold on a two dimensional triangular lattice (see Table 1.1).

Moreover, by means of the renormalization group approach, we can evaluate the critical exponents. If we start from a density p close to p_c, the correlation length ξ of the initial configuration is much bigger than the linear dimension b of the blocks (in our case $b = \sqrt{3}$). That means that the blocking introduces changes only at a scale which is by far smaller than ξ. The correlation length of the renormalized configuration ξ' has thus the same functional dependence of ξ, i.e.

$$\xi' = \; c\;|p' - p_c|^{-\nu} \tag{1.31}$$

with the same constant c and exponent ν of ξ. Moreover, since all the lengths of the initial system are rescaled by a factor b, we have $\xi' = \xi/b$, which establishes the following relation

between p, p' and ν

$$b\,|p' - p_c|^{-\nu} \;=\; |p - p_c|^{-\nu}, \tag{1.32}$$

from which we derive

$$\frac{1}{\nu} = \frac{\log[(p' - p_c)/(p - p_c)]}{\log\, b} = \frac{\log\left(\frac{dp'}{dp}\right)_{p_c}}{\log\, b}, \tag{1.33}$$

where the last step is justified since we assume that both p and p' are very close to p_c. In our case, knowing the function p' from Eq. (1.30) and $p_c = 1/2$, we get finally

$$\nu = \frac{\log(\sqrt{3})}{\log(3/2)} = 1.355, \tag{1.34}$$

which is a good approximation of the exact value 4/3.

We have then shown the power of the renormalization group approach. We must admit, however, that we have chosen a particularly suitable example, and that the agreement between the values derived in this way and the exact values is seldom as good as in our case. As we have said, in fact, there is some freedom in the procedure that leads to the renormalized configurations: we may choose several ways of blocking the lattice, and the rule to establish which of the sites of the renormalized lattice are occupied and which are free is not fixed either. In general, each of the possible ways we may adopt to renormalize the initial lattice leads to different results, which could also be rather far from the exact ones. The original assumption that, around the critical point, we can 'rescale' the lattice structures by simply replacing groups of sites by single super-sites is indeed quite strong and not completely legitimate. It is easy to convince oneself that, for instance, a cluster of the initial lattice could be broken into pieces in the renormalized lattice or, vice versa, separate clusters can be fused together after the blocking transformation. Since the crucial feature is the fact that the *average* properties of the initial configuration are not changed, sometimes we can be lucky enough to choose a procedure that induces a sort of compensation of these two effects: our case of the triangular lattice is an example of that. However, generally speaking, renormalizing a configuration involves correlations between sites at a block distance b from each other. After the transformations, in fact, the relative super-sites can become neighbours and form structures. But, if we want to preserve the initial cluster distribution after any transformation, we must forbid that new structures are formed or that some of the old ones disappear. Reynolds et al. showed that using large cells one can reduce very much this drawback and get quite precise results for several systems [26].

From what we have said it emerges that blocking the lattice does not only imply a new occupation density p' for the sites of the renormalized configuration, but also some *probability* x that neighbouring sites are connected to each other. This probability is introduced to eliminate correlations among sites which are not neighbour in the initial configuration. If we start from a pure site percolation problem, we will thus end up with a *site-bond* one. Repeating the transformation over and over, longer range correlations will be introduced, and, in order to cancel them, the number of parameters which characterize the percolation system after any transformation

will increase. But, around criticality, as long as the range of the correlation between sites can be, it will be always negligible compared to the (basically) infinite correlation length and, following the same reasoning of our example, we deduce that the exponent ν is the same for all the percolation systems mapped onto each other by renormalization transformations. Analogously, if we consider other percolation variables, instead of the correlation length ξ, it is easy to show that each critical exponent is not changed by blocking transformations. At some stage, one finds that the set of parameters does not vary after performing blocking transformations. In an ideal parameter space where all percolation systems can be represented by points according to the values of p, x, etc., the final set of parameters represents the so-called *fixed point* of the renormalization transformation. If one starts from some percolation system at criticality in d space dimensions, successive blockings will lead to the *same* fixed point. From what we have said, a consequence of that is the fact that the critical exponents are the same for all percolation systems in d dimensions, which explains the *universality* for the percolation phenomenon. In so far, we can say that the local differences between the various percolation systems can be smoothed out by means of renormalization transformations without changing the main features (e.g. the exponents) of the phenomenon. These features remain unchanged all the way up to the fixed point and are, because of that, equal for all possible systems.

1.5 Finite Size Scaling

As we said at the beginning, the percolation problem is relatively old. The simplicity of its formulation and the useful symmetries of several lattices have allowed to derive a number of results by means of rigorous analytic proofs: the demonstration that the critical density for bond percolation on a square lattice is 1/2 is probably the most spectacular achievement [27]. Indeed, percolation as a critical phenomenon makes sense only on an infinite lattice, and such an ideal system can be properly handled by probability theory, which is at the basis of the proofs we mentioned. Many features of apparently simple systems are, however, still out of reach. For instance, nobody could so far find an analytical expression for the value of the critical density ($p_c = 0.592746$) for the site percolation problem on a square lattice.

The study of percolation systems received new impulse since fast computers became available. Monte Carlo simulations are, in fact, a powerful tool to analyze complex systems. The data we have shown in our plots so far have been derived by means of this numerical approach. Computer simulations are *experiments*: they reproduce the system one wants to study by creating a big number of possible copies of it, and obtain the results by averaging the values corresponding to the different configurations. In this way, one can investigate any system with a degree of accuracy which depends mainly on the computer time one invests in the project. The results can then be made, in principle, arbitrarily precise.

By simulating a system, however, we are forced to use *finite lattices*. The infinite lattice, which is the ideal system we would like to investigate, remains an unreachable limit for a computer, as big as it can be. The rapid evolution of fast machines in the last years has allowed to push the size of the lattices that can be realistically studied up to values which were unthinkable only ten

years before. Any progress in this direction is always welcome, but the fundamental problem of computer simulations is always the same: how can we extrapolate the infinite volume results out of values relative to finite lattices? One could assume that a huge lattice is already 'infinite' in the sense that the difference between the critical indices (threshold, exponents) that one can derive from it and the exact ones is smaller than the degree of accuracy we want to reach. For some random percolation systems this turns out to be a good assumption. But in most cases, especially when one wishes to perform percolation studies on interacting systems, it does not work. Because of the dynamics, in fact, the simulations are by far more time consuming than for ordinary random percolation, and the largest lattices one can use for the latter are out of reach. As a matter of fact, there is a way to extract the required infinite volume information out of values calculated on finite lattices: instead of using a single lattice size, one has to take several ones, and exploit the *scaling* behaviour of the percolation systems. This procedure is called *finite size scaling* and is usually applied to all systems which undergo second order phase transitions. In this section we shall describe finite size scaling, focusing in particular on the techniques we adopted to extract the final results for the systems we have investigated all through this work.

If we take a look at the plots we have presented in this chapter, we can already see a number of characteristic *finite size effects*, i.e. features due to the finite size of the system. In Fig. 1.6a, for example the divergence of the average cluster size S becomes a finite peak, which gets sharper and higher for bigger systems; the corresponding percolation strength curves (Fig. 1.7a) show a little tail to the left of the critical point, whereas on an infinite lattice $P = 0$ for $p < p_c$. The main reason of these perturbations is obviously the finite number of sites of the lattice, which introduces a cut-off for the upper size of the clusters. Another problem is the fact that the configuration looks different at the boundaries of the system than far from them. We can see it in Fig. 1.2c: the edges of the lattice cut the clusters close to them. This factor can be considerably reduced by using *periodic boundary conditions*, i.e., by connecting opposite sides (surfaces) of the lattice to each other in some way, so that each site is always surrounded by other sites. Such a trick is regularly adopted in simulating systems on the lattice but in all our cluster analyses we will dispense with it (*free boundaries*).

We have seen that the scaling laws are effective already for rather small lattices. In the previous section we pointed out that self similarity at the critical point is responsible of that. From renormalization group theory it is possible to find out what the scaling laws look like on finite lattices. In general, if a variable $\mathcal{O}$ is supposed to scale as $|p - p_c|^{-\rho}$, on a finite lattice of linear dimension L at a density p close to p_c, one observes the following behaviour:

$$\mathcal{O}(p - p_c, L) \;=\; L^{\rho/\nu}\, Q_{\mathcal{O}}\Big[\Big(\frac{p - p_c}{p_c}\Big)\, L^{1/\nu}, g_i L^{y_i}\Big]\,, \tag{1.35}$$

where ν is the critical exponent we have already met and $Q_{\mathcal{O}}$ is a function related to the variable $\mathcal{O}$ whose form does not depend on the dimension L of the lattice. Besides, one could have an eventual dependence on other parameters, which we indicate by g_i: y_i are the exponents correspondent to these other parameters. The further dependence of $\mathcal{O}$ on g_i is the main source of the so-called *corrections to scaling*, since it modifies the otherwise simple scaling assumption expressed by Eq. (1.35). Such perturbations are sometimes relevant and one should take them

into account. However, for all the systems we have investigated in this work, we will disregard them [‡]. We shall thus always make use of the simple scaling assumption

$$\mathcal{O}(p - p_c, L) \;=\; L^{\rho/\nu}\, Q_{\mathcal{O}}\Big[\Big(\frac{p - p_c}{p_c}\Big)\, L^{1/\nu}\Big]\,. \tag{1.36}$$

Eq. (1.36) shows that the infinite volume information we look for (p_c and the exponent ρ) is 'hidden' in the finite size results: we have only to extract it in some clever way. At the critical density p_c, Eq. (1.36) becomes

$$\mathcal{O}(L)_{p_c} \;=\; L^{\rho/\nu}\, Q_{\mathcal{O}}[0]\,. \tag{1.37}$$

We notice that there is no L-dependence in the values of the function $Q_{\mathcal{O}}$. By plotting $\mathcal{O}$ as a function of L at p_c, we can then obtain the exponents' ratio ρ/ν directly from the slope of the data points in a log-log plot. If we have an idea of where the critical point could be, e.g. from the positions of the peaks of the average cluster size curves, we can evaluate $\mathcal{O}$ at different values of p for several lattices and check for which value of the density we get the best χ^2 for the simple linear fit in the log-log plot. In this way we would be able to evaluate p_c as well. The errors on p_c and on the exponents are calculated by determining the p-range containing p_c such that for each value of p one still gets a good χ^2 for the scaling fit[§].

As a matter of fact, there is also another method to determine quite precisely the critical point of the percolation transition. Because of the finite size of the lattices we may find spanning clusters at any value of the density p of occupied sites, in particular also for $p < p_c$. For the same reason there may be lattice configurations at densities above the critical threshold for which percolation does not occur. The probability of finding a spanning cluster on a finite lattice of linear dimension L at a density p is a well defined function Π, which we call *percolation cumulant* [28]: for $p \approx p_c$ and big values of L, it has the following behaviour

$$\Pi \;=\; \Phi\Big[\Big(\frac{p - p_c}{p_c}\Big)\, L^{1/\nu}\Big]. \tag{1.38}$$

We recognize the typical functional dependence of an observable $\mathcal{O}$ given by Eq. (1.36) with $\rho = 0$. The function Π is not a real variable for percolation because it has a non-trivial meaning only on finite lattices. On an infinite lattice it reduces itself to a step function: it is zero for $p < p_c$ and one $p > p_c$. Nevertheless the special features of Π make it a powerful tool to extract information about critical properties of the percolation phenomenon. In particular, for $p = p_c$, $\Pi = \Phi(0)$ for any value of L. That means that if we calculate the percolation cumulant as a function of p for different lattice sizes, all curves will cross in correspondence of the critical density p_c (Fig. 1.12a). Besides, if we replot the different curves as a function of $X = (\frac{p-p_c}{p_c})L^{1/\nu}$, the result must be just the function $\Phi(X)$ for each lattice size and all curves will fall on top of each other (Fig. 1.12b). This represents a good technique to determine the critical point and we will adopt this method all through our calculations. Once we have determined the position of the critical threshold p_c with its error σ, we examine the range $[p_c - \sigma, p_c + \sigma]$: by exploiting

[‡] This point will be discussed more extensively in the summary.

[§] A common criterion is that the value of the χ^2 must be within the 95 % confidence level.

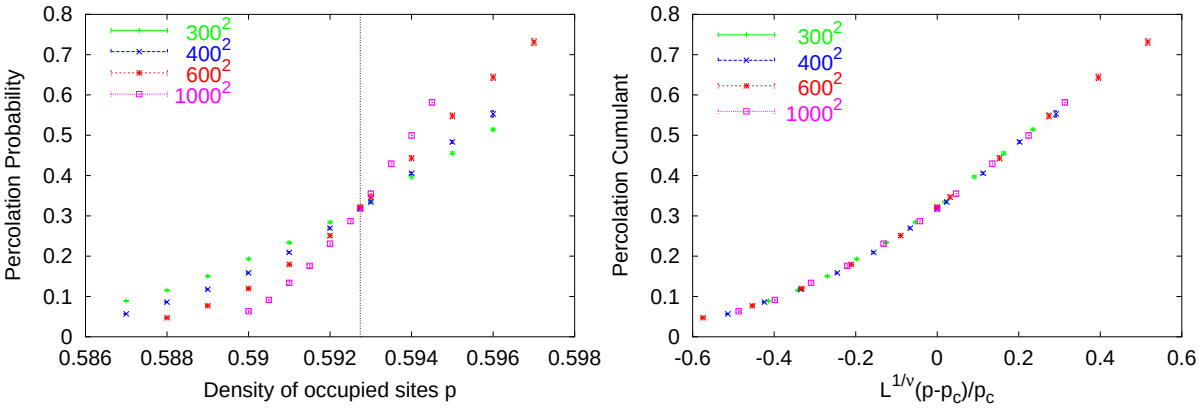

(a) (b)

Figure 1.12: (a) Percolation cumulant as a function of the density p for pure site percolation on a square lattice. The curves cross remarkably well at the same point, in excellent agreement with the infinite volume threshold, whose value is marked by the dotted line. (b) The data points in (a) are plotted as a function of $(\frac{p-p_c}{p_c})L^{1/\nu}$. Both p_c and ν for this problem are well known from the literature: $p_c = 0.592746$ and $\nu = 4/3$. All data points fall on the same curve, which is the scaling curve $\Phi(X)$ of equation (1.38) for our system.

the scaling of the percolation variables one can see how the exponents's ratios ρ/ν of Eq. (1.37) vary with p within the range. In this way one determines the errors on ρ/ν.

To get the scaling function $\Phi(X)$, one needs also to know the value of the exponent ν: if we don't know this value we can evaluate it by making some guesses until we find the best scaling for the percolation cumulant curves. This method can indeed help to restrict the range of possible values of ν; unfortunately Φ varies quite slowly with ν and the errors on its value can be rather big ($\approx 5\%$ in some of our investigations).

An alternative way of evaluating the exponent ν consists in determining, for a given lattice of dimension L, the so-called *pseudocritical point*. Looking at Fig. 1.6a we notice that the peaks are not centered at the same value of p. In fact, because of the finite size, each lattice 'feels' itself at criticality when the correlation length ξ reaches the dimension of the lattice. Since, around the critical point, ξ varies with p according to Eq. (1.25), the condition $\xi \approx L$ is reached for the density $\bar{p}\,(L)$ for which

$$|\bar{p}(L) - p_c| \propto L^{-1/\nu} \tag{1.39}$$

The value of $\bar{p}$ is called pseudocritical point: we stress that it depends on the linear dimension L of the lattice. Plotting in logarithmic scale the values of the 'distances' from the critical point $|\bar{p}(L) - p_c|$ as a function of L, we should then get a straight line, whose slope gives $1/\nu$. If we have a precise value for the critical density p_c, Eq. (1.39) allows us then to derive the exponent ν. Anyway, if our determination of the critical point is not accurate enough but we have data

in correspondence of several lattice sizes, we could obtain p_c by considering it a parameter of the fit like $1/\nu$ and the proportionality constant of the power law of Eq. (1.39). This method leads to more precise estimates of ν than the ones got by means of the scaling of the percolation cumulant; because of that, in our studies we shall determine the percolation exponent ν from the scaling of the pseudocritical points.

Chapter 2

Percolation and Critical Behaviour in the Ising Model

2.1 Critical Behaviour

In this section we shall introduce the formal definition of phase transition and point out the main aspects related to it.

In general, if we have a system at a temperature T, from its Hamiltonian $\mathcal{H}$ one defines the *partition function* $\mathcal{Z}(T)$ as follows

$$\mathcal{Z}(T) = \sum_{\{n\}} e^{-\beta \mathcal{H}}, \quad \beta = \frac{1}{kT}, \tag{2.1}$$

where $\sum_{\{n\}}$ runs over all possible states of the system. From $\mathcal{Z}(T)$ one can derive all the *thermodynamic potentials* of the system, which give us the whole thermal information. In particular, one defines the *free energy* $\mathcal{F}(T)$

$$\mathcal{F}(T) = -\frac{1}{\beta} \log \mathcal{Z}(T). \tag{2.2}$$

By means of the free energy one usually classifies phase transitions in two main categories:

- *first order* phase transitions, if the first derivative of the free energy $\mathcal{F}$ as a function of T is discontinuous;
- *continuous* phase transitions, if the n^{th} derivative of the free energy $\mathcal{F}$ as a function of T is discontinuous, all the previous n-1 derivatives are continuous ($n = 2, 3, etc.$).

For first order phase transitions, the discontinuity of the first derivative of the free energy implies the discontinuity of the *energy density* ϵ,

$$\epsilon = \frac{E}{V} = \frac{\mathcal{F} + T\,\frac{\partial \mathcal{F}}{\partial T}}{V} \tag{2.3}$$

(E and V are the energy and the volume of the system, respectively). Because of that, once we reach the critical temperature T_c by heating or cooling our system, we need to extract (or add) some energy (*latent heat*) for the system to pass to the other phase, and during this process the temperature does not vary. This is exactly what happens during the water-ice transition: the latent heat $L \simeq 334 Jg^{-1}$ is the energy released when H_2O molecules neatly pack themselves into a face-centered cubic lattice, rather than wandering around.

The most famous example of a continuous phase transition is the conversion of iron from paramagnetic to ferromagnetic form at the Curie temperature $T_c = 1043^0 K$. At $T > T_c$ iron is paramagnetic, i.e., it is not magnetized in absence of an external magnetic field; for $T < T_c$ the material acquires a *spontaneous magnetization* $\mathbf{m}$. The magnetization as a function of T is continuous and the energy density changes as well smoothly. The phase change is thus continuous.

In this work we will deal with second order phase transitions, therefore we shall briefly introduce here the main features of these special phenomena.

A common feature of phase transitions is the existence of a variable Φ, called *order parameter*: Φ is defined in each point $\vec{\mathbf{r}}$ of the volume occupied by the system and its average value allows to identify the phase of the system. For the paramagnetic-ferromagnetic transition we have mentioned, Φ is just the magnetization $\mathbf{m}$, which is zero in the paramagnetic phase and non-zero in the ferromagnetic one. To express the relationship between two points of the system at various distances, one defines the *two-point correlation function*:

$$G^{(2)}(r) \equiv \langle \Phi(\mathbf{0}) \cdot \Phi(\vec{\mathbf{r}}) \rangle. \tag{2.4}$$

The brackets indicate thermal averaging, i.e., over many configurations at some temperature T. In the ordered phase, $G^{(2)}(r)$ includes the contribution of the non-vanishing average of the order parameter $|\langle \Phi \rangle|^2$. In order to determine the *fluctuations* of Φ with respect to its average value, one needs to subtract that contribution. Therefore one often uses the *connected two-point correlation function*

$$G_c{}^{(2)}(r) \equiv \langle \Phi(\mathbf{0}) \cdot \Phi(\vec{\mathbf{r}}) \rangle - |\langle \Phi \rangle|^2. \tag{2.5}$$

Experimental evidence leads to the following form of the function $G_c{}^{(2)}(r)$ for T close to the critical temperature T_c:

$$G_c{}^{(2)}(r) \sim e^{-r/\xi}. \tag{2.6}$$

The length ξ is the *correlation length* of the system. It expresses the distance within which the fluctuations of the order parameter are important. For second order phase transitions at $T \approx T_c$,

$$\xi \sim |T - T_c|^{-\nu} \tag{2.7}$$

where ν is a critical exponent. The correlation length is thus divergent at T_c, which means that at the critical point large scale fluctuations of the order parameter occur. Because of that big dynamical structures are generated, though the interactions within the system are short-ranged.

The divergence of ξ at criticality is described by a simple power law. Actually it turns out that the behaviour of all variables around the critical point is described by simple power laws and corresponding critical exponents (Table 2.1).

α	$c_H \propto \alpha^{-1}\left(\left(\lvert T-T_c\rvert/T_c\right)^{-\alpha}-1\right)$,	$T \to T_c$,	$H=0$
β	$m \propto (T_c-T)^{\beta}$,	$T \to T_c^-$,	$H=0$
γ	$\chi \propto \lvert T-T_c\rvert^{-\gamma}$,	$T \to T_c$,	$H=0$
δ	$m \propto H^{1/\delta}$,	$T=T_c$,	$H \to 0$
η	$G_c^{(2)}(r) \propto r^{2-d-\eta}$,	$T=T_c$,	$H=0$
ν	$\xi \propto \lvert T-T_c\rvert^{-\nu}$,	$T \to T_c$,	$H=0$

Table 2.1: Behaviour at criticality of the main variables that characterize a system which undergoes a second order phase transition. We indicate by c_H the specific heat, by m the order parameter, by χ the susceptibility. The presence of another degree of freedom besides the temperature T, like a (small) external field (labeled by H), leads to other interesting power laws when $H \to 0$. In the first column we have listed the relative critical exponents. The d present in the expression of $G_c^{(2)}(r)$ is the space dimension of the system.

Some laws are valid both to the right and to the left of the critical point; the values of the relative proportionality constants, or *amplitudes*, are in general different for the two branches of the function, whereas the exponent is the same. From Table 2.1 we see that there are altogether six exponents. Nevertheless they are not independent of each other, but related by some simple scaling laws

$$\alpha + 2\beta + \gamma = 2, \qquad \alpha + \beta(\delta+1) = 2, \qquad (2-\eta)\nu = \gamma, \qquad \nu\, d = 2-\alpha, \tag{2.8}$$

so that there are only two independent exponents. One of the most interesting aspects of second order phase transitions is the so-called *universality*, i.e., the fact that systems which can be very different from each other share the same set of critical indices (exponents and some amplitudes' ratios). One can thus subdivide all systems into *classes*, each of them being identified by a set of critical indices.

The divergence of the correlation length at T_c implies self-similarity at the critical point and opens the way to analogous arguments as those we have presented in Section 1.4. Real space renormalization [29] gives an account of the scaling behaviour and the universality of the critical indices; moreover, starting from a general ansatz for the free energy, it allows to derive the scaling relations (2.8) and the values of the exponents.

2.2 Percolation vs Second Order Thermal Phase Transitions

The onset of percolation marks a borderline between two different *geometrical phases* of the system: on one side we never have a spanning cluster, on the other we always have one. When we introduced the percolation problem, we stressed the fact that each site of the lattice is occupied with a probability p *independently of the other sites*. There is *no communication* between different sites, which is in contrast to what one has in real systems, whose costituents normally interact with each other.

Nevertheless, the geometrical transition of a percolation system has many features in common with the thermal phase transitions we have dealt with in the previous section. We summarize here the most important ones:

- In the neighbourhood of the critical point, both the percolation and the thermal variables vary according to power laws:

$$P \propto (p - p_c)^{\beta} \quad \textit{for } p > p_c \qquad\qquad m \propto (T_c - T)^{\beta} \quad \textit{for } T < T_c$$

$$S \propto |p - p_c|^{-\gamma} \qquad\qquad \chi \propto |T_c - T|^{-\gamma}$$

- Simple scaling relations are valid, some of which, like the *hyperscaling* relation

$$d = \frac{\gamma}{\nu} + 2\,\frac{\beta}{\nu} \tag{2.9}$$

  (d= number of space dimensions), are identical for both kinds of systems;

- Universality of the critical indices.

Indeed, for several 'physical' systems, it is possible to single out some cluster-like structures: the magnetic domains of a piece of iron are a clear example. The interplay of such structures in correspondence of different states of the system can be quite interesting. In the case of the magnetic domains of iron, for instance, one observes that they grow by lowering the temperature of the sample until they fuse into macroscopic structures below the Curie point. One could ask oneself whether the critical behaviour of a system could be described in terms of the properties of some 'physical clusters'. The growth of correlations approaching the critical point would be represented by the growth of the size of the clusters. Moreover, the spontaneous order appearing below the critical temperature T_c could be related to the formation of an infinite cluster, which would map the thermal transition into a geometrical percolation transition. Cluster-like pictures of phase transitions have been discussed since about 1940. Their first applications concerned the liquid-gas transition: the droplet model proposed by Fisher was already able to make

quantitative predictions and the size distribution of its 'droplets' is very close to the cluster size distribution in percolation theory [30].

In general, one establishes the following correspondence between the thermal properties of the model and the geometrical features of the 'physical' droplets:

- they diverge at the thermal critical point;
- the connectedness length diverges as the thermal correlation length (same exponent);
- the percolation strength P near the threshold varies like the order parameter m of the model (same exponent);
- the average cluster size S diverges as the physical susceptibility χ (same exponent).

By turning a thermal system into a percolation one, we introduce a new feature with respect to the simple geometrical problem we introduced in the previous chapter: *the sites of the lattice are no longer independent of each other*, because of the interaction. This may lead to different cluster distributions compared to the ones of random percolation[†]. The distribution of the 'physical' clusters depends on the temperature of the system and on its dynamics. If the percolation transition takes place at a temperature $T_p \neq T_c$, the thermal correlation length of the system, ξ_{th}, is finite at T_p. That means that two sites of the lattice separated by a distance $r > \xi_{th}(T_p)$ will be uncorrelated; the large clusters which are responsible of the singularities of the percolation variables are then basically formed by randomly distributed (occupied) sites, and for this reason they will carry the exponents of random percolation. We can easily convince ourselves by simple space renormalization arguments. At T_p, ξ_{th} is finite but the percolation correlation length, ξ_p, is infinite. By applying successive blocking transformations, at some stage we will have reduced ξ_{th} to very small values, i.e., the sites of the renormalized configuration will be all uncorrelated. But ξ_p remains infinite and, for percolation purposes, the renormalized system is characterized by the same exponents of the original one, as we have explained in Section 1.4. Since the sites of the final configuration are uncorrelated, the percolation exponents must be the random percolation ones. Numerical analyses performed on several systems have confirmed that without exception.

On the other hand, if $T_p = T_c$, each site has a non vanishing correlation on any other, and the properties of all clusters of the system, including the largest ones, will be influenced by this correlation. Therefore, the exponents describing the percolation variables need not be the ones of random percolation, and may be related to the exponents describing the singularities of thermal variables at criticality: in particular, their values could coincide.

The early attempts to explore quantitatively this possibility date back to the 70's, and the first system to be investigated was the Ising model.

[†]In this case one usually speaks of *correlated percolation*.

2.3 The Ising Model

The Ising model is by far the simplest of all spin systems. Suppose we have a regular lattice in d space dimensions and place two-valued *spins* at each lattice site. The Ising model is characterized by the following Hamiltonian:

$$\mathcal{H} = -J \sum_{ij} s_i s_j - H \sum_i s_i, \tag{2.10}$$

where $J(> 0)$ is the coupling of the interaction between nearest neighbouring spins s_i and s_j and H an external field. The values of the spins are conventionally taken to be +1 (up) and -1 (down). For $H = 0$ and space dimension $d \geq 2$, a macroscopic system ruled by (2.10) undergoes a second order phase transition, going from a high temperature phase without spin alignment to a low temperature phase with spin alignment. In particular, at $T = 0$, all spins point to the same direction, either up or down. In this way the state of the system at low temperatures breaks the global symmetry under spin inversion enjoyed by the Hamiltonian (*spontaneous symmetry breaking*). The *order parameter* of the Ising model is the lattice average of the spin variable s, or *specific magnetization* m:

$$m = \frac{1}{V} \sum_i s_i, \tag{2.11}$$

being V the lattice volume (number of sites of the lattice). Fig. 2.1 shows the behaviour of m as a function of the temperature T.

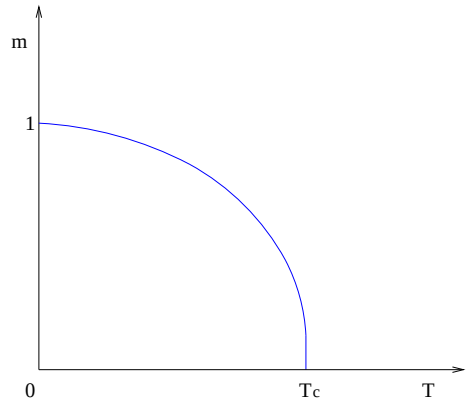

Figure 2.1: Behaviour of the specific magnetization of the Ising model as a function of the temperature T. Below the critical temperature T_c, m is different from zero, that is the system 'chooses' one of the two equivalent directions for the spins.

The Ising model without external field was exactly solved in two dimensions by Onsager [31]. The behaviour of the thermodynamic potentials close to the critical temperature is thus known analytically and the values of the critical exponents are exactly determined. In three dimensions no rigorous solution has been found so far, and all of what is known about it comes from numerical analyses, like high- and low-temperature expansions and Monte Carlo simulations. However, the simplicity of the system is such that most aspects can be investigated with remarkable precision. In Table 2.2 we put the values of the critical exponents of the Ising model in two and three space dimensions, because we will often refer to them for comparisons all along this work.

If we take a configuration of the Ising model around T_c, it will look like in Fig. 2.2.

	α	β	γ	δ	η	ν
2D	0	1/8	7/4	15	1/4	1
3D	0.1118(30)	0.3265(4)	1.2353(25)	4.783(16)	0.0374(12)	0.6294(10)

Table 2.2: Critical exponents of the Ising model in two and three dimensions. For the latter ones we report the recent numerical evaluations given in [23].

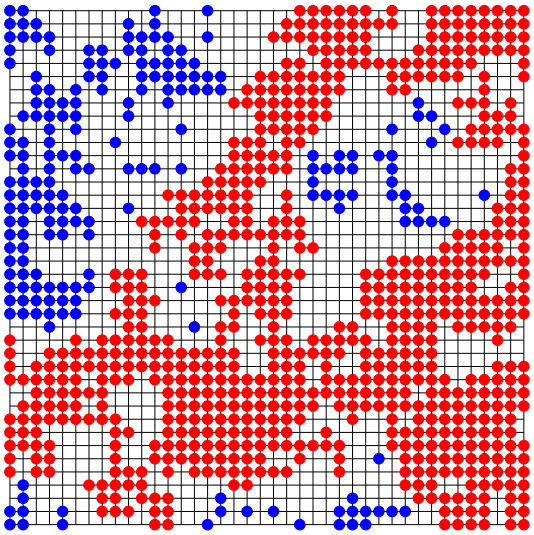

Figure 2.2: Ising model with no external field in two dimensions. The figure shows a typical configuration near the critical temperature T_c. We have marked all up spins with balls. It is visible the tendency of the spins to clusterize, because of the interaction. If we treat the spins up like pawns in a percolation game and we form clusters according to the pure site percolation scheme, there is a spanning network (red cluster in the figure).

Because of the spin alignment at low temperatures, the system will be finally dominated by spins of one type (up or down). If we think of these spins as occupied sites in a percolation picture, the clusters formed by the aligned spins will increase their size the lower the temperature is, and at a certain value T_p, there will be an infinite network. The easiest thing to think of is to consider as clusters all structures formed by nearest neighbouring spins of the same sign, which is the pure site percolation scheme we have very often discussed in the previous chapter. If we adopt this scheme, the configuration of Fig. 2.2 presents a spanning cluster, represented by the red structure. The first percolation studies on the Ising model indeed focused on these clusters.

In the two-dimensional Ising model, topological considerations imply that the percolation transition of the pure site clusters and the thermal critical point must coincide [4]. It thus became interesting to study the behaviour of the percolation variables around criticality to determine the critical exponents. As we have seen in Chapter 1, the percolation variables near the critical point vary as power laws of the 'reduced' density of occupied sites $p - p_c$. That is valid for pure random percolation. If we analyze the clusters formed by interacting systems, their features do not depend on the density alone, and the dynamics plays a major role. For example, if we take the Ising model at temperatures above T_c, there will be as many spins up as spins down. So, the density of occupied sites (considering either the up or the down spins) remains constant above T_c. But the features of the clusters change if we go from $T = T_c$, where the correlations between spins are long-ranged, to $T \to \infty$, where spins are uncorrelated. It

turns out that, for 'dynamical' clusters, the percolation variables vary as simple power laws of the reduced temperature $T - T_c$, like the thermal ones. In the case of the two dimensional Ising model, the average cluster size S of the pure site clusters was shown to diverge as

$$S \propto |T - T_c|^{-\gamma_p}, \tag{2.12}$$

where $\gamma_p = 1.91$ [5]. The result, derived by means of series expansions, is not in agreement with the thermal value for the susceptibility exponent found by Onsager ($\gamma = 7/4$). Besides, in three dimensions, the spins which are favoured by the onset of magnetization form an infinite network at any temperature, whereas the unfavoured spins happen to percolate at temperatures higher than T_p, with $T_p \approx 0.96\, T_c$ [6].

So, if it is at all possible to describe the thermal phase transition of the Ising model as a percolation transition, one must look for a different cluster definition than the pure site one.

2.4 The Random Cluster Model

At the beginning of the 70's, contemporary to the research activities mentioned in the previous section, Fortuin and Kasteleyn [7] introduced a correlated bond-percolation model (the *Random Cluster Model*) indexed by a parameter q, and proved identities relating the partition function and connectedness probabilities in this model to the partition function and correlation functions of the q-state Potts model ($q = 2, 3, ...$). The q-state Potts model has the following Hamiltonian:

$$\mathcal{H} = J_P \sum_{ij} (1 - \delta_{\sigma_i \sigma_j}), \tag{2.13}$$

where $J_P (> 0)$ is the coupling and the σ's represent the spin variable of the model, which can take q different values. For $q = 2$ it is easy to see that the Hamiltonian (2.13) is equivalent to the one of an Ising model, whose coupling $J_I = J_P/2$. In this section, however, we will keep the Potts notation because it simplifies the mathematical expressions.

To give a feeling of the work of Fortuin and Kasteleyn, we will show that their Random Cluster Model and the q-state Potts model are equivalent to each other. In particular, we will see that the partition function of the q-state Potts model can be rewritten in purely geometrical terms, as sum over cluster configurations. The clusters are built in the following way: taking two nearest neighbouring spins σ_i and σ_j, if $\sigma_i \neq \sigma_j$ they are *always* disjoint; if $\sigma_i = \sigma_j$, they are joined together with a temperature dependent probability $p_{ij} = 1 - \exp(-J_P/kT)$. So, the Fortuin-Kasteleyn clusters are *site-bond* clusters: once we have a spin configuration, we need to distribute bonds with the probability p_{ij} among nearest neighbouring spins of the same value to build the clusters. A cluster configuration will be therefore completely determined by a spin configuration $\{\sigma\}$ and a bond configuration $\{n\}$ superimposed to the former. For the bond variables n_{ij}, we assign $n_{ij} = 0$ (open bond) and $n_{ij} = 1$ (closed bond).

We won't follow the original Fortuin-Kasteleyn derivation, because it is too technical, but a simplified version proposed by Sokal and Edwards [32]. Given a lattice with Potts spins $\sigma_i = 1, ..., q$ on the sites and bond variables n_{ij} on the edges (links), we define the joint probability of a certain cluster configuration (spins + bonds) as

$$P(\sigma, n) = \mathcal{Z}^{-1} \prod_{<ij>} [(1 - p_{ij})\delta_{n_{ij},0} + p_{ij}\delta_{\sigma_i\sigma_j}\delta_{n_{ij},1}], \tag{2.14}$$

with

$$\mathcal{Z} = \sum_{\sigma} \sum_{n} \prod_{<ij>} [(1 - p_{ij})\delta_{n_{ij},0} + p_{ij}\delta_{\sigma_i\sigma_j}\delta_{n_{ij},1}]. \tag{2.15}$$

This is the so-called FKSW model (Fortuin-Kasteleyn-Swendsen-Wang), which has, a priori, nothing to do with the dynamics of a spin model. If we sum over all bond configurations we get

$$\begin{aligned} P(\sigma) &= \sum_{n} P(\sigma, n) \\ &= \mathcal{Z}^{-1} \prod_{<i,j>} \sum_{n_{ij}=0}^{1} [(1 - p_{ij})\delta_{n_{ij},0} + p_{ij}\delta_{\sigma_i\sigma_j}\delta_{n_{ij},1}] \\ &= \mathcal{Z}^{-1} \prod_{<i,j>} [(1 - p_{ij}) + p_{ij}\delta_{\sigma_i\sigma_j}] \\ &= \mathcal{Z}^{-1} \exp\Big[- \frac{J_P}{kT} \sum_{<ij>} (1 - \delta_{\sigma_i\sigma_j}) \Big] \\ &= \mathcal{Z}^{-1} \exp\Big[- \frac{\mathcal{H}(\sigma)}{kT} \Big], \end{aligned} \tag{2.16}$$

where $\mathcal{H}(\sigma)$ is the Hamiltonian (2.13). Now we have got rid of the bonds. $P(\sigma)$ is the probability associated to the spin configuration $\{\sigma\}$ in the FKSW model. If we sum over all spin configurations, we obviously obtain

$$\sum_{\sigma} P(\sigma) = 1. \tag{2.17}$$

From Eqs. (2.16) and (2.17) one gets

$$\mathcal{Z} = \sum_{\sigma} \exp\Big[- \frac{\mathcal{H}(\sigma)}{kT} \Big]. \tag{2.18}$$

We have then found that the partition function of the FKSW model coincides with the one of the Potts model (see Eq. (2.13)). The expression of the probability $P(\sigma)$ we have derived in Eq. (2.16) is just the Boltzmann probability to have the spin configuration $\{\sigma\}$ in a system ruled by the Potts dynamics. We conclude that, after integrating out the bond configurations, the FKSW model is equivalent to the Potts model.

Next, we want to see what happens if we reduce the FKSW model to a bond model, by eliminating the spin degrees of freedom. For that, we start again from Eq. (2.14) and sum over all

spin configurations. We obtain

$$\begin{aligned} P(n) &= \sum_{\sigma} P(\sigma, n) \\ &= \mathcal{Z}^{-1} \sum_{\sigma} \Big[\prod_{<ij>, n_{ij}=1} p_{ij} \delta_{\sigma_i \sigma_j} \prod_{<ij>, n_{ij}=0} (1 - p_{ij}) \Big]. \end{aligned} \tag{2.19}$$

In the last expression all the terms in the sum with a closed bond between two spins in distinct states will vanish (they are not allowed by definition), so if we denote by σ^n a spin configuration compatible with the restriction for two spins to be parallel if connected by a closed bond, we get

$$P(n) = \mathcal{Z}^{-1} \sum_{\sigma^n} \Big[\prod_{<ij>, n_{ij}=1} p_{ij} \prod_{<ij>, n_{ij}=0} (1 - p_{ij}) \Big]. \tag{2.20}$$

The terms in the sum are now independent of the spin configuration. Given the bond configuration, the sum just counts the number of compatible spin configurations. Defining as a cluster each set of bond-connected spins, we get

$$P(n) = \mathcal{Z}^{-1} \prod_{<ij>, n_{ij}=1} p_{ij} \prod_{<ij>, n_{ij}=0} (1 - p_{ij}) q^{c(n)}, \tag{2.21}$$

where $c(n)$ is the number of clusters of the given bond configuration n. Again, we have the normalization

$$\sum_{n} P(n) = 1, \tag{2.22}$$

so that

$$\mathcal{Z} = \sum_{n} \Big[\prod_{<ij>, n_{ij}=1} p_{ij} \prod_{<ij>, n_{ij}=0} (1 - p_{ij}) q^{c(n)} \Big]. \tag{2.23}$$

The (2.23) is just the partition function of the Random Cluster model introduced by Fortuin and Kasteleyn, which is then equivalent to the FKSW model when the spins are integrated out.

Summarizing the results we have derived so far, we can say that the Potts and the Fortuin-Kasteleyn models are nothing but the FKSW model when one eliminates the bonds or the spins, respectively. Consequently, the Potts model is equivalent to the one of Fortuin and Kasteleyn.

The site-bond clusters we have used look like artificial structures, because the bond probability breaks existing geometrical connections between the spins. Nevertheless, on the grounds of the result we have just presented, it seems that such "artificial structures" have a close relationship to the dynamics of the Potts model. A confirmation of such relationship is represented by the fact that the Fortuin-Kasteleyn clusters can be used to implement a non-local Monte Carlo update of the Potts model. This algorithm was proposed by Swendsen and Wang [33] and it reduces considerably the problem of *critical slowing down*, which makes the simulations around the critical point very lengthy with traditional local methods. We conclude the section describing this algorithm.

As we have already said, in order to identify the clusters, we have a superposition of a spin configuration $\{\sigma\}$ and a bond configuration $\{n\}$. But if we take a spin configuration $\{\sigma\}$, it will not be compatible with each bond configuration $\{n\}$. So, the probability to have $\{\sigma\}$ *and* $\{n\}$ is not simply given by the product of the probability of having $\{\sigma\}$ by the probability of having $\{n\}$ independently, but it is a more involved expression which requires the introduction of the concept of *joint probability*. If we have two events A and B, one defines joint probability $P(A|B)$ as the probability of the event A *given* the event B. According to this definition one gets, trivially

$$P(\sigma, n) = P(\sigma|n)\, P(n) = P(n|\sigma)\, P(\sigma) \tag{2.24}$$

Now we can calculate the conditional probabilities to get from a bond configuration to a spin configuration and vice versa:

$$\begin{aligned}
P(n|\sigma) &= \frac{P(\sigma,n)}{P(\sigma)} \\
&= \frac{\prod\limits_{<i,j>} [(1-p_{ij})\delta_{n_{ij},0} + p_{ij}\delta_{\sigma_i\sigma_j}\delta_{n_{ij},1}]}{\exp[-H(\sigma)/kT]} \\
&= \frac{\prod\limits_{<i,j>,\sigma_i=\sigma_j} [(1-p_{ij})\delta_{n_{ij},0} + p_{ij}\delta_{n_{ij},1}] \prod\limits_{<i,j>,\sigma_i\neq\sigma_j} [(1-p_{ij})\delta_{n_{ij},0}]}{\exp[-\sum_{ij}\frac{J_P}{kT}(1-\delta_{\sigma_i\sigma_j})]} \\
&= \frac{\prod\limits_{<i,j>,\sigma_i=\sigma_j} [(1-p_{ij})\delta_{n_{ij},0} + p_{ij}\delta_{n_{ij},1}] \prod\limits_{<i,j>,\sigma_i\neq\sigma_j} \delta_{n_{ij},0} \prod\limits_{<i,j>,\sigma_i\neq\sigma_j} \exp[-\frac{J_P}{kT}]}{\prod\limits_{<i,j>,\sigma_i\neq\sigma_j} \exp[-\frac{J_P}{kT}]} \\
&= \prod_{<i,j>,\sigma_i=\sigma_j} [(1-p_{ij})\delta_{n_{ij},0} + p_{ij}\delta_{n_{ij},1}] \prod_{<i,j>,\sigma_i\neq\sigma_j} \delta_{n_{ij},0}
\end{aligned} \tag{2.25}$$

is the probability to obtain the bond configuration $\{n\}$ given the spin configuration $\{\sigma\}$. In the case $\sigma_i \neq \sigma_j$ only open bonds are allowed; in the case $\sigma_i = \sigma_j$ a closed bond is put with a probability p_{ij} and an open bond with probability $1 - p_{ij}$.

$$\begin{aligned}
P(\sigma|n) &= \frac{P(\sigma,n)}{P(n)} \\
&= \frac{\prod\limits_{<i,j>} [(1-p_{ij})\delta_{n_{ij},0} + p_{ij}\delta_{\sigma_i\sigma_j}\delta_{n_{ij},1}]}{\prod\limits_{<ij>,n_{ij}=1} p_{ij} \prod\limits_{<ij>,n_{ij}=0} (1-p_{ij}) q^{c(n)}} \\
&= q^{-c(n)} \frac{\prod\limits_{<i,j>,n_{ij}=1} p_{ij}\delta_{\sigma_i\sigma_j} \prod\limits_{<i,j>,n_{ij}=0} (1-p_{ij})}{\prod\limits_{<ij>,n_{ij}=1} p_{ij} \prod\limits_{<ij>,n_{ij}=0} (1-p_{ij})} \\
&= q^{-c(n)} \prod_{<ij>,n_{ij}=1} \delta_{\sigma_i\sigma_j}
\end{aligned} \tag{2.26}$$

is the probability to obtain the spin configuration $\{\sigma\}$ given the bond configuration $\{n\}$. In order to have compatibility, the spin configuration $\{\sigma\}$ must be one of the configurations which

can be obtained by flipping the spins of the $c(n)$ clusters formed by the bond $\{n\}$, under the condition that the flipped spins within a cluster take the same value q.

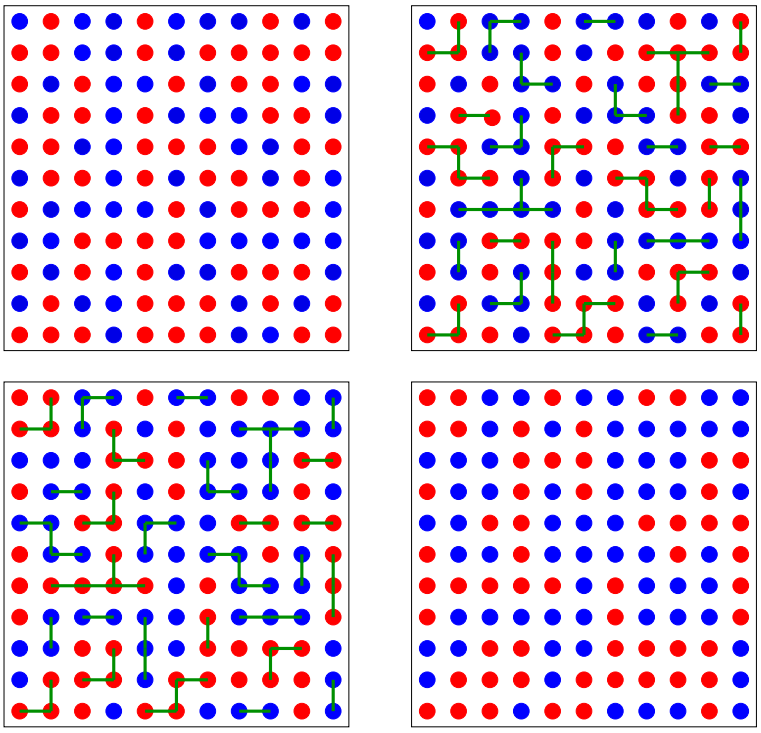

Figure 2.3: Scheme of the Swendsen-Wang cluster update for the 2D Ising model. The two possible spin values are labeled by the two colors, blue and red, of the sites. One starts from some spin configuration (top left); bonds between nearest neighbouring spins of the same color are distributed with probability p_{ij} (green links in the top right diagram); the color of all sites which are bond-connected to each other (including isolated sites) is set to blue or red with equal probability, provided the color remains uniform within each cluster (lower left); taking the bonds away one obtains a new spin configuration (lower right).

The Swendsen-Wang cluster update is based exactly on this procedure (see Fig. 2.3). We can divide it in two steps:

- Take a spin configuration and distribute bonds between nearest neighbouring spins of the same value with the probability $p_{ij} = 1 - \exp(-J_P/kT)$;
- Set the values of all spins belonging to each cluster of bond-connected sites to one of the possible q values with equal probability.

It is clear that the algorithm respects the accessibility criterium, i.e. any spin configuration can be produced provided we update the system a sufficiently large number of times. The probability

$P_{\sigma,\sigma'}$ of getting from the spin configuration $\{\sigma\}$ to $\{\sigma'\}$ is given by:

$$P_{\sigma,\sigma'} = \sum_n P(\sigma|n)\, P(n|\sigma') \tag{2.27}$$

It is easy to show that $P_{\sigma,\sigma'}$ satisfies the detailed balance condition, so that the algorithm indeed produces a Markov chain which leads the system to the canonical equilibrium distribution of the Potts model.

2.5 Percolation of Fortuin-Kasteleyn clusters

As we have seen, the pure site-clusters of the Ising model do not allow to map the thermal transition into a geometrical percolation transition. The known properties of the Ising site-clusters suggest that they are too big to describe the critical behaviour of the Ising model. The reason is that there are two contributions to the Ising clusters: one is due to the correlations, and the other is due to purely geometric effects. The latter becomes evident in the limit of infinite temperature. In this case there are no correlations but the cluster size is different from zero. In fact, since the density of occupied sites is 1/2, they tend to form clusters just because they happen to be close to each other; in the 3-dimensional Ising model there is even a spanning pure-site network at $T \to \infty$, because the critical density of 3D random percolation is 0.3116, well below 1/2.

It is thus necessary to reduce the size of the clusters in some way. We notice that the Fortuin-Kasteleyn clusters are indeed smaller than the pure-site ones. In particular, the bond probability $p_{ij} = 1 - \exp(-J_P/kT)$ varies strongly with the temperature T, going from the value 1 at $T = 0$ to the value 0 at $T \to \infty$, which expresses the absence of correlation between the sites that are, therefore, all disjoint. Moreover, from the previous section, it turns out that these clusters have a close relationship with the dynamics of the q-state Potts model (Ising model for $q = 2$). For all that they might be good candidates for the droplets we are looking for.

A. Coniglio and W. Klein [8] showed that the Fortuin-Kasteleyn clusters really have the required properties of the physical droplets, i. e. they percolate at the thermal critical point and the geometrical critical exponents coincide with the thermal ones. This result, obtained independently of the Fortuin-Kasteleyn work, is analytical and is valid for any space dimension $d \geq 2$ and any lattice geometry, as long as it is homogeneous (Fig. 2.4). In the Ising notation, the bond weight of Fortuin and Kasteleyn is

$$p_{ij} = 1 - \exp(-\frac{2J}{kT}) \tag{2.28}$$

(see Section 2.4).

For the 2-dimensional Ising model, the result of Coniglio and Klein leads to an apparent paradox. In fact we have seen that the pure site clusters percolate at the thermal threshold. On the other

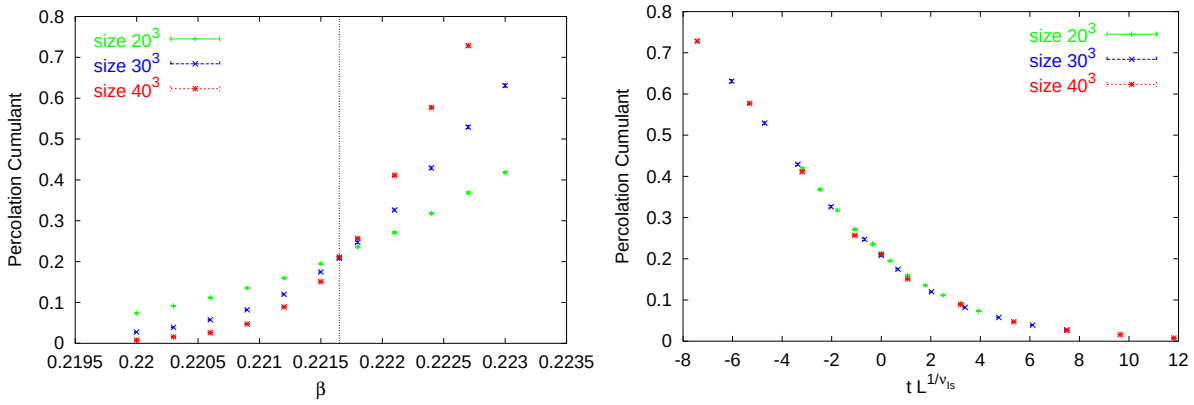

(a) (b)

Figure 2.4: (a) Percolation cumulant as a function of $\beta = J/kT$ for Fortuin-Kasteleyn clusters of the 3-dimensional Ising model. The curves, corresponding to three different lattice sizes, cross remarkably well at the thermal critical point, represented by the dashed line in the plot. (b) Rescaled percolation cumulants taking as a variable on the X-axis the expression $tL^{1/\nu}$ ($t = (T - T_c)/T_c$, L is the lattice side), where ν is set to the 3D Ising model value $\nu_{Is} = 0.6294$ (see Table 2.2). The curves fall on top of each other, so that $\nu_{perc} = \nu_{Is}$.

hand, the Fortuin-Kasteleyn clusters, which are smaller than the pure site ones, form as well an infinite network at the Ising critical point. From this fact, which is indeed unexpected but legitimate, it follows that site-bond clusters built using a bond probability p such that $p_{ij} < p < 1$ will also give rise to a spanning cluster at the thermal critical point, as their size is intermediate between the size of the pure site clusters and the one of the Fortuin-Kasteleyn clusters. However, the geometrical critical exponents relative to the percolation transition of these intermediate clusters are different from the thermal ones, with which they coincide *only* if $p = p_{ij}$. This fact shows the key role played by the bond weight p_{ij}.

2.6 The Kertész Line

So far we have been dealing with the Ising model in absence of an external magnetic field. The reason of that is clear: the Ising model shows critical behaviour in the usual sense only if $H = 0$. That means that introducing an external field H, none of the thermodynamic potentials will exhibit discontinuities of any kind, because the partition function is analytical. This result, already proved by Yang and Lee [34], inserts itself in a quite old debate concerning phase transitions. It has been known for a long time that phases separated by a line of first order phase transitions can be connected without thermodynamic singularities when using paths around the critical endpoint. This was discovered experimentally by Andrews (1869) and explained by the Van der Waals theory of liquid and gaseous states (1873). Because of that, it was suggested that, along the 'continuous' paths, something interesting may happen, in spite of the absence of

standard thermodynamic singularities. This is indeed true, and is strictly related to the droplet description of phase transitions that we have discussed in this chapter.

The Fortuin-Kasteleyn clusters are perfectly defined also in the presence of a magnetic field. Because of the field, the system has a non vanishing magnetization m parallel to the direction of the field for any value of the temperature T. However, for $T \to \infty$, $m \to 0$. For $T = 0$, $m = 1$ again. This suggests that also in this case, for a fixed value of the field H, the clusters will form an infinite network at some temperature $T_p(H)$. Varying the intensity of the field one gets a curve $T_p(H)$, which is called *Kertész line* [35]. We have plotted it schematically in Fig. 2.5.

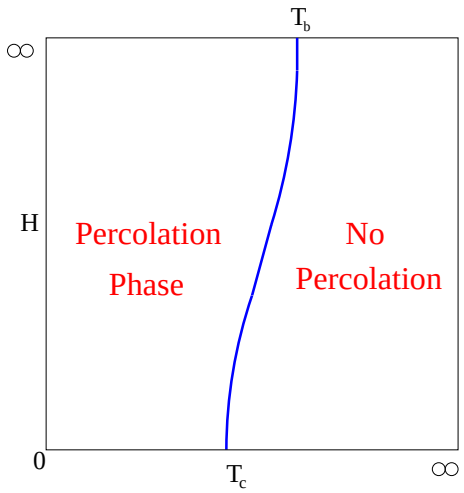

Figure 2.5: Kertész line. For $H = 0$, T_p is equal to the Ising critical point; for $H \to \infty$, T_p tends to the endpoint T_b, solution of Eq. (2.29).

When the field $H = 0$, we obviously get the thermal threshold of the Ising model. When $H \to \infty$, at any temperature T the lattice spins will be all aligned with the field. The bonds will be then distributed among all pairs of nearest neighbouring spins, and the site-bond problem turns in a pure bond percolation problem. The geometric transition will then take place for that value of the temperature T_b for which the probability p_{ij} equals the critical density $p_B(d)$ of random bond percolation in d dimensions:

$$\begin{aligned} p_{ij} &= p_B(d) \\ 1 - \exp(-\frac{2J}{kT_b}) &= p_B(d) \\ \log[1 - p_B(d)] &= -\frac{2J}{kT_b} \\ T_b &= -\frac{2J}{k \log[1 - p_B(d)]} \end{aligned} \tag{2.29}$$

So, we have a whole curve whose points are percolation points, with the usual singular behaviour of cluster-related quantities, though the corresponding thermal variables are continuous.

One can ask oneself how 'physical' the Kertész line is. We have already seen that some definitions of clusters may lead to behaviours which have nothing to do with the critical behaviour of the system: one example is represented by the pure site-clusters of the Ising model. In the same way, we could conclude that the Fortuin-Kasteleyn clusters are not the 'physical droplets' of the system if we switch on a magnetic field, and that we have to look for an appropriate definition. Swendsen and Wang [36] proposed to introduce a *ghost spin* oriented parallel to the magnetic field. This ghost spin is connected to each spin (oriented like the field) with a probability $p_H = 1-\exp(-2H/kT)$, formally similar to the Fortuin-Kasteleyn bond weight. Since, for $H \neq 0$, such probability is non-zero, no matter how small, spins arbitrarily far from each other will be connected together through the ghost spin, giving rise to a loose infinite network. Therefore, as long as $H \neq 0$, at any temperature there will be percolation in this general sense, with the sites being not directly but indirectly connected. That seems to provide the desired mapping to the thermal counterpart, in which there is always a non-zero magnetization and no divergences. An indirect confirmation of that is given by the fact that, by means of this general definition of clusters, it is possible to implement a cluster update which leads to the canonical equilibrium distribution of the Ising (Potts) model with an external field.

The success of the Swendsen-Wang definition of clusters does not imply that we can simply forget the Kertész line or treat it like an artificial construction. In fact, it turns out to have some remarkable properties. Fig. 2.6 shows some preliminary results of an investigation we are

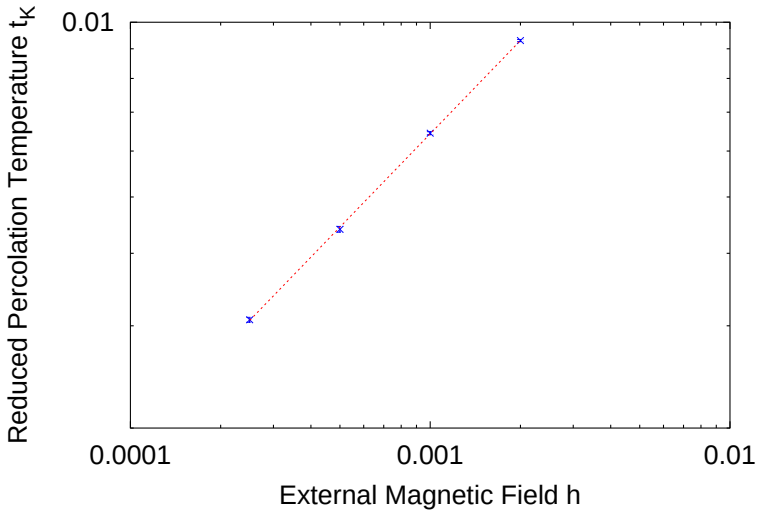

Figure 2.6: Kertész line for the 2D Ising model for small values of the external field h.

carrying on. The system is the 2D Ising model, and we calculated few points of the Kertész line for very small values of the external field $h = H/J$ (see Eq. (2.10)). The variable on the y-axis is the reduced percolation temperature $t_K = (T_K - T_c)/T_c$, where T_c is as usual the critical temperature of the Ising model without field. In the logarithmic scale of the plot the data points fall remarkably well on a straight line. We thus conclude that, for the Kertész line,

$$t_K \propto h^{\kappa}, \qquad for\ h \to 0. \tag{2.30}$$

From the slope of the straight line in the plot we obtain $\kappa = 0.534(3)$. This result might have an interesting connection with some thermal properties of the Ising model with external field. In fact, even if the susceptibility χ is not divergent at any T when $H \neq 0$, it has anyhow a well defined peak. From the renormalization group ansatz for the free energy of thermal systems undergoing second order phase transitions, it is possible to determine in general how the position of the susceptibility peak t_χ is related to the magnetic field h, when $h \to 0$. It turns out that

$$t_\chi \propto h^{1/(\beta\delta)}, \qquad for\ h \to 0, \tag{2.31}$$

where β and δ are the critical exponents we have introduced in Section 2.1. For the 2D Ising model $1/(\beta\delta) = 0.533$, which coincides with our estimate of the Kertész exponent κ. That could mean that there is a relationship between the two curves. In particular, it would be interesting to check whether they overlap, at least for small values of h[‡]. Work in this direction is still in progress.

If we take the cluster number distribution n_s of the general Swendsen-Wang droplets, it behaves differently on the two sides of the Kertész line [35]. On the low-temperature side

$$\log n_s \propto -\frac{2H}{kT}s - ?\, s^{2/3}, \tag{2.32}$$

where ? is a surface tension term; instead, on the high-temperature side, there is no surface tension and one has

$$\log n_s \propto -\frac{2H}{kT}s - const{\cdot}s, \tag{2.33}$$

Similar percolation-type singularities appear when one studies the behaviour of the Fortuin-Kasteleyn droplets around the Kertész line. According to some numerical investigations [37], there seems to be evidence that Taylor expansions of the free energy as a function of H or T have a different convergence behaviour (i.e. radius) on the two sides of this line. That might be related to the geometrical singularities we have just mentioned and could represent an argument for a generalization of the definition of phase change, not exclusively based on standard singularities of the thermodynamic potentials.

[‡]For $h \to \infty$, the position of the susceptibility peak $t_\chi \to \infty$, whereas we have seen that the Kertész line has an endpoint, given by Eq. (2.29). So, the two curves will certainly differ for sufficiently high values of h. Nevertheless, one could introduce a dependence on the field h into the Coniglio-Klein factor. Simple expressions like $1 - \exp[-2\beta(1+h)]$, for example, would still lead to the same power law behaviour of Eq. (2.30) with the same exponent κ we have found, because for the small h-values of the points we have considered, the difference from the Coniglio-Klein factor is negligible. On the other hand, the Kertész line obtained by using the new factor tends to infinity for $h \to \infty$, which might allow a global comparison with the thermal curve of the susceptibility peaks.

Chapter 3

Percolation and Magnetization in Continuous Spin Models

Starting from this chapter we shall present the results of our investigations. We will initially try to extend the Coniglio-Klein result to models characterized by continuous spin variables, which represents a first step towards the definition of a percolation picture for lattice field theory.

3.1 The Continuous Spin Ising Model

The easiest thing to start with is just to take the Ising model without external field, and replace its two-valued spins by continuous variables. The Hamiltonian is again given by

$$\mathcal{H} = -J \sum_{ij} S_i S_j, \tag{3.1}$$

with the sum over nearest neighbours, but the spin S_i can now take all values within some range, which we assume to be $[-1, +1]$. This model is the classical continuous spin Ising model introduced by Griffiths [38], who studied its behaviour in two space dimensions. In [38], Griffiths deduced that this model has the same critical behaviour of the Ising model, i. e. it undergoes a second order phase transition with the magnetization as order parameter, and its exponents are in the Ising universality class. For practical reasons, it is convenient to rewrite the spin variable S in the following way

$$S = sign(S)\,\sigma, \tag{3.2}$$

separating the sign from the amplitude σ (e.g. the absolute value) of the spin. The Hamiltonian (3.1) satisfies a $Z(2)$ global symmetry, i. e. it remains invariant after a simultaneous sign change of all spins of the system. This symmetry will play an important role all through our studies and it implies that the signs of the spins are equally distributed in the canonical ensemble of the

system. In contrast, the amplitudes can in general be weighted in different ways by choosing a distribution function $f(\sigma)$. Therefore, the partition function of the continuous spin Ising model has the following general form:

$$Z(T) = \prod_i \int_0^1 d\sigma_i f(\sigma_i) \ \exp\{\kappa \sum_{\langle i,j \rangle} S_i S_j\}, \tag{3.3}$$

where $\kappa \equiv J/kT$. In the model studied by Griffiths, $f(\sigma) = 1 \ \forall \sigma$. We will begin by studying this special case, but we will see that our result is valid also for the more general expression (3.3).

We have carried on a detailed numerical study of the model on a simple square lattice. The Monte Carlo update method we have used is a version of the Wolff algorithm [39] adapted to our system. We briefly describe this algorithm, that we will often use, in the case of the Ising model.

The Wolff algorithm is a cluster update which improves the Swendsen-Wang procedure we have illustrated in Section 2.4. Starting from a randomly chosen spin S_0, one visits all nearest neighbours of the same sign as S_0 and connects them to it with probability $p = 1 - \exp(-2J/kT)$. Repeating iteratively this procedure with newly added spins in the cluster, at some stage no more neighbours will fulfill the above compatibility condition. Flipping all spins of the cluster one gets a new spin configuration. It turns out that this dynamics verifies the detailed balance condition, i.e. it samples the Gibbs distribution of the Ising model (see [39]). The analogies with the Swendsen-Wang method are clear. The Wolff cluster is constructed in the same way as the Fortuin-Kasteleyn-Swendsen-Wang clusters, being the bond probability the same in both cases. But with the Wolff method one flips a single cluster at a time, a feature that succeeds in eliminating the old problem of critical slowing down of Monte Carlo simulations.

Because of its effectiveness, we tried to implement a Wolff-like cluster update for our system, exploiting its analogies with the Ising model. We basically repeat the Wolff procedure, but adopting for the bond probability the expression below

$$p(i,j) = 1 - \exp(-\frac{2J}{kT}\sigma_i\sigma_j), \tag{3.4}$$

which explicitly depends on the spin amplitudes. If we simply flip the spins, the dynamics is no longer ergodic, as the spin amplitudes would remain unchanged. So, the cluster flipping must be supplemented by a local update method (like Metropolis or heat bath), in order to respect the accessibility criterium. We chose to alternate heat bath and Wolff steps. The proof that the resulting update fulfills both ergodicity criteria and the detailed balance condition will be omitted here since it follows closely the derivations that can be found in [40, 41, 42, 43].

Our version of the Wolff algorithm for the continuous Ising model suggests that the Fortuin-Kasteleyn clusters in this case should probably be built as usual, the only difference being represented by the local bond probability (3.4).

To check whether these clusters are indeed the physical droplets we are looking for, we have performed extensive simulations of our model, choosing six different lattice sizes, namely 64^2, 96^2, 128^2, 160^2, 200^2 and 300^2. Our update step consisted of one heat bath sweep for the spin amplitudes and three Wolff flippings for the signs, which turned out to be a good compromise to reduce sensibly the correlation of the data without making the move be too much time-consuming. The thermal quantities are the energy density

$$\epsilon = \frac{\sum_{ij} S_i S_j}{V} \tag{3.5}$$

(V is the lattice volume), and the magnetization

$$m = \frac{|\sum_i S_i|}{V}, \tag{3.6}$$

where the absolute value is necessary to take into account the two equivalent directions of the spins.

As far as the percolation variables are concerned, after grouping all spins into clusters by means of the Hoshen and Kopelman labeling (see Appendix A), we measure the percolation strength P and the average cluster size S, as defined in Sections 1.2.2 and 1.2.3. For the cluster labeling we have used free boundary conditions. We say that a cluster percolates if it spans the lattice in both directions, that is if it touches all four sides of the lattice. This choice was made to avoid the possibility that, due to the finite lattice size, one could find more than one percolating cluster, making ambiguous the evaluation of our variables[†]. The three fundamental features we have just mentioned, i. e. the Hoshen-Kopelman algorithm, the use of free boundary conditions and the definition of percolating cluster in all directions, will be always present in our percolation investigations, unless stated otherwise.

The statistical errors of all variables were determined by using the Jackknife method [44] with ten bins of data: such method will be applied in all our studies. The quantities of interest were measured every five updates for any temperature and lattice size. That makes both the percolation and the thermal variables basically uncorrelated.

After some preliminary scans of our program for several values of the temperature κ ($\kappa = J/kT$), we focused on the κ-range between 1.07 and 1.11, where the transition seems to take place. The number of iterations for each run goes from 20000 (for κ values close to the extremes of the range) to 50000 (around the center of the range). The thermal results have been interpolated by means of the density of state method (DSM) [45], which contributes to reduce the errors relative to the data points. We shall regularly apply this method to study thermal phase transitions. Unfortunately the DSM fails if one tries to interpolate the percolation data, because the probability of having a given cluster configuration must take into account not only the distribution of the spins, which is weighted by the Hamiltonian of the model, but also the

[†]In three dimensions even this definition of spanning cluster does not exclude the possibility of having more than one of such clusters for the same configuration. Nevertheless the occurrence of such cases is so rare that we can safely ignore them.

distribution of the bonds. Besides, for the percolation quantities, standard interpolation methods (like cubic spline) do not help to improve the situation because of the fluctuations of the data at criticality. Therefore we used directly the data points to extract the critical indices.

To locate the critical point of the thermal transition we used the Binder cumulant[‡]

$$g_r = 3 - \frac{\langle m^4 \rangle}{\langle m^2 \rangle^2} \ . \tag{3.7}$$

Fig. 3.1 shows g_r as a function of κ for the different lattice sizes we used. The lines cross remarkably well at the same point, which suggests that also in our case g_r is a scaling function. As a numerical proof we replot the lines as a function of $tL^{1/\nu}$ ($t = (T - T_c)/T_c$, L is the lattice side), choosing for the exponent ν the 2D Ising value 1. The plot (Fig. 3.2) shows that indeed g_r is a scaling function with the critical exponent ν equal to the 2D Ising one.

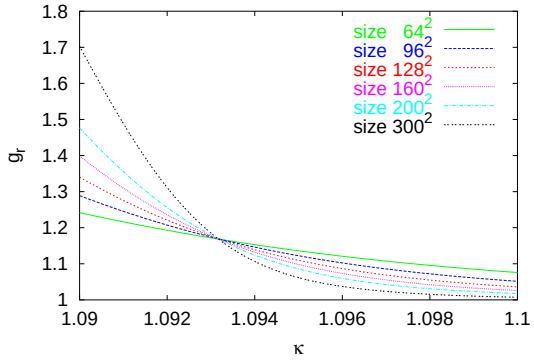

Figure 3.1: Classical continuous Ising model of Griffiths. Binder cumulant as a function of κ for six lattice sizes.

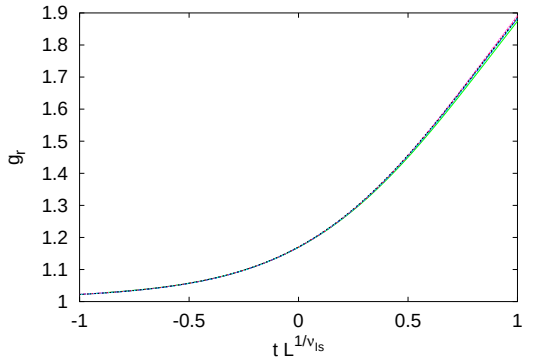

Figure 3.2: Rescaling of the Binder cumulant curves shown in Fig. 3.1. We took $\kappa_{crit} = 1.0932$ and for the exponent ν the 2D Ising value $\nu_{Is} = 1$.

[‡]In all figures of this work showing the Binder cumulant we will just plot the ratio $\langle m^4 \rangle / \langle m^2 \rangle^2$; that allows to separate neatly the Binder and the percolation cumulant in the same figure, which provides a visual comparison of the critical thresholds.

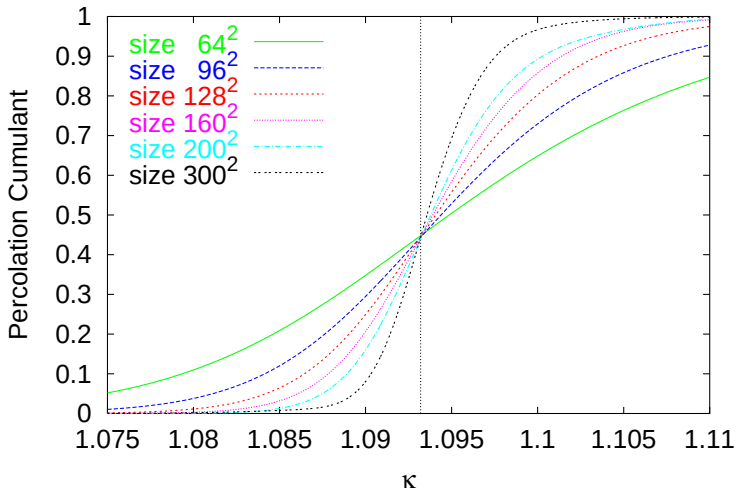

Figure 3.3: Classical continuous Ising model of Griffiths. Percolation cumulant as a function of κ for six lattice sizes. The dashed line indicates the thermal critical threshold.

To find the critical point of the percolation transition we use the percolation cumulant introduced in Section 1.5. The results can be seen in Fig. 3.3. The agreement between the thermal threshold and the geometrical one is excellent.

For the evaluation of the exponents we used standard finite size scaling techniques (see Section 1.5). To obtain the thermal exponents we adopted the χ^2 method [10], a procedure that we will apply to most of the models we are interested in. The results we got are reported in Table 3.1, from which it is clear that the critical exponents of the two transitions agree with each other and with the 2D Ising model values.

	Critical point	β/ν	γ/ν	ν
Thermal results	$1.09312^{+0.00012}_{-0.00008}$	$0.128^{+0.005}_{-0.006}$	$1.745^{+0.007}_{-0.007}$	$1.01^{+0.01}_{-0.02}$
Percolation results	$1.09320^{+0.00008}_{-0.00008}$	$0.130^{+0.008}_{-0.010}$	$1.753^{+0.006}_{-0.006}$	$0.98^{+0.03}_{-0.02}$
2D Ising values		$1/8 = 0.125$	$7/4 = 1.75$	1

Table 3.1: Thermal and percolation critical indices for the classical continuous Ising model of Griffiths.

So far we have investigated a relatively simple case, namely a model with the uniform amplitudes distribution $f(\sigma) = 1$. One can ask whether the result remains valid for the general ansatz (3.3). As a matter of fact, the distribution $f(\sigma)$ plays an important role as far as the thermal properties of the system are concerned; in particular, it may influence the order of the phase transition. For this reason, since we want to study models with continuous transitions, the choice of the

function $f(\sigma)$ is not arbitrary. It can be proved that it must obey certain regularity conditions, which are not very restrictive, however [46]. Here we consider the following form for $f(\sigma)$:

$$f(\sigma) = \sqrt{1-\sigma^2} \tag{3.8}$$

which is the Haar measure of the $SU(2)$ group. We have made this choice because our final target is to define a percolation picture for $SU(2)$ gauge theory, and the function (3.8) appears quite often in formal expressions of this theory, like series expansions.

It is reasonable to presume that the bond weight we need to define our clusters is determined by the Hamiltonian of the system, and not by eventual distribution functions. That is why we tried to test the same cluster definition we adopted in the previous case. So, our droplets will be again clusters of like-signed nearest neighbouring spins bound to each other with the probability (3.4).

We have carried on a complete numerical investigation of the model, performing simulations on four lattice sizes, 64^2, 128^2, 160^2 and 240^2. Our algorithm consists in heat bath steps for the update of the spin amplitudes followed by Wolff-like cluster updates for the flipping of the signs. That is basically the same method as used before, although the heat bath procedure is slightly modified to take into account the presence of the distribution function $f(\sigma)$: the procedure is analogous as the heat bath algorithm of Creutz for $SU(2)$ gauge theory [47]. Also in this case, the proof of the detailed balance condition is simply obtained from the results in [40] - [43]. Again, we alternated one heat bath sweep and three Wolff flippings and took the measurements every five updates: that makes negligeable the correlation of all quantities.

Fig. 3.4 shows a comparison between the Binder cumulant $g_r(\kappa)$ and the percolation cumulant, both as functions of the temperature variable κ, for different lattice sizes. The agreement between the two thresholds is excellent.

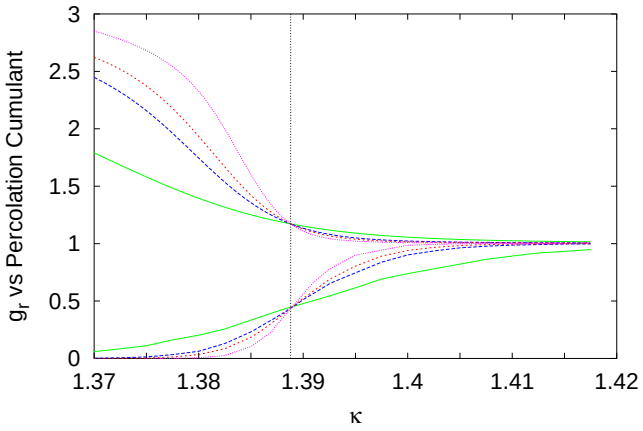

Figure 3.4: Comparison of the thermal and the geometrical critical point for the continuous Ising model with the distribution (3.8).

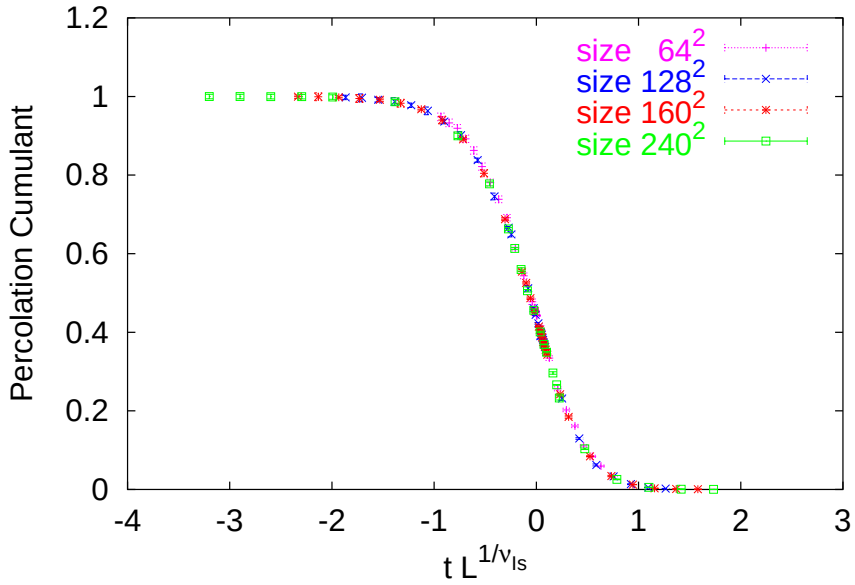

Figure 3.5: Continuous Ising model with the distribution (3.8). Rescaled percolation cumulant for four lattice sizes, using the 2D Ising exponent $\nu_{Is} = 1$. The errors on the data points are smaller than the size of the symbols in the plot.

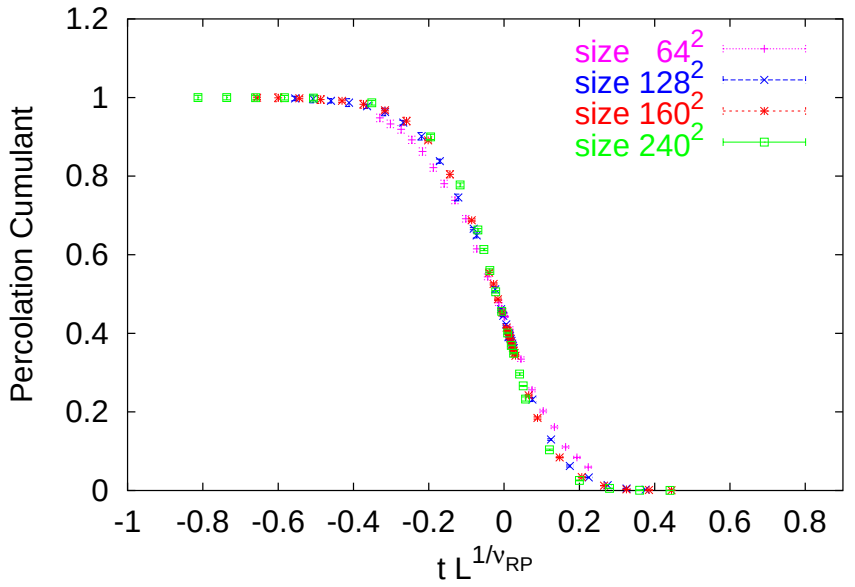

Figure 3.6: Continuous Ising model with the distribution (3.8). Rescaled percolation cumulant for four lattice sizes, using the 2D random percolation exponent $\nu_{RP} = 4/3$. The errors on the data points are smaller than the size of the symbols in the plot.

We can also get an estimate for the percolation critical exponent ν, by rescaling the percolation cumulant curves as a function of $tL^{1/\nu}$. Figs. 3.5 and 3.6 show the rescaled curves: $\kappa_{crit} = 1.3888$ and for ν we have taken the random percolation value $\nu_{RP} = 4/3$ and Ising one $\nu_{Is} = 1$, respectively. It is clear that the curves scale for $\nu = \nu_{Is}$ and do not for $\nu = \nu_{RP}$. To determine the critical exponents' ratios β/ν and γ/ν, we have performed high-statistics simulations around the critical point, with the number of measurements for each value of the coupling varying from 50000 to 100000. We have listed the results in Table 3.2. It is evident that the percolation behaviour coincides fully with the thermal critical behaviour. This conclusion is likely to hold in general for the admissable spin distribution functions.

	Critical point	β/ν	γ/ν	ν
Thermal results	$1.3887^{+0.0002}_{-0.0001}$	$0.128^{+0.007}_{-0.010}$	$1.754^{+0.007}_{-0.008}$	$0.99^{+0.03}_{-0.02}$
Percolation results	$1.3888^{+0.0002}_{-0.0003}$	$0.121^{+0.008}_{-0.006}$	$1.745^{+0.011}_{-0.007}$	$1.01^{+0.02}_{-0.03}$
2D Ising values		$1/8 = 0.125$	$7/4 = 1.75$	1

Table 3.2: Thermal and percolation critical indices for the continuous Ising model with the amplitude distribution (3.8).

3.2 Extension to Generalized Continuous Ising-like Models

We shall now address the question whether the introduction of additional longer range spin-spin interactions still allows a description of the thermal transition in terms of percolation. This will turn out to be very useful in our attempt to define suitable clusters in $SU(2)$ gauge theory. Besides, we will examine the effects of eventual self-interaction terms, and show that they don't play any role in the cluster definition.

Our study is still based on continuous spin Ising models, in which the individual spins s_i at each lattice site can take on all values in the finite range $[-1, 1]$. Since these models are more general than the ones characterized by discrete valued spins, the results can be then trivially extended to the latter ones. Here we will consider three more general models of this type; d denotes the space dimension:

A) $d = 2$, nearest-neighbour (NN) and diagonal next-nearest-neighbour (NTN) interaction (Fig. 3.7a);

B) $d = 3$, NN and two types of NTN interactions (see Fig. 3.7b);

C) as case B), but including an additional self-interaction term proportional to $S_i^2 \ \forall \ i$.

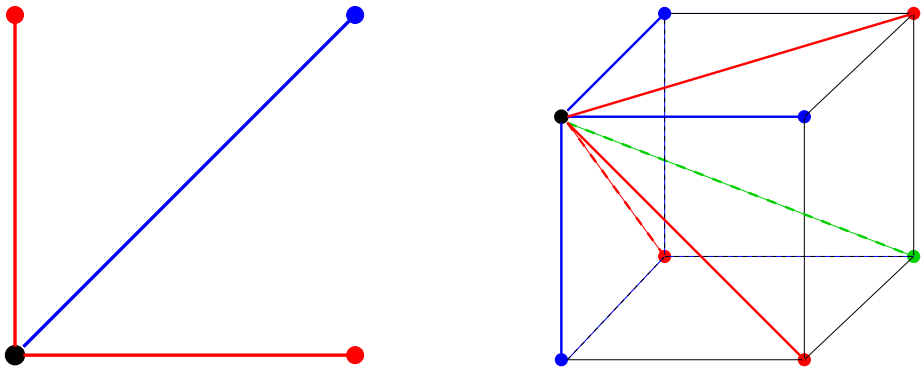

(a) (b)

Figure 3.7: Scheme of the spin-spin interactions in the models we have studied. The figures indicate the interactions of the spin represented by the black circle with its neighbours. Lines of the same color are associated to the same coupling. a) Model A. b) Models B and C.

The couplings J_i relative to the spin-spin interactions are all positive (ferromagnetic). In each case, we will assume a uniform distribution for the spin amplitudes. This has only practical reasons, since it simplifies the numerical analysis, but, according to the results of the previous section, it does not affect the generality of our conclusions.

3.2.1 Model A: Next-to-Nearest Neighbour Interactions

We have now two terms, with a Hamiltonian of the form

$$\mathcal{H} = -J_{NN} \sum_{\langle i,j \rangle}^{NN} S_i S_j - J_{NTN} \sum_{\langle i,j \rangle}^{NTN} S_i S_j \tag{3.9}$$

where the first sum describes nearest-neighbour and the second diagonal next-to-nearest neighbour interactions (Fig. 3.7a). Since longer range interactions are generally weaker, we have fixed the ratio between the two couplings at $J_{NN}/J_{NTN} = 10$; however, we do not believe that our results depend on the choice of the couplings, as long as both are ferromagnetic.

To define clusters, we now extend the Coniglio-Klein method and define for each two spins i, j of the same sign, for NN as well as NTN, a bond probability

$$p_B^x(i,j) = 1 - \exp(-2\kappa_x \sigma_i \sigma_j), \tag{3.10}$$

where x specifies $\kappa_{NN} = J_{NN}/kT$ and $\kappa_{NTN} = J_{NTN}/kT$, respectively. This hypothesis seems to us the most natural, and we will test it in the following B and C models.

We have studied model A using two different Monte Carlo algorithms, in order to test if a Wolff-type algorithm can also be applied in the presence of NTN interactions. The first is the standard Metropolis update, while the second alternates heat bath steps and a generalized Wolff flipping, for which the clusters are formed taking into account both interactions. The generalization of the cluster update is trivial. After several runs, some with high statistics, we found excellent agreement with the Metropolis results in all cases. So, the mixed algorithm with heat bath and Wolff flippings appears to remain viable also in the presence of more than the standard NN interaction. Subsequently we have therefore used this mixed algorithm. The update alternates like before one heat bath sweep and three Wolff flippings. The lattice sizes ranged from 100^2 to 400^2. We measured our variables every 5 updates for the smaller lattice sizes and every 10 for the larger ones, keeping these numbers fixed at any temperature. All variables of interest turn out to be basically uncorrelated. We accumulated up to 50000 measures for temperatures close to the critical point.

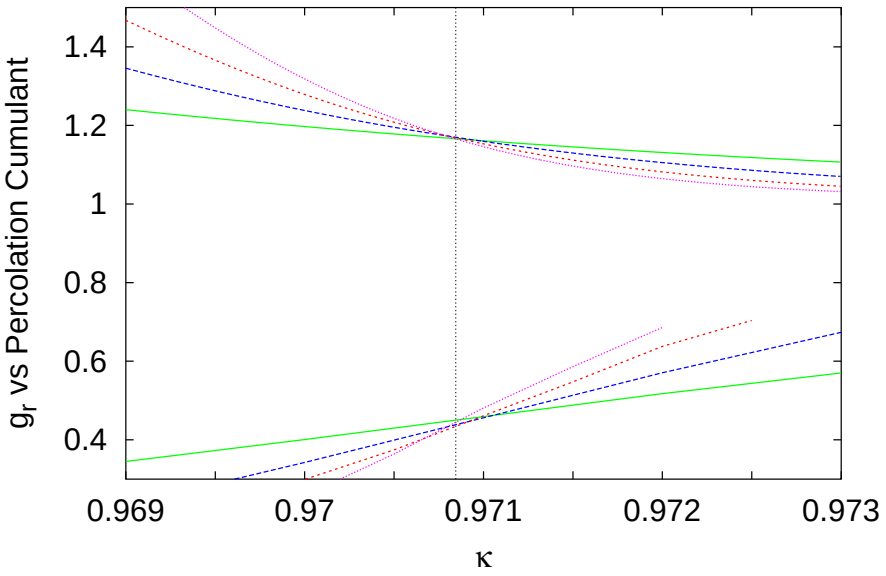

Figure 3.8: Comparison of the thermal and the geometrical critical point for Model A obtained respectively from the Binder cumulant g_r and the percolation cumulant.

We present again the comparison between percolation and Binder cumulants, in order to test that the critical points coincide (Fig. 3.8). The crossing point of the percolation curves looks less defined than the thermal one because we used a simple linear interpolation of the data. Anyhow, simulations of the model at the thermal threshold lead to values of the percolation cumulant that, within errors, are the same for all lattice sizes. We then rescale the percolation cumulant, using the critical κ determined in Fig. 3.8 together with the two main options for the exponent ν, that is the value of 2D random percolation and the one of the 2D Ising model. In Fig. 3.9 we show the rescaling done using ν_{Is}: the curves fall clearly on top of each other.

The determination of the two exponents ratios β/ν and γ/ν confirms that indeed the exponents

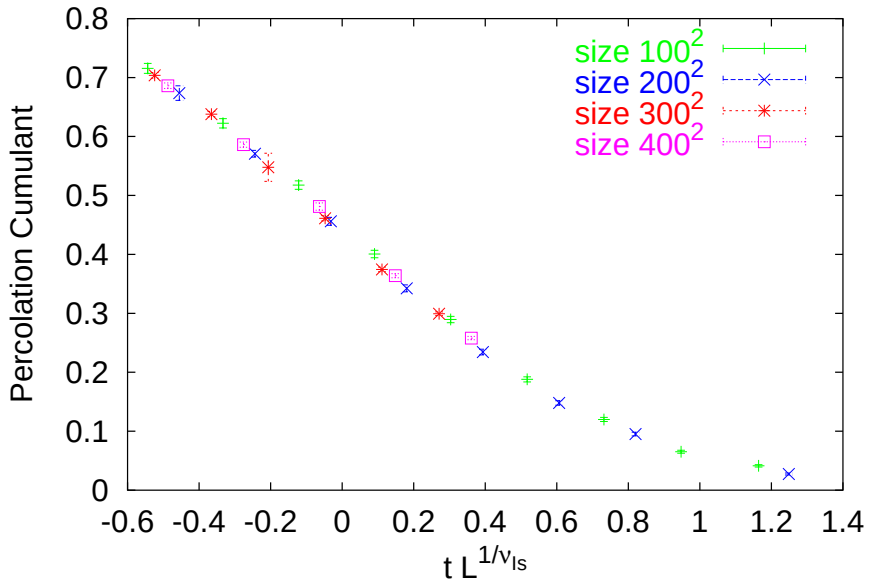

Figure 3.9: Rescaled percolation cumulant curves for model A, using the 2D Ising exponent $\nu_{Is} = 1$. The errors on the data points are smaller than the size of the symbols in the plot.

of our geometrical islands belong to the 2D Ising universality class (Table 3.3).

	Critical point	β/ν	γ/ν	ν
Thermal results	$0.9707^{+0.0003}_{-0.0002}$	$0.124^{+0.007}_{-0.005}$	$1.747^{+0.009}_{-0.007}$	$0.993^{+0.014}_{-0.010}$
Percolation results	$0.9708^{+0.0002}_{-0.0002}$	$0.129^{+0.008}_{-0.009}$	$1.752^{+0.009}_{-0.011}$	$1.005^{+0.012}_{-0.020}$
2D Ising Model		$1/8 = 0.125$	$7/4 = 1.75$	1

Table 3.3: Thermal and percolation critical indices for model A, compared to those of the 2D Ising model.

3.2.2 Model B: Extension to Three Dimensions

We now go one step further and repeat the study for a $d = 3$ model with three different interactions (Fig. 3.7b).

To fix the model, we have to specify the ratios of the nearest-neighbour coupling J_{NN} to J_{NTN} and J_{diag}. We chose them to be $10:2$ and $10:1$, respectively. Our calculations are performed on lattices ranging from 12^3 to 40^3.

Also here we have first compared the results from a mixed algorithm of the same kind as for the previous case to those from a standard Metropolis algorithm; again, the agreement turns out to be very good. The heat bath sweeps and the Wolff flippings are in the ratio $1:3$. We measured our variables every 5 updates for any temperature and lattice size. The percolation variables are not correlated, whereas the thermal ones show a correlation which is, however, rather small (the autocorrelation time τ is of about $2-3$ for the magnetization on the 40^3 lattice near criticality). The number of measurements we took varies from 20000 to 40000.

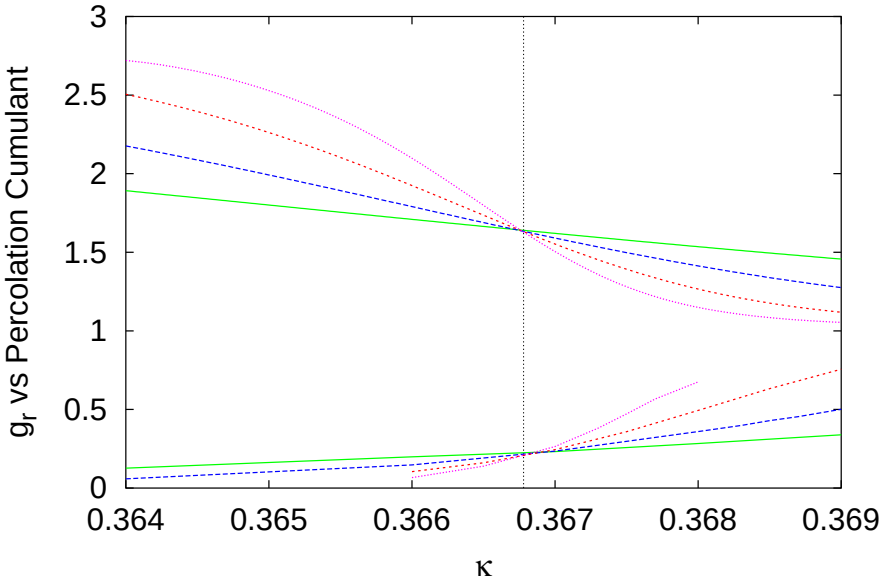

Figure 3.10: Comparison of the thermal and the geometrical critical point for Model B obtained respectively from the Binder cumulant g_r and the percolation cumulant.

Figs. 3.10 and 3.11 then show the comparison of the thresholds and the scaling of the percolation probability. As before, the correspondence between percolation and thermal variables is evident (Table 3.4).

	Critical point	β/ν	γ/ν	ν
Thermal results	$0.36677^{+0.00010}_{-0.00008}$	$0.530^{+0.012}_{-0.018}$	$1.943^{+0.019}_{-0.008}$	$0.640^{+0.012}_{-0.018}$
Percolation results	$0.36673^{+0.00012}_{-0.00010}$	$0.528^{+0.012}_{-0.015}$	$1.975^{+0.010}_{-0.015}$	$0.632^{+0.010}_{-0.015}$
3D Ising Model		0.5187(14)	1.963(7)	0.6294(10)

Table 3.4: Thermal and percolation critical indices for model B, compared to those of the 3D Ising model.

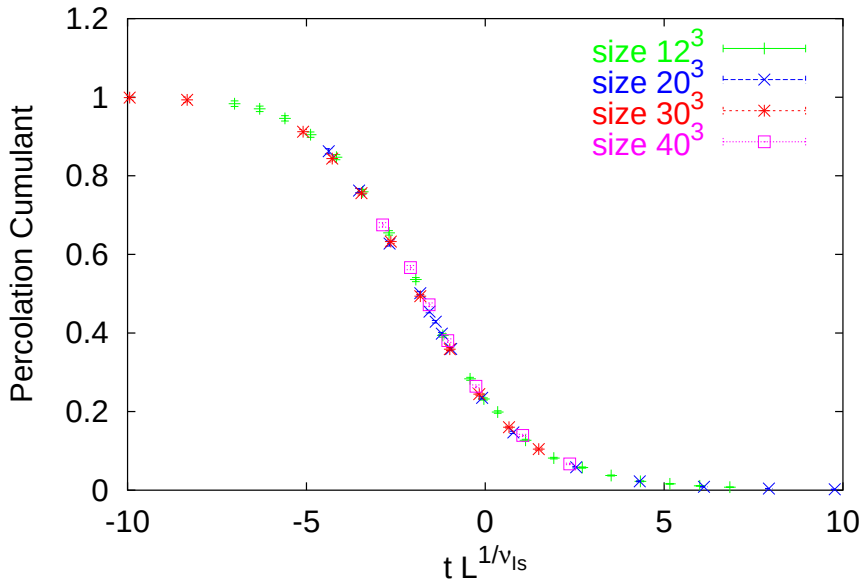

Figure 3.11: Rescaled percolation cumulant curves for model B, using the 3D Ising exponent $\nu_{Is} = 0.6294$. The errors on the data points are smaller than the size of the symbols in the plot.

3.2.3 Model C: Adding Self-Interactions

From what we have seen up to now, it seems to be clear that the correct cluster definition can readily be extended to models including several (ferromagnetic) spin-spin interactions. However, such terms are not the only possible interactions in a model with Z(2) symmetry and a continuous transition. There could be anti-ferromagnetic spin-spin couplings as well as multispin terms, coupling an even number of spins greater than two (four, six, etc.). Moreover, since the spins are continuous, the presence of self-interaction terms is possible, determined by S^2, S^4, etc. The treatment for antiferromagnetic and multispin couplings so far remains an open question. In contrast, self-interactions are not expected to play a role in the cluster building, since such terms do not relate different spins. Therefore, we test a cluster definition ignoring any self-interaction term.

We thus consider in Model C the same interactions as in Model B, plus a term proportional to $J_0 \sum_i S_i^2$. We chose a negative value for the self-interaction coupling J_0; this is the more interesting case since the corresponding interaction tries to resist the approach of the system to the ground state at low temperatures ($\sigma = 1$ everywhere). The ratios of the NN coupling to the others were chosen as $J_{NN} : J_{NTN} : J_{diag} : |J_0| = 6 : 2 : 1 : 2$.

We first verify the viability of the mixed algorithm. The check was successful so that we could apply the algorithm for our purposes. The update consists again in one heat bath sweep and three Wolff flippings. In order to eliminate the correlation of the data we measured our quantities every 40 updates. We collected up to 70000 measurements for temperatures close to criticality.

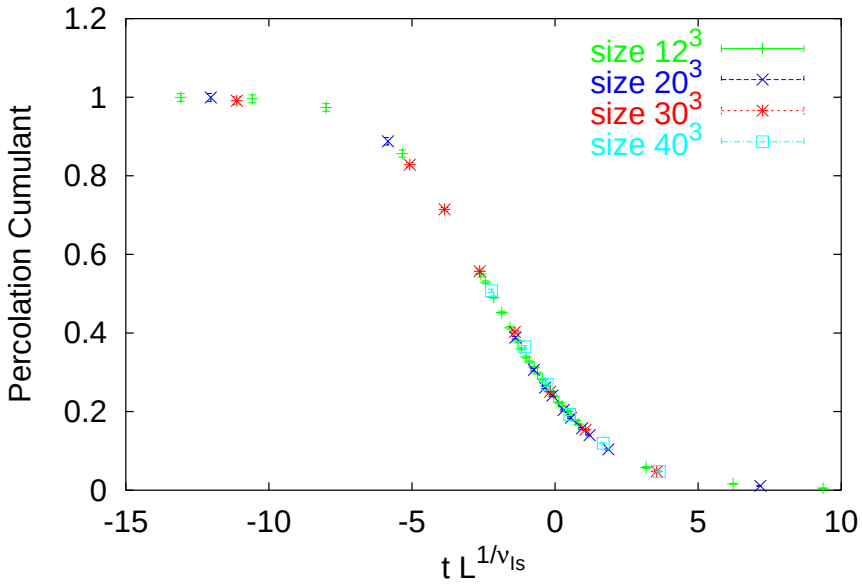

Figure 3.12: Rescaled percolation cumulant curves for model C, using the 3D Ising exponent $\nu_{Is} = 0.6294$. The errors on the data points are smaller than the size of the symbols in the plot.

The critical points were determined by means of the cumulants. In Fig. 3.12 we present the rescaling of the percolation cumulant curves in correspondence of the 3D Ising exponent $\nu_{Is} = 0.6294$. The scaling function can be clearly seen. Successively we have determined the critical exponents (Table 3.5). It is evident that percolation and the thermal transition again fall into the same universality class.

	Critical point	β/ν	γ/ν	ν
Thermal results	$0.3004^{+0.0002}_{-0.0001}$	$0.513^{+0.012}_{-0.010}$	$1.963^{+0.014}_{-0.009}$	$0.626^{+0.011}_{-0.010}$
Percolation results	$0.3005^{+0.0001}_{-0.0001}$	$0.524^{+0.010}_{-0.011}$	$1.975^{+0.008}_{-0.009}$	$0.636^{+0.011}_{-0.017}$
3D Ising Model		0.5187(14)	1.963(7)	0.6294(10)

Table 3.5: Thermal and percolation critical indices for model C, compared to those of the 3D Ising model.

We have shown that the equivalence of cluster percolation and spin ordering in the description of critical behaviour in the continuous spin Ising model can be extended to a rather wide class of theories. In particular, it remains valid also in the presence of more than just nearest neighbour interactions, if ferromagnetic, and of spin distribution functions. Moreover, the introduction of self-energy contributions does not affect the equivalence.

3.3 Cluster Percolation in O(n) Spin Models

An interesting extension of the Coniglio-Klein result concerns the $O(n)$ spin models.

The $O(n)$ spin models with no external magnetic field have the following Hamiltonian:

$$H = -J \sum_{\langle \mathbf{i},\mathbf{j} \rangle} \mathbf{s_i} \mathbf{s_j}, \tag{3.11}$$

where i and j are nearest-neighbour sites on a d-dimensional hypercubic lattice, and $\mathbf{s_i}$ is an n-component unit vector at site i ($J > 0$ is the coupling). The partition function of these models at the temperature T is

$$Z(T) = \int \mathcal{D}[\mathbf{s}] \exp\{\beta \sum_{\langle \mathbf{i},\mathbf{j} \rangle} \mathbf{s_i} \mathbf{s_j}\} \tag{3.12}$$

where $\beta = J/kT$ and the integral is extended over all spin configurations $\{\mathbf{s}\}$ of the system.

In three space dimensions, such models undergo a second order phase transition due to the spontaneous breaking of the continuous rotational symmetry of their Hamiltonian. The $O(n)$ models are very interesting: some physical systems in condensed matter physics are directly associated to them. The three-dimensional $O(3)$ model is the low-temperature effective model for a bidimensional quantum antiferromagnet [48]. The $O(2)$ model in three dimensions is known to be in the same universality class as superfluid ^4He. $O(n)$ models are also very useful to study relativistic field theories. The $O(4)$ model in three dimensions has been conjectured to be in the same universality class as the finite-temperature chiral phase transition of QCD with two flavours massless quarks [49].

Numerical simulations of $O(n)$ models became much quicker and more effective after U. Wolff introduced his Monte Carlo cluster update [39]. We have already described it in the particular case of the Ising model (see Section 3.1). As a matter of fact, the Wolff update was devised for $O(n)$ spin models, of which the Ising model is a special case (for $n = 1$).

The procedure, as we have said, consists in flipping all spins of a cluster which is built in some way. For details of the flipping procedure, see [39]. Here we are interested in the way to build up the clusters. We can split this procedure in two steps:

a) choose a random n-component unit vector $\mathbf{r}$;

b) bind together pairs of nearest-neighbouring sites i, j with the probability

$$p(i,j) = 1 - \exp\{min[0, -2\beta(\mathbf{s_i} \cdot \mathbf{r})(\mathbf{s_j} \cdot \mathbf{r})]\}. \tag{3.13}$$

From this prescription it follows that if the two spins at two nearest-neighbouring sites i and j are such that their projections onto the random vector $\mathbf{r}$ are of opposite signs, they will never belong

to the same cluster ($p(i,j) = 0$). The random vector $\mathbf{r}$, therefore, divides the spin space in two hemispheres, separating the spins which have a positive projection onto it from the ones which have a negative projection. The Wolff clusters are made out of spins which all lie either in the one or in the other hemisphere. In this respect, we can again speak of 'up' and 'down' spins, like for the Ising model. In addition to that, the bond probability is local, since it depends explicitly on the spin vectors $\mathbf{s_i}$ and $\mathbf{s_j}$, and not only on the temperature like the Fortuin-Kasteleyn factor.

The analogies with the Ising model are however clear, motivating the attempt to study the percolation properties of these clusters.

Indeed, for $O(2)$ and $O(3)$, it was analytically proven that the Wolff clusters percolate at the thermal critical point [50, 51]. Nevertheless, in [50, 51] nothing about the relationship between the critical exponents was said.

We have investigated numerically the 3-dimensional $O(2)$ and $O(4)$ models performing computer simulations for several lattice sizes. The Monte Carlo update was performed by the Wolff algorithm. At the end of an iteration, the percolation strength P and the average cluster size S were measured. This has been done for each of the models using two different approaches.

The **first approach** is the traditional one, based on a complete analysis of the lattice configuration. Once we have the configuration we want to analyze, we build Wolff clusters until all spins are set into clusters. We assign to P the value zero if there is no percolating cluster, the ratio between the size of the percolating cluster and the lattice volume otherwise. We calculate S using the standard formula (1.7). We say that a cluster percolates if it spans the lattice from a face to the opposite one in each of the three directions x, y, z. In this approach we have used as usual free boundary conditions.

The **second approach** is based on a single-cluster analysis. Basically one studies the percolation properties of the cluster built during the update procedure. For the cluster building we have considered periodic boundary conditions. Suppose that s_c is the size of the cluster we built. If it percolates, we assign value one to the strength P and zero to the size S; otherwise, we write zero for P and s_c for S. These definitions of P and S look different from the standard definitions we have introduced above, but it is easy to see that they are instead equivalent to them.

In fact, we build the cluster starting from a lattice site taken at random. In this way, the probability that the cluster percolates (expressed by the new P) coincides with the probability that a site taken at random belongs to the percolating cluster (standard definition of P). As far as the average cluster size is concerned, we can repeat the same reasoning: the probability that the cluster we built is a non-percolating cluster of size s_c is just the probability w_{s_c} that a randomly taken lattice site belongs to a non-percolating cluster of size s_c; w_{s_c} is given by

$$w_{s_c} = n_{s_c} s_c \, . \tag{3.14}$$

Because of that, whenever we get a non-vanishing size s_c, such value will be weighted by the probability w_{s_c} in the final average S, which is then given by the following formula:

$$S = \sum_{s_c} w_{s_c} s_c = \sum_{s_c} n_{s_c} {s_c}^2, \tag{3.15}$$

where the sum runs over the non-percolating clusters. We notice that Eq. (3.15) coincides with Eq. (1.7), apart from the denominator $\sum_s n_s\, s$, which is just the density of the sites belonging to finite clusters. Since this term does not contribute to the divergence of the average cluster size, the power law behaviour of the two S's at criticality is identical, so that the critical exponent γ is the same in both cases.

As we have said, in the second approach we select a single cluster at a time from the whole configuration. Because of that we have now some freedom of choosing the definition of percolating cluster, as we do not risk, like in the first approach, to find more spanning structures. We say that the cluster percolates if it connects at least one face with the opposite one.

In this way, also the definitions of percolating clusters are different in the two approaches. This certainly influences the results on finite lattices, but has no effects on the infinite-volume properties we are interested in. In fact, we have seen in Section 1.3.2 that one can have at most a unique spanning cluster above the critical density p_c (in our case below the critical temperature T_c). Exactly at p_c (T_c) there is a finite probability to have more than a spanning cluster. So, the two different definitions of percolating cluster we have adopted can lead to differences between the infinite-volume values *only* at the critical point p_c (T_c). But the critical exponents are, of course, not influenced by that, as they are determined by the behaviour of the percolation variables *near* the critical point, not exactly at p_c (T_c).

The second approach has the advantage that it does not require a procedure to reduce the configuration of the system to a set of clusters; on the other hand, since it gets the information out of a single cluster, it requires a higher number of samples in order to measure the percolation variables with the same accuracy of the first method. Nevertheless, the iterations are faster due to the simpler measurement of observables, and are less correlated than in the first approach, since only a (random) limited region of the lattice is considered in each sample. We find that both methods are efficient, and that it is important to be able to compare results obtained in two such different ways.

We collected up to 150000 measurements for temperatures close to the critical point. We measured our quantities every N updates, with N ranging from 50 for the smaller lattice sizes to 100 for the greater ones: that eliminates the correlation of the percolation data.

Figs. 3.13 and 3.14 show percolation cumulant curves for $O(2)$ and $O(4)$, respectively. The agreement with the physical thresholds (dashed lines) is clear. Successively, we perform the usual scaling tests to check whether the exponents ν_{perc} of the geometrical transitions coincide with the ones of the model, $\nu_{O2} = 0.6723$ and $\nu_{O4} = 0.7479$ respectively, or rather with the 3-dimensional random percolation exponent $\nu_{RP} = 0.8765$. Figs. 3.15 and 3.16 show that, by taking the thermal exponents, the curves fall on top of each other, confirming that $\nu_{perc} = \nu_{therm}$ in both cases.

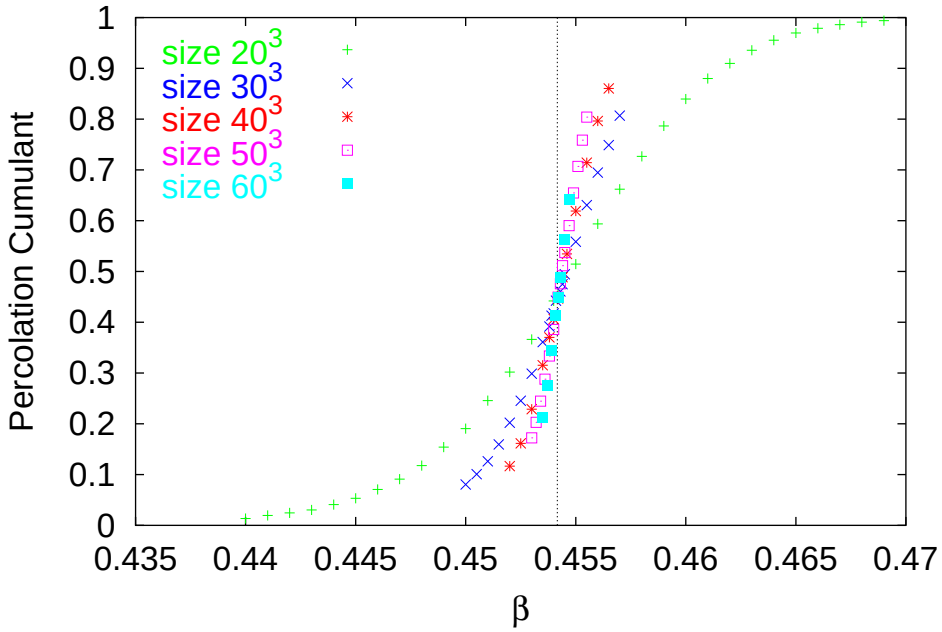

Figure 3.13: Percolation cumulant as function of β for $O(2)$ and five lattice sizes. The dashed line indicates the position of the thermal threshold [52].

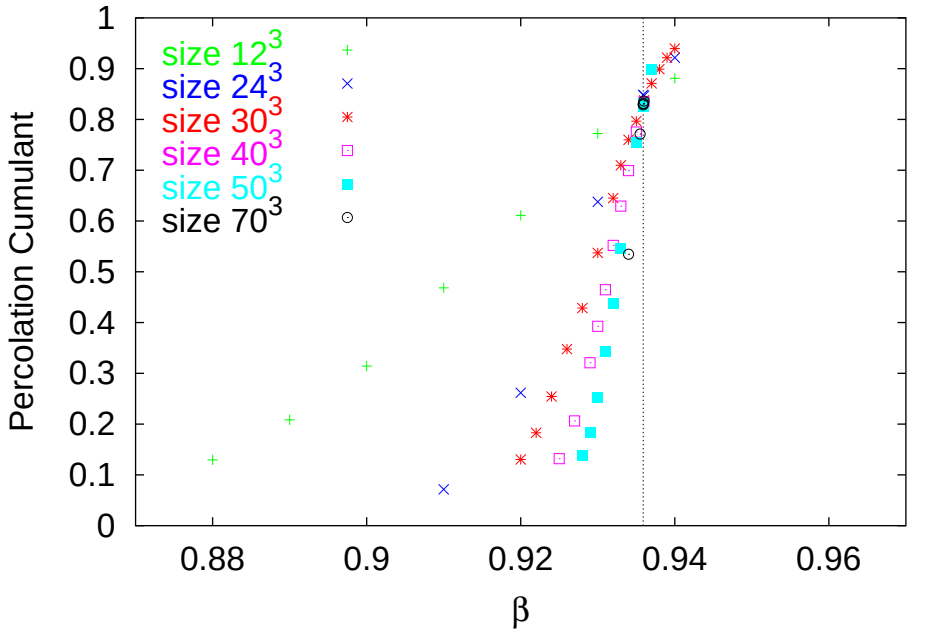

Figure 3.14: Percolation cumulant as function of β for $O(4)$ and six lattice sizes. The dashed line indicates the position of the thermal threshold [53].

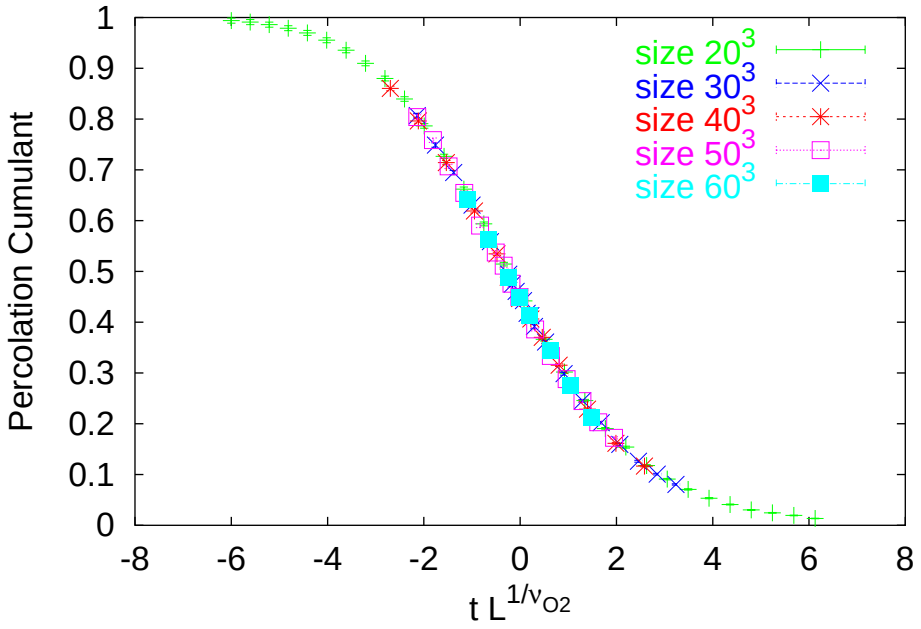

Figure 3.15: Rescaled percolation cumulant for $O(2)$ using $\beta_c = 0.45416$ and the $O(2)$ exponent $\nu_{O2} = 0.6723$. The values of the thermal critical indices are taken from [52]. The errors on the data points are smaller than the size of the symbols in the plot.

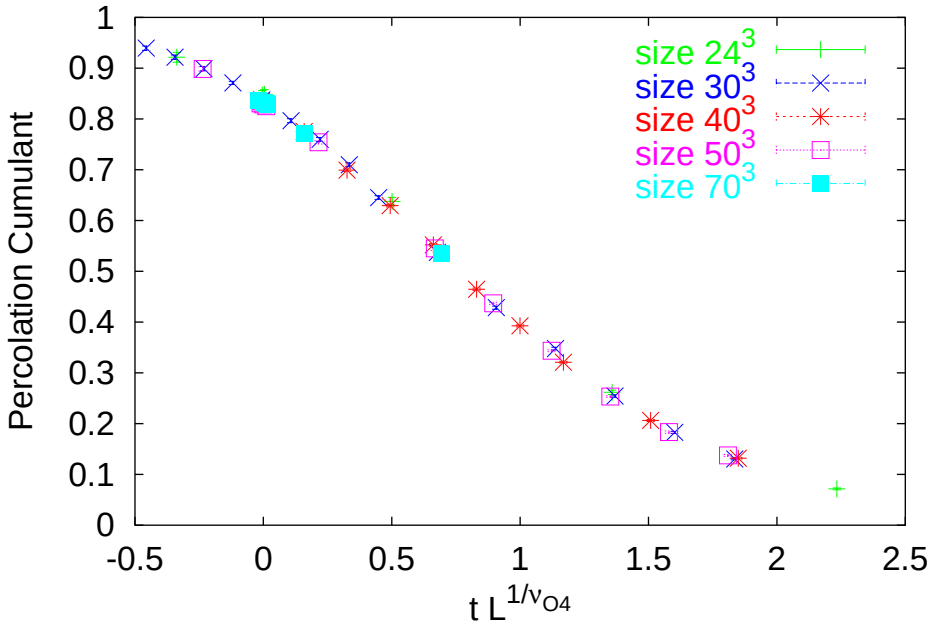

Figure 3.16: Rescaled percolation cumulant for $O(4)$ using $\beta_c = 0.9359$ and the $O(4)$ exponent $\nu_{O4} = 0.7479$. The values of the thermal critical indices are taken from [53] (the threshold) and [54] (the exponent ν_{O4}). The errors on the data points are smaller than the size of the symbols in the plot.

To complete our investigation, we have determined the critical exponents' ratios making use, as usually, of standard finite size scaling techniques. We list all the critical indices relative to the percolation transition for $O(2)$ and $O(4)$ in Tables 3.6 and 3.7, respectively. In the tables we have reported, for comparison, the values of the thermal critical indices. The agreement with the physical values in [52, 53, 54] is good.

	β_c	β/ν	γ/ν	ν
Thermal results [52]	0.454165(4)	0.5189(3)	1.9619(5)	0.6723(3)
Percolation results	0.45418(2)	0.516(5)	1.971(15)	0.670(4)

Table 3.6: Comparison of the thermal and percolation thresholds and exponents for $O(2)$.

	β_c	β/ν	γ/ν	ν
Thermal results	0.93590(5)[53]	0.5129(11)[54]	1.9746(38)[54]	0.7479(90)[54]
Percolation results	0.93595(3)	0.515(5)	1.961(15)	0.751(6)

Table 3.7: Comparison of the thermal and percolation thresholds and exponents for $O(4)$.

So far we have presented the results obtained using the first approach. The results derived using the second approach are essentially the same; besides, we observe an improved quality of the scaling, mainly because of the use of periodic boundary conditions, which reduce considerably the finite size effects.

In particular we show in Figs. 3.17, 3.18 the scaling of P and S at the thermal thresholds reported in [52, 53]. We observe very small finite size effects (lattices of $L \geq 20$ are used in the fits), especially for the $O(2)$ case, which is in contrast to what is observed for thermal observables [55]. The slopes of the straight lines are in agreement with the values of the thermal exponents' ratios β/ν, γ/ν.

In conclusion, we have shown that the spontaneous breaking of the continuous rotational symmetry for the 3-dimensional $O(2)$ and $O(4)$ spin models can be described as percolation of Wolff clusters. In both cases, the number n of components of the spin vectors $\mathbf{s}$ does not seem to play a role; the result is thus likely to be valid for any $O(n)$ model.

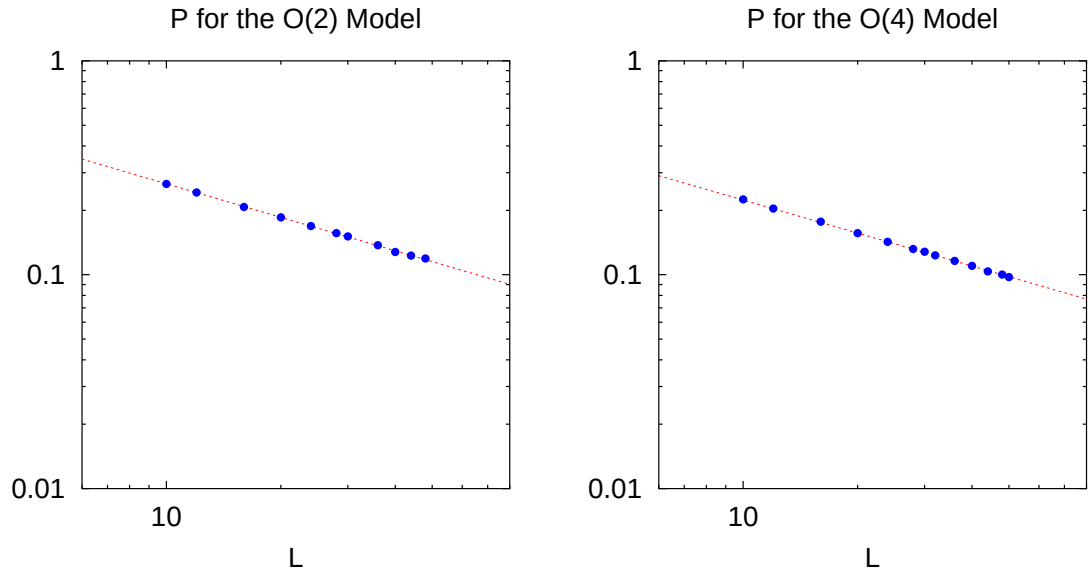

Figure 3.17: Finite size scaling plot at T_c for the percolation observable P as a function of the lattice size L. The slopes in the plots correspond to $\beta/\nu = 0.521(3), 0.513(6)$ respectively for O(2) and O(4). The errors on the data points are smaller than the size of the points in the plot.

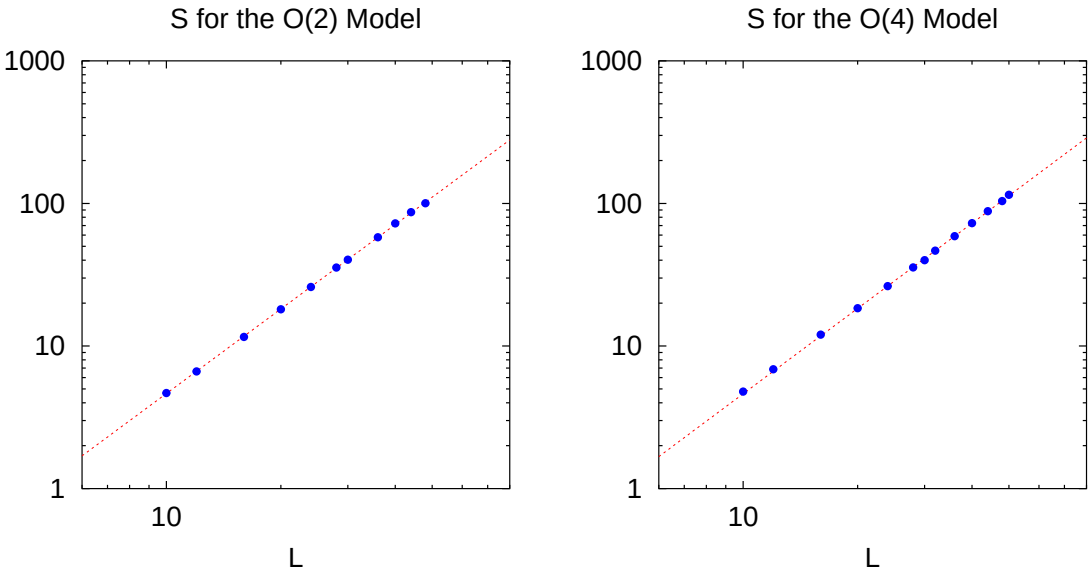

Figure 3.18: Finite size scaling plot at T_c for the percolation observable S as a function of the lattice size L. The slopes in the plots correspond to $\gamma/\nu = 1.97(1), 1.99(1)$ respectively for O(2) and O(4). The two curves look surprisingly similar to each other. The errors on the data points are smaller than the size of the points in the plot.

Chapter 4

Polyakov Loop Percolation in SU(2) Gauge Theory

4.1 Finite Temperature SU(N) on the lattice

Finite temperature Quantum Chromodynamics (QCD) has been extensively simulated on the lattice over the last two decades, in order to test the hypothesis that, at high temperatures and (or) high densities, quark matter should pass from the (confined) hadronic phase to the (deconfined) phase represented by a plasma of quarks and gluons.

QCD, like all theories describing fundamental forces (except gravitation), is a quantum field theory with local gauge invariance. The gauge group which rules this invariance is $SU(3)$: the quarks form a triplet in the fundamental representation of $SU(3)$, and the gluons, which are the carriers of the interaction, form an octet in the adjoint representation.

The non-abelian character of the $SU(3)$ group leads to an important feature that distinguishes QCD from Quantum Electrodynamics (QED), which is ruled by the abelian group $U(1)$: the gluons carry a charge and can interact among each others, in contrast to the photons. Therefore, it makes sense to study systems constitued only by gluons, and to check whether the interaction gives rise to a confinement-deconfinement transition from a phase in which the gluons are bound in glueballs to a phase of free gluons. This simpler situation is described by the so-called *pure gauge* $SU(3)$.

Since any $SU(N)$ group is non abelian, the study of the relative pure gauge theories may be of interest also for $N \neq 3$.

The Lagrangian density of the $SU(N)$ pure gauge theories is

$$\mathcal{L} = -\frac{1}{4} F^a_{\mu\nu}(x)\, F^{a\mu\nu}(x), \tag{4.1}$$

where

$$F^a_{\mu\nu}(x) \equiv \partial_\mu A^a_\nu(x) - \partial_\nu A^a_\mu(x) + g\, f^{abc}\, A^b_\mu(x) A^c_\nu(x). \tag{4.2}$$

Here A^a_μ are the gauge fields ($a = 1, 2, ..., N^2 - 1$), g is the gauge coupling constant and f_{abc} the structure constants of the $SU(N)$ group. The rightmost term of (4.2), present because for the $SU(N)$ group $f_{abc} \neq 0$, is responsible of the gluon-gluon interaction.

The renormalizability of $SU(N)$ gauge theories [56] assures the convergence of perturbative series expansions: QCD was established as theory of the strong interaction after a great deal of perturbative results were confirmed by experiments. However, the important phenomenon of confinement lies well beyond the realm of perturbation theory.

The need of getting predictions from the theory in the non-perturbative domain led to an alternative calculation pattern, the *lattice regularization*, characterized by a discretization of space-time which gets rid automatically of troublesome divergences [57].

With the Lagrangian density (4.1) provided, the formulation of statistical $SU(N)$ theories is, at least in principle, a well-defined problem. We have to calculate the partition function

$$\mathcal{Z}(\beta, V) \;=\; Tr\{e^{-\beta H}\}. \tag{4.3}$$

In the trace we have to sum over all physical states accessible to the system in a spatial volume V; $\beta = 1/T$, where T is the physical temperature and H is the Hamiltonian of the system, which can be expressed by means of $\mathcal{L}$. Once we have $\mathcal{Z}(\beta, V)$, we can proceed to derive all thermodynamic observables. Thus,

$$\epsilon \;=\; -\frac{1}{V}\Big(\frac{\partial\, ln\mathcal{Z}}{\partial\beta}\Big)_V \tag{4.4}$$

is the energy density, and

$$P \;=\; \frac{1}{\beta}\Big(\frac{\partial\, ln\mathcal{Z}}{\partial V}\Big)_\beta \tag{4.5}$$

gives us the pressure.

The lattice formulation of statistical $SU(N)$ is obtained in three steps. First we replace the Hamiltonian form (Eq. (4.3)) of the partition function by the corresponding Euclidean functional integral

$$\mathcal{Z}_E(\beta, V) \;=\; \int\limits_{A_\mu(\beta,\vec{x})=A_\mu(0,\vec{x})} (dA)\, \exp\Big[-\int_V d^3x \int_0^\beta d\tau\, \mathcal{L}(A)\Big]. \tag{4.6}$$

This form involves directly the Lagrangian density and the sum over states in (4.3) is replaced by the integration over the field configurations A. The periodicity condition $A_\mu(\beta, \vec{x}) = A_\mu(0, \vec{x})$ is a consequence of the trace form of Eq. (4.3). The spatial integration of (4.6) is performed over

the whole volume of the system, while in the imaginary time $\tau \equiv ix_0$, the integration runs over a finite slice determined by the temperature. The finite temperature behaviour of the partition function thus becomes a finite size effect in the integration over τ.

Next, the Euclidean $\vec{x} - \tau$ manifold is replaced by a discrete lattice, with N_σ points in each space direction and N_τ points for the τ axis. The lattice spacing is a. The overall space volume becomes $V = (N_\sigma a)^3$, the inverse temperature $\beta^{-1} = N_\tau a$. To ensure the gauge invariance of the formulation, the gauge fields A must be defined on the links connecting each pair of adjacent sites.

In the final step, the integration over the gluon fields is replaced by one over the corresponding gauge group variables, or *link variables*,

$$U_{ij} = \exp\Big[- ig(x_i - x_j)^\mu A_\mu\Big(\frac{x_i + x_j}{2}\Big)\Big], \tag{4.7}$$

with x_i and x_j denoting two adjacent lattice sites, so that U_{ij} is an $SU(N)$ matrix associated to the links between these two sites.

The partition function of finite temperature $SU(N)$ pure gauge theories takes then the form

$$\mathcal{Z}(N_\sigma, N_\tau; g^2) = \int \prod_{links} dU_{ij} \, \exp[-S(U)], \tag{4.8}$$

where $S(U)$ is the *Wilson action*

$$S(U) = \frac{2N}{g^2} \sum_{plaq} \Big(1 - \frac{1}{N} Re\, Tr\, UUUU\Big). \tag{4.9}$$

The sum is over all the smallest closed paths of the lattice (*plaquettes*), which are formed by four links; $UUUU$ is the product of the link variables corresponding to each side of a plaquette.

By letting the lattice spacing a go to zero, one recovers the continuum limit (4.6). This assures that, for a small enough, the lattice regularization does not influence the physical observables and that we can rely on the results derived by this approach.

4.2 Z(N) Symmetry and Deconfinement

Pure $SU(N)$ gauge theories have a global symmetry, resulting from the periodicity of the gauge fields in the temperature direction, that rules the behaviour of the system at finite temperatures. Gauge transformations which are compatible with the periodicity condition need only be periodic up to an element z of the center $Z(N)$ of the gauge group $SU(N)$. Thus a gauge transformation must obey:

$$A(\vec{x},0) \;=\; zA(\vec{x},\beta), \quad for\ all\ \vec{x}, \tag{4.10}$$

where $A(\vec{x},\tau)$ is the $SU(N)$ matrix associated to the gauge field at the point $(\vec{x},\tau)$ and $z \in Z(N)$. The n-th element of $Z(N)$ is given as $\exp(2\pi in/N)$ $(n = 0, ..., N-1)$. It is easy to see that, under (4.10), the action (4.9) remains unchanged. In contrast, the *Polyakov loop*,

$$L_{\vec{x}} \;=\; \frac{1}{N} Tr \prod_{t=1}^{N_\tau} U_{\vec{x};t,t+1}, \tag{4.11}$$

consisting of the product of all the U's in the temperature direction taken at a given spatial site $\vec{x}$, transforms non-trivially under this transformation,

$$L_{\vec{x}} \;\rightarrow\; z\, L_{\vec{x}}. \tag{4.12}$$

The same relation is valid if we take the average $L = \langle L_{\vec{x}} \rangle$ over the lattice and over configurations. L is an indicator of the state in which the system finds itself. It is clear that, if $L \neq 0$, the transformation (4.10) will *not* leave invariant the value of L, as it would happen if $L = 0$. That means that the state of the system may spontaneously break the global $Z(N)$ symmetry, just as the ordered phase of the Ising model breaks the global $Z(2)$ symmetry of its Hamiltonian.

The quantity L is then the *order parameter* of the phase transition associated to the spontaneous breaking of the $Z(N)$ symmetry. Is this transition somehow related to deconfinement?

The state of a gluons system can be probed qualitativey by a heavy test quark. The free energy F of this test quark should be infinite in the confinement phase, but finite in the deconfinement phase. It turns out that such free energy is related to the lattice average of the Polyakov loop by the following expression

$$L \;\propto\; e^{-\beta F}. \tag{4.13}$$

In the confinement regime, $F = \infty$ and Eq. (4.13) implies $L = 0$. If the gluons are free, F is finite and, consequently, $L \neq 0$. The (eventual) transition from the confined to the deconfined state of the $SU(N)$ gauge system is thus characterized by the spontaneous breaking of the global center $Z(N)$ symmetry.

Lattice studies have shown that this phase transition indeed takes place. The first computer simulations of finite temperature lattice gauge theories were performed in the early 80's and concerned the $SU(2)$ theory [47], basically because it is the simplest one and the relative simulations are not so lengthy as the $SU(3)$ simulations.

Fig. 4.1 shows $SU(2)$ data relative to the Polyakov loop, from which the typical behaviour of a second order phase transition is clearly visible.

In spite of their higher complexity, $SU(3)$ simulations could be performed shortly after the $SU(2)$ ones. However, it took a while before one could be sure to understand what was happening there. Now it is well established that $SU(3)$ gauge theory undergoes a (weak) first order confinement-deconfinement phase transition (Fig. 4.2).

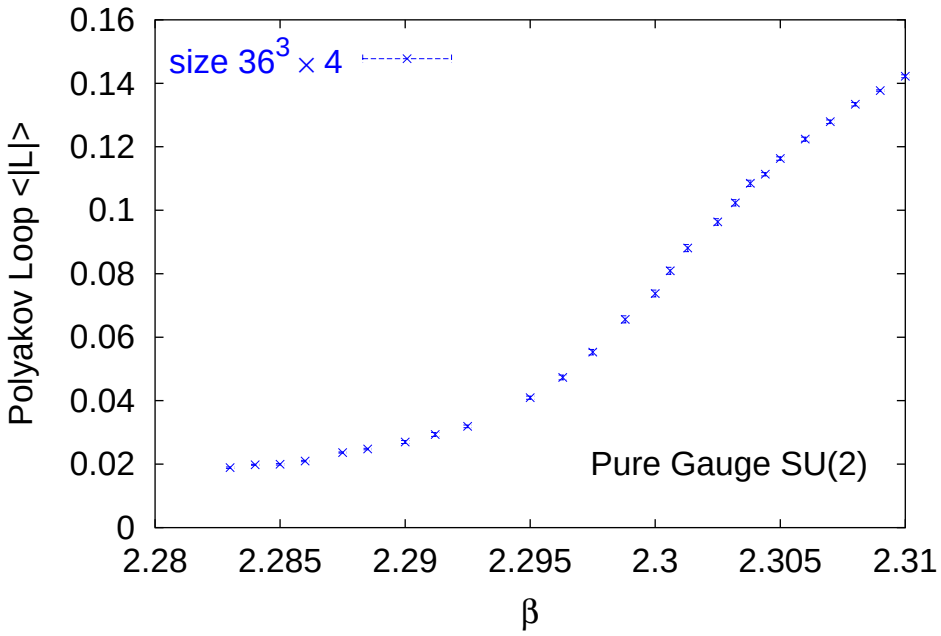

Figure 4.1: Lattice average of the Polyakov loop as a function of the coupling $\beta = 4/g^2$ for pure gauge $SU(2)$ on a $N_\sigma^3 \times N_\tau$ lattice with $N_\sigma = 36$ and $N_\tau = 4$.

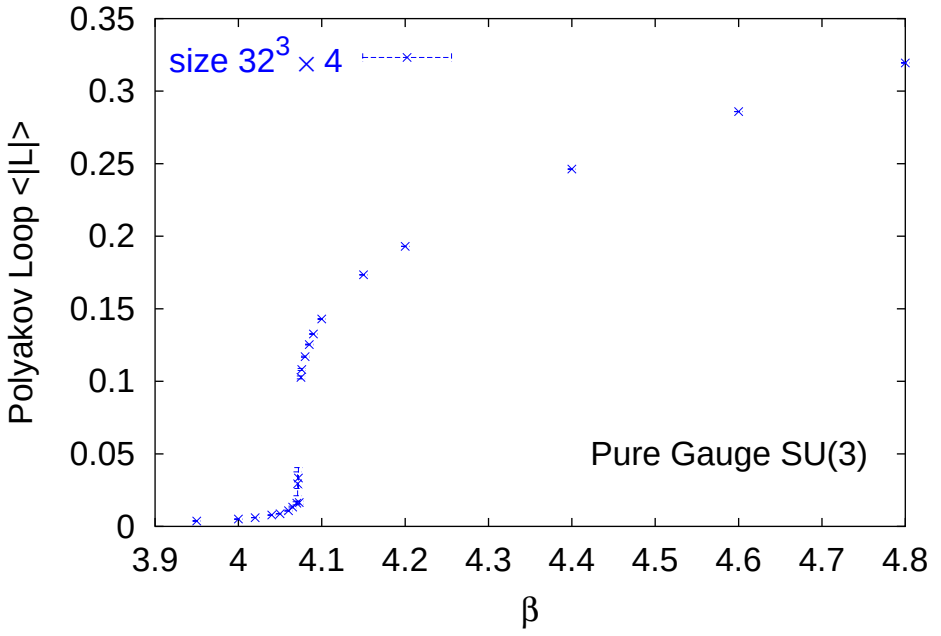

Figure 4.2: Polyakov loop as a function of the coupling $\beta = 6/g^2$ for pure gauge $SU(3)$ on a $32^3 \times 4$ lattice; the data points are taken from [58].

4.3 SU(N) Gauge Theories vs Z(N) Spin Models

In the previous section we have stressed the key role played by the $Z(N)$ symmetry in the confinement-deconfinement mechanism of $SU(N)$ gauge theories. It is easy to check that any $Z(N)$ rotation leaves invariant the product of link variables around each closed path which includes spatial links (*Wilson loops*). However, we have seen that the topologically nontrivial Polyakov loop $L_{\vec{x}}$ changes after such rotations (see Eq. (4.12)). If we consider that, from Eq. (4.11), $L_{\vec{x}}$ is determined *only* by the links in the imaginary time/temperature direction, we realize that the $Z(N)$ symmetry introduces a distinction between spatial links and time links: the latter ones alone seem to have the control of the phase transition.

It is then natural to try to get rid of the 'irrelevant' degrees of freedom represented by the spatial links and to express the $SU(N)$ action in terms only of the order parameter field $L_{\vec{x}}$. This can be achieved by integrating out the spatial gauge fields; the resulting effective theory is simpler than the original model and could facilitate the investigation of the confinement-deconfinement phase transition.

Svetitsky and Yaffe [9] presented a number of arguments that lead to some interesting conclusions about the properties of such $SU(N)$ effective theories. Their arguments are essentially based on dynamical considerations and simple renormalization group ideas and allow to deduce, among other things, the order of the phase transition and, in case of a continuous transition, the exponents which characterize the critical fluctuations.

The main point of [9] is the hypothesis that, integrating out all degrees of freedom except the Polyakov loops, one yields an effective theory with short range interactions, which is invariant under the center $Z(N)$ symmetry. In case of a continuous transition, one could in principle locate the renormalization fixed point which governs the relative critical behaviour. If it happens that, in the space of d-dimensional theories with short range interactions invariant under the center symmetry, there exists only a single fixed point, then the critical behaviour of the original $(d+1)$-dimensional finite-temperature $SU(N)$ gauge theory *will be the same as that of simple d-dimensional spin models invariant under the same global symmetry $Z(N)$*.

In many cases theories, related by the same symmetry, are indeed associated to a single fixed point: this implies that results for the critical behaviour of simple spin models may be used to predict the critical behaviour in finite-temperature gauge theories.

It is, for example, the case of the $Z(2)$ symmetry, for which only one fixed point is known. Consequently, since $SU(2)$ pure gauge theory undergoes a continuous transition, its critical exponents should fall in the universality class of the $Z(2)$ spin model, which is the Ising model. Lattice studies have provided strong evidence that the conjecture is indeed true [10].

As a counter-example, in the space of three-dimensional $Z(3)$ symmetric theories, no stable renormalization group fixed point is known. That led the authors of [9] to conjecture that $(3+1)$-d $SU(3)$ pure gauge theory undergoes a first order phase transition, as it was successively confirmed by lattice simulations (see Section 4.2).

4.4 Polyakov Loop Percolation

$Z(N)$ spin models have been extensively investigated, both analytically and numerically. It is natural to check to which extent the analogy between such models and $SU(N)$ gauge theories is valid.

In particular, we know that the critical behaviour of the Ising model can be equivalently described as percolation of well defined clusters of like-sign spins (see Chapter 2). It is thus spontaneous to ask ourselves whether it is possible to find a description of critical behaviour in terms of percolation also for the deconfinement transition in $SU(2)$ gauge theory.

This could provide a suggestive view of the confinement-deconfinement mechanism. If we take a typical SU(2) configuration at a certain temperature, there will be areas where the Polyakov loop L takes negative values, and areas where L takes positive values. Both the positive and the negative 'islands' can be seen as local regions of deconfinement. But as long as there are finite islands of both signs, deconfinement remains a local phenomenon and the whole system is in the confined phase. When one of this islands percolates, that is it becomes infinite, then we can talk of deconfinement as a global phase of the system.

The rest of this chapter is devoted to find a solution to this problem. The main difficulty is the fact that the $SU(2)$ Lagrangian is not directly a function of the Polyakov loop, due to the presence of the spatial gauge fields. Moreover, if we integrate out the spatial link variables, we yield an effective theory that contains non trivial combination of operators, which cannot in general be replaced by suitable combinations of Polyakov loops.

Therefore it is not clear how one can extract the expression of the bond probability which is necessary to build the clusters like in the Ising model.

The only way to face the problem is to try to approximate $SU(2)$ by means of effective theories which are easy to handle. This will allow us to exploit the percolation pictures for general spin models presented in Chapter 3.

We propose two alternative procedures to look for a suitable definition of cluster building.

The *first approach* adopts a Polyakov loop effective theory derived by means of series expansions of the $SU(2)$ partition function in the strong coupling limit.

The *second approach* searches for simple Ising-like spin models which approximate the Ising-projected Polyakov loop configurations and, even if it is more involved than the first one, it can also be applied in a case which approaches the weak coupling region.

4.5 First Approach: Strong Coupling Expansions

4.5.1 The Green-Karsch Effective Theory

One of the most successful techniques adopted to deduce results from the lattice formulation of gauge theories is the so-called *strong coupling expansion*, which consists in expanding quantities like the action, the partition function, etc., in powers of the inverse coupling $1/g^2$. This procedure, analogous as the well known high-temperature expansions in statistical physics, allows to obtain interesting information about the system. It was by means of analyses of the strong coupling limit that Polyakov [59] and Susskind [60] could show for the first time that QCD may lose its confining property, if the temperature is sufficiently high.

We present here a strong coupling expansion of $SU(N)$ gauge theories derived by Green and Karsch [11]. Their aim was to perform a mean field analysis of the $SU(N)$ deconfinement transition in the presence of dynamical quarks, but we will limit ourselves to introduce the expressions relative to the pure gauge sector, in particular to pure gauge $SU(2)$, which is the one we are interested in.

We start from the formula (4.8) for the lattice action. We can write

$$\begin{aligned} S(U) &= \sum_P S_P(U) \\ S_P(U) &= \frac{4}{g^2}\Big(1 - \frac{1}{2} Re\, Tr\, UUUU\Big) \end{aligned} \tag{4.14}$$

where the action $S(U)$ is divided in the contributions $S_P(U)$ coming from each plaquette P. $S_P(U)$ can be expanded [61] in terms of the characters χ_r of the $SU(2)$ group (r is an integer which indicates the representation of the group)

$$e^{-S_P} = \mathcal{Z}_0\Big(\frac{1}{g^2}\Big)\Big[1 + \sum_r d_r z_r\Big(\frac{1}{g^2}\Big)\chi_r(U_P)\Big]. \tag{4.15}$$

In (4.15) $d_r = r + 1$, $z_r(1/g^2) = I_{r+1}(4/g^2)/I_1(4/g^2)$ and $\mathcal{Z}_0 = g^2 I_1(4/g^2)/2$, where the I_r are the modified Bessel functions.

Next, we remark that we can neglect all spacelike plaquettes P_s by setting $U_{P_s} = 1$ without affecting appreciably the critical behaviour of the system, as long as the coupling $\beta = 4/g^2$ is small. The validity of this approximation, which corresponds to dropping the magnetic term in the hamiltonian of the theory, relies on the fact that spacelike plaquettes tend to decrease the string tension (see [61]). Hence if a phase transition is found in the strongly coupled theory, there is almost certainly one in the full theory.

For little values of β we can thus write the $SU(2)$ partition function

$$\mathcal{Z}_{eff} = \int [dU] \prod_{P_t}\Big[1 + \sum_r d_r z_r\Big(\frac{1}{g^2}\Big)\chi_r(U_{P_t})\Big], \tag{4.16}$$

where the product is exclusively over the timelike plaquettes P_t. Integrating over the spacelike links and grouping the timelike links associated to the same spatial site $\mathbf{x}$, we easily get

$$\mathcal{Z}_{eff} \;=\; \int \prod_{\mathbf{x}} dW_{\mathbf{x}} \prod_{\mathbf{x},\mathbf{e}} \Big[1 + \sum_r z_r^{N_\tau}\Big(\frac{1}{g^2}\Big)\chi_r(W_{\mathbf{x}})\chi_r(W^\dagger_{\mathbf{x}+\mathbf{e}})\Big]. \tag{4.17}$$

In the expression above $\{\mathbf{x},\mathbf{e}\}$ indicates a link, N_τ is the number of lattice spacings in the temperature direction and $W_{\mathbf{x}}$ the Wilson line variable

$$W_{\mathbf{x}} \;=\; \prod_{t=1}^{N_\tau} U_{\mathbf{x};t,t+1}. \tag{4.18}$$

We stress that the the original $(d+1)$-dimensional lattice has now become a simple d-dimensional lattice; the first product in Eq. (4.17) runs over its sites, the second one over its links.

If β is small enough, we can keep only the fundamental $r = 1$ term of the expansion, and we finally get

$$\mathcal{Z}_{eff} \;\approx\; \int \prod_{\mathbf{x}} dW_{\mathbf{x}} \, \exp\Big[\beta' \sum_{ij} L_i L_j\Big], \tag{4.19}$$

with $\beta' = 4z_1^{N_\tau}$ and L_i the value of the Polyakov loop at the site i (see Eq. (4.11)); the sum is over nearest neighbours. For β small,

$$z_1\Big(\frac{1}{g^2}\Big) \;=\; \frac{I_2\big(\frac{4}{g^2}\big)}{I_1\big(\frac{4}{g^2}\big)} \;\approx\; \frac{1}{g^2} \;=\; \frac{\beta}{4}. \tag{4.20}$$

The final expression for the coupling β' of the effective theory is then

$$\beta' \;=\; 4\Big(\frac{\beta}{4}\Big)^{N_\tau}. \tag{4.21}$$

The partition function $\mathcal{Z}_{eff}$ of Eq. (4.19) looks very much like the one of a spin model with simple nearest-neighbour interactions, with the Polyakov loop playing the role of the spin variable. There is, however, an essential difference: the integration variables in $\mathcal{Z}_{eff}$ are not the Polyakov loops $L_{\mathbf{x}}$, but the Wilson line operators $W_{\mathbf{x}}$, which are $SU(2)$ matrices. We know that

$$L_{\mathbf{x}} \;=\; \frac{1}{2} Tr\, W_{\mathbf{x}}, \tag{4.22}$$

but it is not clear whether we can rewrite the sum in Eq. (4.19) as a sum over Polyakov loops *only*.

The properties of the $SU(2)$ group may help us to solve the problem. If U is an $SU(2)$ matrix, we can use a parametrization in terms of an angle ϕ and a 3-dimensional unit vector $\vec{n}$:

$$U \;=\; e^{i\phi\vec{n}\cdot\vec{\tau}/2} \;=\; \Big(\cos\frac{\phi}{2}\Big)\mathbf{1} \;+\; i\Big(\sin\frac{\phi}{2}\Big)\,\vec{n}\cdot\vec{\tau}, \qquad 0 \le \phi < 2\pi,\ |\vec{n}| = 1. \tag{4.23}$$

In (4.23), $\vec{\tau}$ are the Pauli matrices. According to Eq. (4.23), one gets

$$Tr\,U \;=\; 2\,\cos\left(\frac{\phi}{2}\right) \tag{4.24}$$

So, the trace of U depends only on the angle ϕ. With this parametrization, the integral over $SU(2)$ matrices can be written as

$$dU \;=\; \frac{1}{4\pi^2}\,d\phi\,d\Omega(\vec{n})\left(\sin\,\frac{\phi}{2}\right)^2, \tag{4.25}$$

where $d\Omega(\vec{n})$ is the measure relative to the angles of $\vec{n}$. Using Eqs. (4.22), (4.24) and (4.25), we can express $\mathcal{Z}_{eff}$ in the following way

$$\mathcal{Z}_{eff} \;\approx\; \int \prod_{\mathbf{x}} \frac{1}{4\pi^2}\,d\phi_{\mathbf{x}}\,d\Omega(\vec{n}_{\mathbf{x}})\left(\sin\,\frac{\phi_{\mathbf{x}}}{2}\right)^2 \exp\left[\beta' \sum_{ij} \cos\left(\frac{\phi_i}{2}\right)\,\cos\left(\frac{\phi_j}{2}\right)\right], \tag{4.26}$$

The exponential of Eq. (4.26) is only a function of the angles ϕ_i associated to the Wilson line operators. The angles of $d\Omega(\vec{n})$ can thus be integrated out; since $L_i = \cos(\phi_i/2)$ and $\sin(\phi_{\mathbf{x}}/2) = \sqrt{1 - {L_{\mathbf{x}}}^2}$, we reach the final expression

$$\mathcal{Z}_{eff} \;\approx\; \int \prod_{\mathbf{x}} dL_{\mathbf{x}}\,\sqrt{1 - L_{\mathbf{x}}^2}\,\exp\left[\beta' \sum_{ij} L_i L_j\right], \tag{4.27}$$

in which we have neglected the irrelevant constant factor due to the integration over $d\Omega(\vec{n})_{\mathbf{x}}$.

We stress that, to derive Eq. (4.27), we made use of two approximations. We have neglected the spacelike plaquettes and we have truncated the expansion of (4.17) to the first term. Both approximations rely on the fact that the coupling β_c, at which the transition occurs, is small enough. Since β_c shifts to higher values the bigger the number of lattice spacings in the time direction, the assumptions are valid only for small values of N_τ. Green and Karsch showed that the mean field analysis of the effective theory of Eq. (4.19) gives results which are compatible with $SU(2)$ lattice simulations for $N_\tau = 1, 2$ [11]. We decided to concentrate ourselves to the more interesting case, i. e. $N_\tau = 2$.

Eq. (4.27) is exactly the partition function of one of the continuous spin Ising models we have studied in Section 3.1, namely the model whose spin amplitudes $\{\sigma\}$ are distributed according to Eq. (3.8). From Section 3.1 we know that the critical behaviour of the continuous Ising models has an equivalent percolation picture; the clusters are formed by binding nearest neighbouring spins of the same sign with the probability (3.4). We have also seen that the distribution (3.8) does not play a role in the cluster definition.

Assuming that, for $N_\tau = 2$, the Polyakov loop configurations of $SU(2)$ are ruled by the partition function (4.27), it is natural to test the same definition of clusters of the continuous Ising model. In our case, the clusters will be then formed by like-signed nearest neighbouring Polyakov loops, bound with the probability

$$p(i,j) = 1 - \exp(-2\beta'\,L_i\,L_j). \tag{4.28}$$

For $N_\tau = 2$, from Eq. (4.21) we get $\beta' = \beta^2/4$, so that

$$p(i,j) = 1 - \exp\Big(- \frac{\beta^2}{2} L_i \, L_j \Big). \tag{4.29}$$

With Eq. (4.29), the Polyakov loop percolation problem is fully defined. We point out that the strong coupling expansion we have shown is independent on the number of space dimensions of the system, as long as the corresponding values of the critical coupling β_c remain small. Because of that, we decided to investigate $SU(2)$ both in $(2+1)$ and in $(3+1)$ dimensions, to test our cluster definition in two different cases.

4.5.2 Numerical Results for (2+1)-d SU(2)

Our analysis is based on four sets of data on $N_\sigma^2 \times 2$ lattices, with N_σ=64, 96, 128 and 160. The Monte Carlo update consists of one heat bath and two overrelaxation steps. For the $64^2 \times 2$ and $96^2 \times 2$ lattices we evaluated configurations every six updates, for $128^2 \times 2$ and $160^2 \times 2$ every eight updates, measuring in each case the percolation strength P and the average cluster size S. The percolation variables are essentially uncorrelated.

A first scan for values $3.1 < \beta < 3.5$ leads to the behaviour of S shown in Fig. 4.3. It is seen that S peaks slightly below β_c; with increasing N_σ, the peak moves towards β_c. Next,

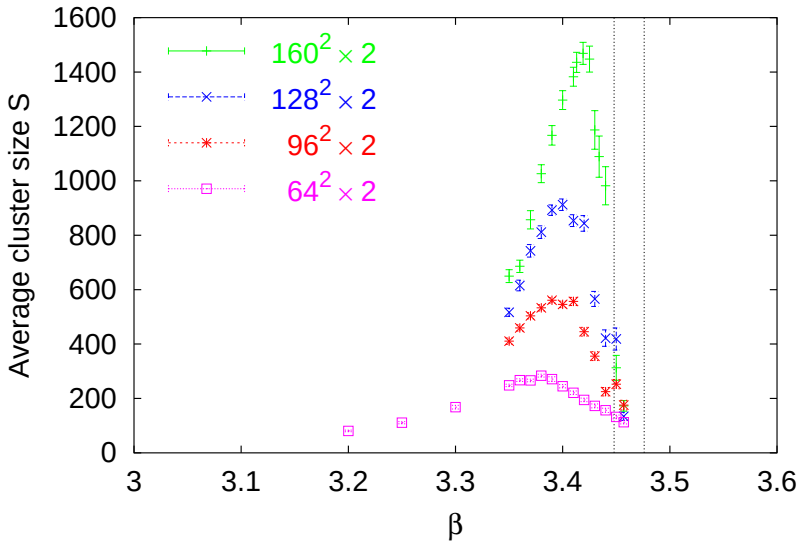

Figure 4.3: $(2+1)$-d $SU(2)$, $N_\tau = 2$. Average cluster size S as function of β for four lattice sizes. The curves peak clearly near the thermal threshold, represented by the dashed lines (within one standard deviation), and tend to approach it the larger the size is.

we carried out high-statistics simulations in a narrower range $3.410 < \beta < 3.457$ around the transition. In general, we performed between 30000 and 55000 measurements per β value, with the higher number taken in the region of the interval closest to the eventual critical point. The high density of points near the threshold allows to determine quite precisely the critical indices after the usual finite size scaling analysis that we have adopted many times in this work.

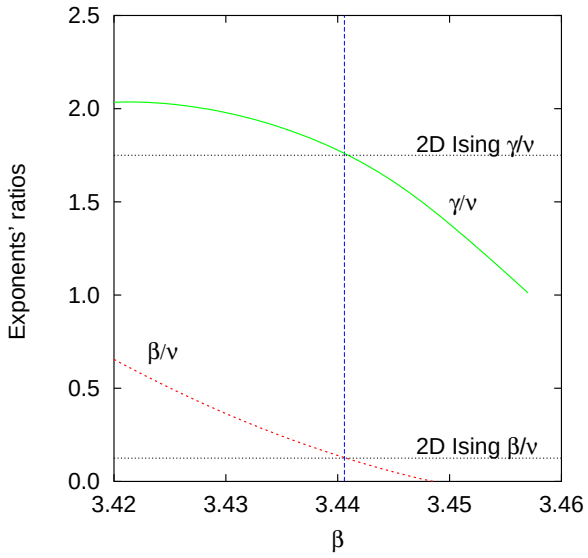

Figure 4.4: $(2+1)$-d $SU(2)$, $N_\tau = 2$. Critical exponents' ratios derived by the slope of finite size scaling fits for P (red line) and S (green line), plotted as a function of the coupling β. The blue line marks the point at which the χ^2 is minimal. The corresponding values of the critical exponents' ratios β/ν and γ/ν (vertical axis in the figure), are in good accord with the 2D Ising values, represented by the horizontal dashed lines.

In Fig. 4.4 we present the variation with β of the values of the exponents' ratios obtained by log-log finite size scaling fits for P and S. The β value corresponding to the best χ^2 is indicated by the vertical line in the figure. The values of β/ν and γ/ν around that point are, within errors, in the universality class of the 2D Ising model. The final results are reported in Table 4.1.

	Critical point	β/ν	γ/ν	ν
Percolation results	$3.443^{+0.001}_{-0.001}$	$0.128^{+0.003}_{-0.005}$	$1.752^{+0.006}_{-0.008}$	$0.98^{+0.07}_{-0.04}$
Thermal results	$3.464^{+0.012}_{-0.016}$	$1/8 = 0.125$	$7/4 = 1.75$	1

Table 4.1: Thermal and percolation critical indices for $(2+1)$-d $SU(2)$, $N_\tau = 2$. As exponents for the thermal transition we adopted the exact 2D Ising exponents, the value of the threshold is taken from [62].

The critical values of the coupling for the thermal and the geometric transition are very close, although they do not overlap within one standard deviation. In view of the inevitable approximations involved by our procedure, small deviations are not unexpected. However, the fact that the critical percolation exponents agree with the Ising values and not with the 2D random percolation ones shows clearly that our clusters are, with good approximation, the physical 'droplets' of the system.

4.5.3 Numerical Results for (3+1)-d SU(2)

As finite temperature $SU(2)$ in $(3+1)$ dimensions is more interesting than in $(2+1)$, because it describes a system in the 'real' 3-dimensional space, we carried on a complete study of the model, analysing both the thermal and the geometrical transition.

We performed four sets of simulations in correspondence to the following lattice sizes: $16^3 \times 2$, $24^3 \times 2$, $30^3 \times 2$, $40^3 \times 2$. The Monte Carlo update is the same we have used in the previous case, i. e. it alternates heat bath and overrelaxation moves, in the ratio $1:2$. We evaluated configurations every ten updates for each lattice size and value of the coupling β. The percolation data are uncorrelated; the thermal variables instead show some important correlation (the autocorrelation time τ is about 10 for the magnetization on the $40^3 \times 2$ lattice near criticality). The number of measurements varies from 10000 to 80000. We used the density of states method (DSM) [45] to interpolate our data. Fig. 4.5 shows the results of the interpolation for the physical susceptibility

$$\chi = V\ (\langle L^2 \rangle - \langle L \rangle^2), \tag{4.30}$$

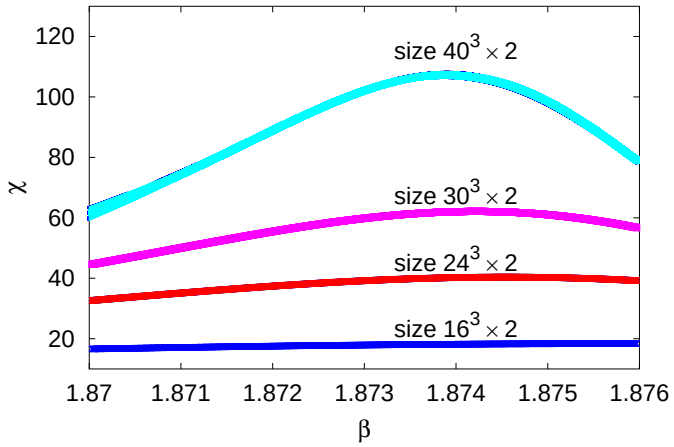

Figure 4.5: $(3+1)$-d $SU(2)$, $N_\tau = 2$. Physical susceptibility χ as function of β for four lattice sizes. For each curve we got 4000 interpolation points.

where L is, as usual, the lattice average of the Polyakov loop and V the spatial lattice volume.

To find the thermal threshold we used the Binder cumulant[†]

$$g_r = 3 - \frac{\langle L^4 \rangle}{\langle L^2 \rangle^2} \,. \tag{4.31}$$

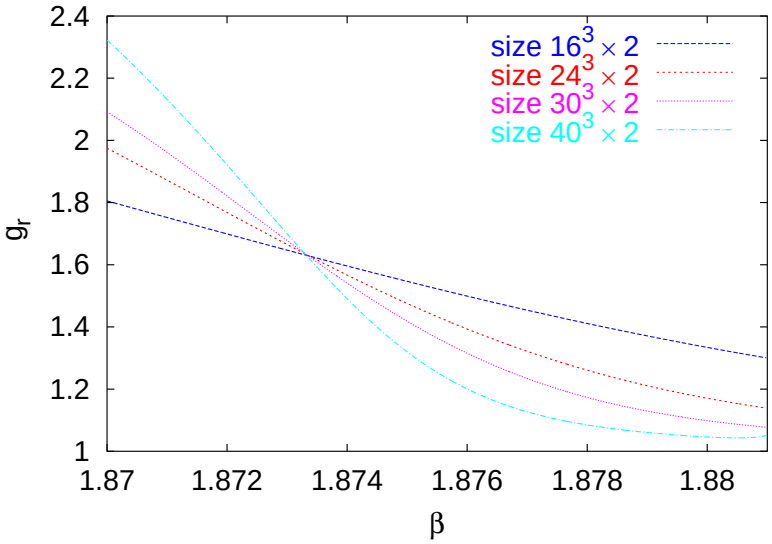

Figure 4.6: Binder cumulant as function of β for $(3+1)$-d $SU(2)$, $N_\tau = 2$.

We put the interpolated curves in Fig. 4.6. They clearly cross at the same point, around $\beta = 1.8734$, which gives a good idea of where the thermal transition takes place.

To determine precisely this point we used the χ^2 method [10]. We applied this method to the absolute value of the lattice average of the Polyakov loop $|L|$, to the physical susceptibility χ and to the derivative of the Binder cumulant with respect to β. In this way we could also evaluate the critical exponents ratios β/ν, γ/ν and $1/\nu$. Both the threshold and the exponents' ratios are shown in Table 4.2.

We began our percolation studies performing some test runs for different lattice sizes to check the behaviour of our percolation variables around criticality. Fig. 4.7 shows the behaviour of the average cluster size S for three lattice sizes, $24^3 \times 2$, $30^3 \times 2$, and $40^3 \times 2$ respectively.

To get the critical point of the geometrical transition we made use of the percolation cumulant. In Fig. 4.8 one can see the percolation cumulant as a function of β for $24^3 \times 2$, $30^3 \times 2$ and $40^3 \times 2$. The lines cross at the same point within the errors and that restricts further the β range for the critical threshold.

[†]See footnote at page 52.

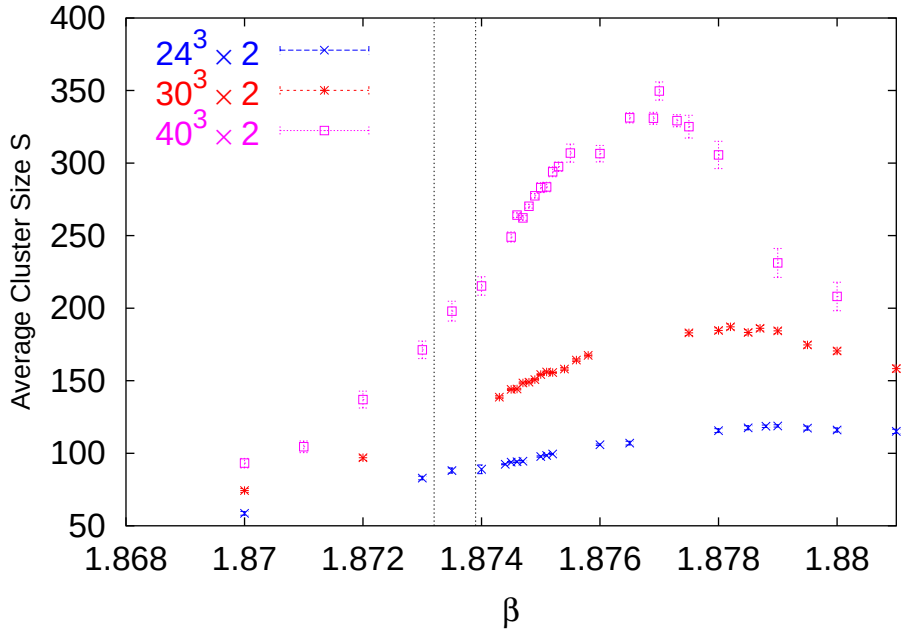

Figure 4.7: $(3+1)$-d $SU(2)$, $N_\tau = 2$. Average cluster size as function of β near the thermal threshold β_c, indicated within one standard deviation by the dashed lines.

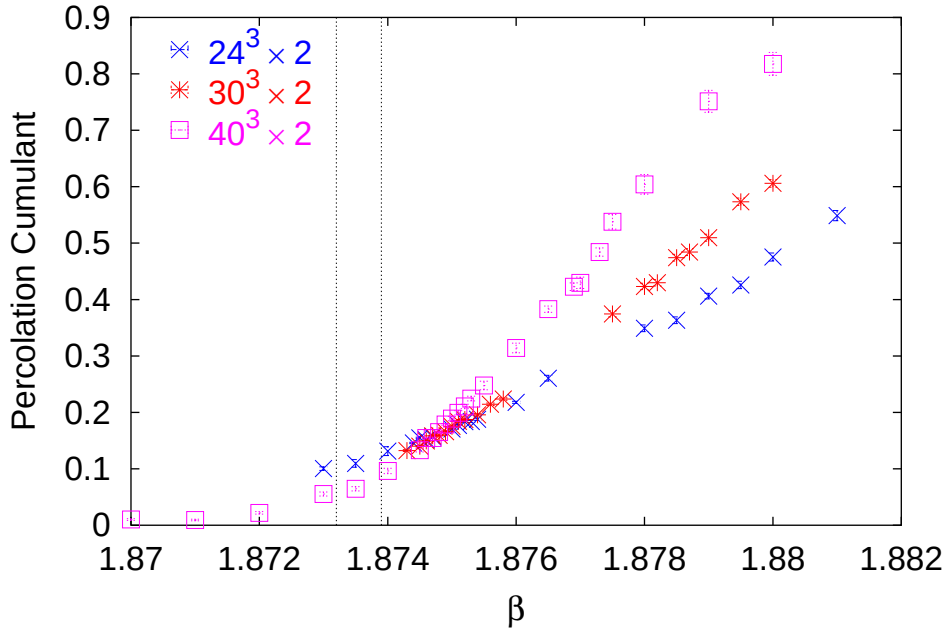

Figure 4.8: $(3+1)$-d $SU(2)$, $N_\tau = 2$. Percolation cumulant as function of β for three lattice sizes. The curves cross close to the thermal threshold (dashed lines).

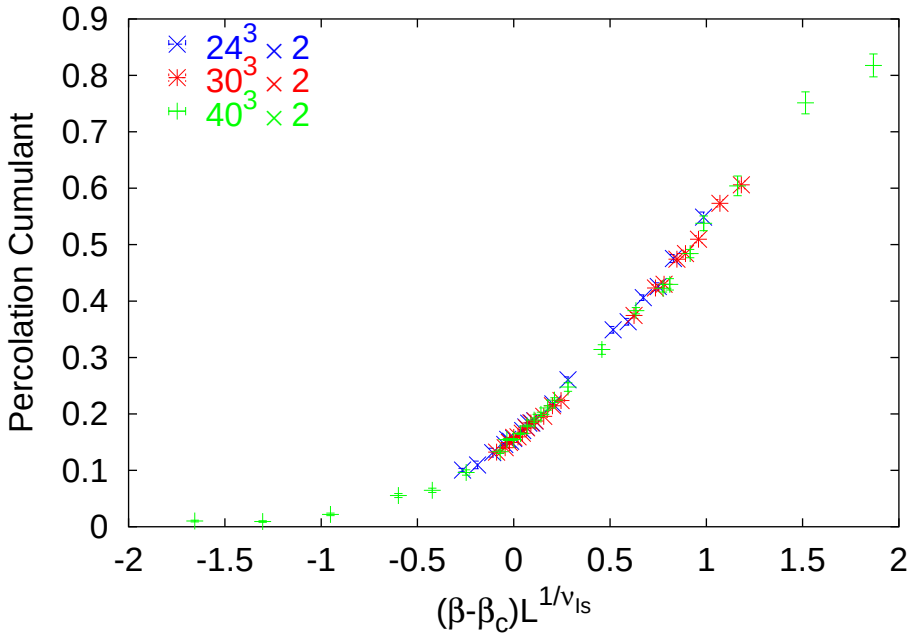

Figure 4.9: $(3+1)$-d $SU(2)$, $N_\tau = 2$. Rescaling of the percolation cumulant curves of Fig. 4.8 using $\beta_c = 1.8747$ and the 3-dimensional Ising exponent $\nu_{Is} = 0.6294$.

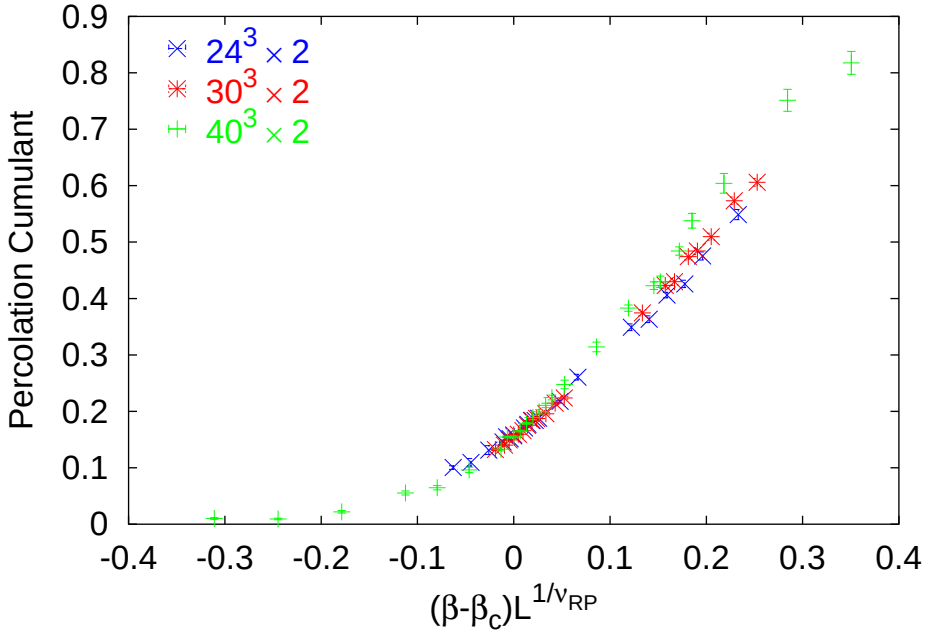

Figure 4.10: $(3+1)$-d $SU(2)$, $N_\tau = 2$. Rescaling of the percolation cumulant curves of Fig. 4.8 using $\beta_c = 1.8747$ and the 3-dimensional random percolation exponent $\nu_{RP} = 0.8765$.

Figs. 4.9 and 4.10 show the rescaled percolation cumulant using $\beta_c = 1.8747$ and the two major options for the exponent ν, respectively the Ising value and the random percolation one. From the figures it is evident that the critical exponent ν_{perc} of the scaling function is the Ising exponent and not the random percolation one.

To evaluate the exponents' ratios β/ν and γ/ν we performed high-statistics simulations in the range where the percolation cumulant curves cross each other. To improve the precision of the scaling fits we considered several lattice sizes (all even values of the lattice side L between 18 and 40). The number of measurements we took for each value of the coupling varies from 50000 to 100000. The final results are reported in Table 4.2.

	Critical point	β/ν	γ/ν	ν
Percolation results	$1.8747^{+0.0002}_{-0.0002}$	$0.528^{+0.012}_{-0.015}$	$1.985^{+0.013}_{-0.018}$	$0.632^{+0.010}_{-0.015}$
Thermal results	$1.8735^{+0.0004}_{-0.0003}$	$0.523^{+0.010}_{-0.013}$	$1.959^{+0.009}_{-0.007}$	$0.630^{+0.010}_{-0.008}$
3D Ising Model		0.5187(14)	1.963(7)	0.6294(10)

Table 4.2: Thermal and percolation critical indices for $(3+1)$-d $SU(2)$, $N_\tau = 2$: first approach.

The critical exponents we found, both for the thermal transition and for the geometrical one, are in good agreement with each other and with the ones of the 3-dimensional Ising model.

Again, the values of the two critical points are very close but they overlap only within two standard deviations, like in the $(2+1)$-d case. However, our value of the thermal threshold is much more precise than the value we adopted for $(2+1)$-d $SU(2)$ (see Table 4.1). In this respect, the accord for $(3+1)$-d is better than the one for $(2+1)$-d. This fact is not a surprise. In fact, the error induced by the truncation of the strong coupling expansion to the first term (see Section 4.5.1) is smaller the smaller β_c is, so that the approximation is better in the $(3+1)$ dimensional case ($\beta_c = 1.8735$) than in the $(2+1)$-d case ($\beta_c = 3.464$).

4.6 Second Approach: Projection on Ising-like Spin Models

4.6.1 Beyond the Strong Coupling Limit

On the ground of our previous investigations, we can say that the effective theory, derived by means of the strong coupling expansion of Section 4.5.1, allows to map the critical behaviour of finite temperature $SU(2)$ pure gauge theory into a geometrical percolation framework. Our procedure was, necessarily, approximate; nevertheless the results are encouraging.

We must point out that a drawback of the method is the fact that its validity is limited to the strong coupling limit of $SU(2)$ (i.e. for small N_τ). If we want to address the deconfinement problem more generally, an investigation of the weak coupling limit becomes compulsory.

Since, in this case, high temperature expansions do not help, the derivation of an effective theory from the $SU(2)$ lattice action seems prohibitively complicated. We thus decided to try to extract the effective theory we need by analysing directly the Polyakov loop configurations. This can be done by using techniques developed in Monte Carlo renormalization group studies [63, 64, 65].

To simplify the things, we assume the $Z(2)$ global symmetry to be the only relevant feature at the basis of the critical behaviour of the theory. This assumption is rather strong but reasonable, since the $Z(2)$ symmetry seems to be the only unifying feature of all theories in the Ising universality class.

In this way, we can limit ourselves to analyze the configurations of the *signs* of the Polyakov loops, so that we perform a sort of projection into Ising-like spin configurations. This approach has been successfully applied by Okawa to define an effective Hamiltonian for SU(2), in order to look for the fixed point of the theory by means of block-spin transformations [12].

The effective Hamiltonian $\mathcal{H}(s)$ of the signs $\{s_{\mathbf{n}}\}$ of the Polyakov loop configurations can be defined through the equation [12]

$$\exp[\mathcal{H}(s)] \;=\; \int [dU] \prod_{\mathbf{n}} \delta[s_{\mathbf{n}}, sgn(L_{\mathbf{n}})] \, \exp(S_{SU2}), \tag{4.32}$$

where $L_{\mathbf{n}}$ is, as usual, the value of the Polyakov loop at the spatial point $\mathbf{n}$ and S_{SU2} the $SU(2)$ lattice action. We stress that we include the factor $-\frac{1}{kT}$ in the definition of the Hamiltonian. Eq. (4.32) shows that all degrees of freedom of the original $SU(2)$ field configurations are integrated out, leaving only the distribution of the corresponding Ising-projected configuration.

The problem is now how to determine the expression of $\mathcal{H}(s)$, starting from the original Polyakov loop configurations.

In general, we write

$$\mathcal{H}(s) \;=\; \kappa_\alpha O^\alpha, \tag{4.33}$$

in which κ_α are the couplings, O^α the spin operators and a sum over the index α is understood (e.g. in the Ising model there would be only a single operator $O = \sum_{ij} s_i s_j$). Once we select the number and the type of operators, to fix the form of $\mathcal{H}(s)$ we need just to calculate the values of the couplings κ_α.

To solve this problem, Okawa proposed to use Schwinger-Dyson equations, which are derived by exploiting the $Z(2)$ symmetry of $\mathcal{H}(s)$ [13].

Suppose to select some point $\mathbf{n}$ of the spatial volume. We can then rewrite Eq. (4.33)

$$\mathcal{H}(s) \;=\; \kappa_\alpha O^\alpha_{\mathbf{n}} + \Delta\, H_{\mathbf{n}}, \tag{4.34}$$

separating the terms depending on the spin $s_{\mathbf{n}}$ at $\mathbf{n}$ ($O^\alpha_{\mathbf{n}}$) from the ones which are independent of $s_{\mathbf{n}}$ ($\Delta\, H_{\mathbf{n}}$). We assume $O^\alpha_{\mathbf{n}}$ to be linear in $s_{\mathbf{n}}$. This assumption is by no means restrictive, since all even powers of the spin variables are equal to 1, and consequently any product of spins can be reduced to a form where each spin appears at most linearly.

The thermal average of the operator $O^\gamma_{\mathbf{n}}$ is

$$\langle O^\gamma_{\mathbf{n}} \rangle \;=\; \frac{\sum\limits_{\{s\}} O^\gamma_{\mathbf{n}}\, \exp[\mathcal{H}(s)]}{\mathcal{Z}} \tag{4.35}$$

($\mathcal{Z}$ is the partition function). If we perform a change of variable inside the sum, 'flipping' the spin variable $s_{\mathbf{n}}$ to $-s_{\mathbf{n}}$, the operator $O^\gamma_{\mathbf{n}}$ will change sign and Eq. (4.35) becomes

$$\begin{aligned}
\langle O^\gamma_{\mathbf{n}} \rangle \;&=\; -\frac{\sum\limits_{\{s\}} O^\gamma_{\mathbf{n}}\, \exp[-\kappa_\alpha O^\alpha_{\mathbf{n}} + \Delta\, H_{\mathbf{n}}]}{\mathcal{Z}} \\
&=\; -\frac{\sum\limits_{\{s\}} O^\gamma_{\mathbf{n}}\, \exp(-2\kappa_\alpha O^\alpha_{\mathbf{n}})\, \exp(\kappa_\alpha O^\alpha_{\mathbf{n}} + \Delta\, H_{\mathbf{n}})}{\mathcal{Z}} \\
&=\; -\langle O^\gamma_{\mathbf{n}}\, \exp(-2\kappa_\alpha O^\alpha_{\mathbf{n}}) \rangle .
\end{aligned} \tag{4.36}$$

Eq. (4.36) establishes a relation between thermal averages of the operators $O^\gamma_{\mathbf{n}}$ and the couplings κ_γ. The equations (4.36) are, however, implicit in the couplings. They can be solved by means of the Newton method, which is based on successive approximations. One starts by making a guess about the values of the couplings; we indicate by $\tilde{\kappa_\gamma}$ such initial values. We can develop the exponential

$$\exp(-2\kappa_\gamma O^\gamma_{\mathbf{n}}) = \exp\{-2[\tilde{\kappa_\gamma} + (\kappa_\gamma - \tilde{\kappa_\gamma})]O^\gamma_{\mathbf{n}}\} \;\approx\; \exp(-2\tilde{\kappa_\gamma} O^\gamma_{\mathbf{n}})[1 - 2(\kappa_\delta - \tilde{\kappa_\delta}) O^\delta_{\mathbf{n}}] \tag{4.37}$$

Combining (4.37) and (4.36), we finally obtain for the first approximation of κ_γ

$$\kappa_\gamma(1) = \tilde{\kappa_\gamma} + \frac{1}{2}\langle O^\gamma_{\mathbf{n}} O^\alpha_{\mathbf{n}} \rangle^{-1} [\langle O^\alpha_{\mathbf{n}} \rangle + \langle O^\alpha_{\mathbf{n}} \exp(-2\tilde{\kappa_\delta} O^\delta_{\mathbf{n}}) \rangle]. \tag{4.38}$$

From the Polyakov loop configurations we can calculate the thermal averages of the operator expressions present in (4.38). Next, we use the results $\kappa_\gamma(1)$ of the first iteration as input values in Eq. (4.38) and we get some values $\kappa_\gamma(2)$. After a sufficient number N of iterations, the series of partial values for the κ_γ's will converge, i. e. $\kappa_\gamma(N+1) \approx \kappa_\gamma(N)$ within errors, $\forall\, \gamma$. The final set of couplings is the solution of Eq. (4.36).

We notice that the general set of equations (4.36) refers to a single point $\mathbf{n}$ of the spatial volume. The thermal averages are independent of the particular point $\mathbf{n}$, so it doesn't matter where we decide to take the averages. Nevertheless, since we aim to reduce as much as possible the errors of the couplings, we chose to determine the thermal averages at *each point* of the lattice, and

to calculate successively the average value of the couplings obtained by solving the equations at any point. This reduces considerably the effect of thermal fluctuations and, consequently, the errors on the final κ_γ's.

So, we have now all necessary tools to derive an effective theory for $SU(2)$ out of the Polyakov loop configurations. We still have to specify what kind of spin operators should appear in the expression (4.33) of the hamiltonian $\mathcal{H}(s)$. We can in principle choose any operator which respects the $Z(2)$ symmetry. Nevertheless, our choice is bound by the condition for the effective spin model to have an equivalent percolation formulation. As far as this is concerned, we know that the original Coniglio-Klein picture of the Ising model can be extended to general spin models, as long as the interactions are spin-spin and ferromagnetic (see Section 3.2.1). We proved this result for continuous spin models, but it remains valid also in the simpler case of Ising spins.

Because of that, we impose that our O^α are spin-spin operators. Our ansatz for the effective Hamiltonian $\mathcal{H}(s)$ is thus

$$\mathcal{H}(s) \,=\, \kappa_1 \sum_{NN} s_i s_j \,+\, \kappa_2 \sum_{NTN} s_k s_l \,+\, \kappa_3 \sum_{NTNTN} s_m s_n \,+\, etc.\,, \tag{4.39}$$

where the distance between coupled spins increases progressively starting from the simple nearest-neighbour (NN) case (NTN =next-to-nearest, $NTNTN$ =next-to-next-to-nearest, and so on).

What we have to do is to check whether, including a sufficient number of operators, the Hamiltonian (4.39) can reproduce the Ising-projected Polyakov loop configurations of finite temperature $SU(2)$. In general, the approximation improves the more operators we include in (4.39), because there will be more parameters. The fact that one must restrict the choice to some subset of operators involves an error (*truncation error*) in addition to the statistical one. The truncation error is, in general, impossible to determine and can be much bigger than the indetermination of the effective theory due to the statistical fluctuations of the thermal averages. In this way, the solution one finds at the end of the procedure is not necessarily a good approximation of the original theory, but only the closest one belonging to the subspace of theories defined by the selected set of operators. We need thus to establish a criterium to judge how well the effective theory approximates the original one. A good option could be to compare average values got from the configurations produced by simulating the effective theory with the corresponding quantities measured on the original Ising-projected Polyakov loop configurations. We used the lattice average of the magnetization m,

$$m \,=\, \frac{1}{V}\Big|\sum_i s_i\Big|\,, \tag{4.40}$$

(V is the spatial lattice volume) as test variable for this quality control.

We point out that the approach we have described is independent of the value of the number N_τ of lattice spacings in the temperature direction. In this respect, the method is general, although it is not possible to predict whether it is able to provide the required solution in all cases.

We applied the method to $SU(2)$ in $(3+1)$ dimensions, for two different lattice regularizations: $N_\tau = 2$ and $N_\tau = 4$. We have already studied the case $N_\tau = 2$ with the first approach (see Section 4.5.3): this gives us the possibility to compare the two different procedures.

4.6.2 Numerical Results for (3+1)-d SU(2), N_τ= 2

As we are interested in the phase transition of $SU(2)$, we focused our attention on the critical point. The value of the critical coupling β_c was already determined quite precisely during the previous investigation; our estimate was $\beta_c = 1.8735^{+0.0004}_{-0.0003}$ (see Table 4.2). So, our aim is to check whether, at $\beta = \beta_c$, we can find a projection of the theory onto the spin model (4.39).

We performed a simulation of $SU(2)$ at β_c on a rather large lattice, $32^3 \times 2$. We chose a large lattice to reduce finite size effects. The algorithm we used is the same described in Section 4.5.2. We measured our quantities every 70 updates, which makes the analyzed configurations basically uncorrelated; the total number of measurements is 2000. As usual, the errors were determined with the Jackknife method.

We began by making a projection on a model with 10 operators. Ten is, in fact, the number of spin-spin operators considered by Okawa in his effective theory of $SU(2)$ [12]. However, his Hamiltonian contains also multispin operators (products of 4, 6 and 8 spins), which we must exclude. The average of the magnetization (4.40) of the effective theory did not agree with the one of the Polyakov loop configurations, so that we progressively enlarged the set of operators, adding further spin-spin interactions, until we reached a set of 15 couplings. The

Coupling	Avg. Value	Coupling	Avg. Value
κ_1	0.1307(1)	κ_9	0.00014(10)
κ_2	0.01905(3)	κ_{10}	0.00058(3)
κ_3	0.00470(5)	κ_{11}	0.00018(3)
κ_4	0.0080(1)	κ_{12}	0.00008(1)
κ_5	0.00192(4)	κ_{13}	0.00001(1)
κ_6	0.00062(8)	κ_{14}	0.00006(1)
κ_7	0.00033(2)	κ_{15}	-0.00005(3)
κ_8	0.00007(2)		

Table 4.3: Couplings of the effective theory for the Polyakov loop configurations of $(3+1)$-d $SU(2)$ ($N_\tau = 2$) at the critical coupling $\beta_c = 1.8735$.

relative operators connect a point (000) to (100), (110), (111), (200), (210), (211), (220), (221), (222), (300), (310), (311), (320), (321), (322). The final set of couplings is reported in Table 4.3.

Fig. 4.11 shows a comparison between the magnetization distribution of the Polyakov loop configurations and the one of the effective theory: the two histograms are very similar. The values of the average magnetization m are also in agreement: for $SU(2)$, $m = 0.091(1)$ and for the spin model, $m = 0.0923(7)$. We notice that all the couplings in Table 4.3 are positive, except the last one. Since the error on κ_{15} is of the order of its average value, we can set $\kappa_{15} = 0$ without appreciable effects. In this way, we have got the effective theory we were looking for, with only ferromagnetic spin-spin interactions. The values of the couplings can then be used to

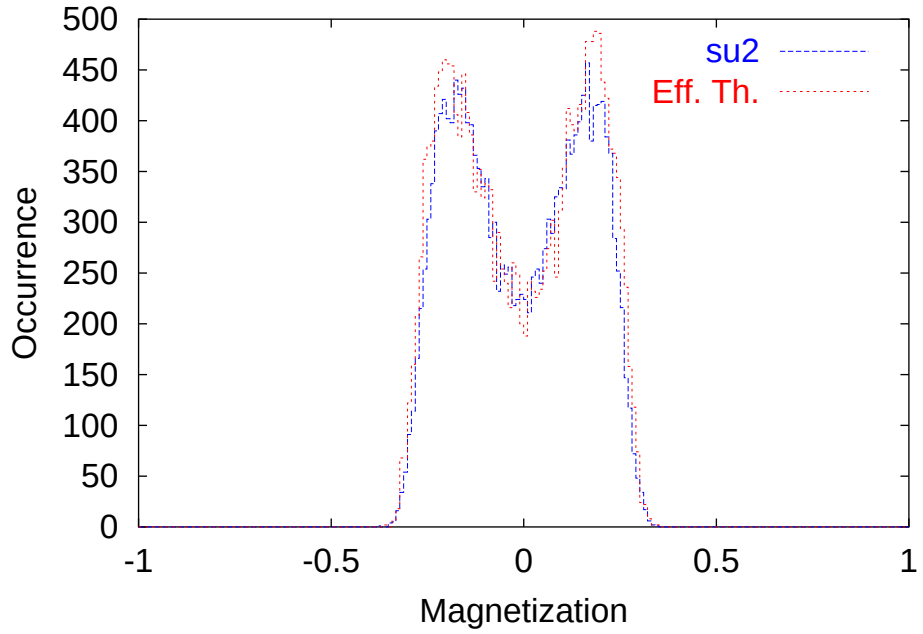

Figure 4.11: (3+1)-d $SU(2)$, $N_\tau = 2$. Comparison of the magnetization histograms derived from the Polyakov loop configurations at β_c and the effective theory (4.39) defined by the couplings of Table 4.3.

determine the bond weights p^α of the corresponding percolation model, according to the usual formula

$$p^\alpha = 1 - \exp(-2\,\kappa_\alpha) \tag{4.41}$$

($\alpha = 1, ..., 15$).

The magnetization check indicates that the effective theory is a fair approximation of $SU(2)$. Anyhow, this does not necessarily imply that the two models are very close to each other, so that we can conclude that the percolation picture of the effective theory indeed works for the original Polyakov loop configurations. The only way to see that is to investigate the geometrical transition of the new clusters in the $SU(2)$ configurations.

Therefore, we performed a percolation analysis of $(3+1)$-d $SU(2)$ ($N_\tau = 2$), building the clusters according to the general definition introduced in Section 3.2.1, with the bond probabilities (4.41). We stress that the bond weights are temperature-dependent. Our effective theory represents a projection of $SU(2)$ for $\beta = \beta_c$. But, in order to carry on our analysis, we need to evaluate the percolation variables at different values of β. Strictly speaking, for each β_i at study we should derive the corresponding effective theory, and use the relative set $\{\kappa\}_i$ to calculate the bond weights (4.41) at β_i. But for our analysis the previous consideration is not important. In fact, we are interested anyhow only in β's which lie near β_c, so that the corresponding couplings of the effective theory will change only slightly from one to the other extreme of the range. In the specific case of our investigations, it turns out that the variation is of the order of the error on the couplings derived by a single projection, and it is thus irrelevant for our purposes. Because of that, at each β, we shall use the same set of bond probabilities, namely the set determined by the couplings of Table 4.3.

We considered four lattice sizes: $24^3\times2$, $30^3\times2$, $40^3\times2$ and $50^3\times2$. Taking the measurements every 10 updates, the percolation data are uncorrelated, even for the $50^3\times2$ lattice. Fig. 4.12 shows the behaviour of the percolation cumulant as a function of β.

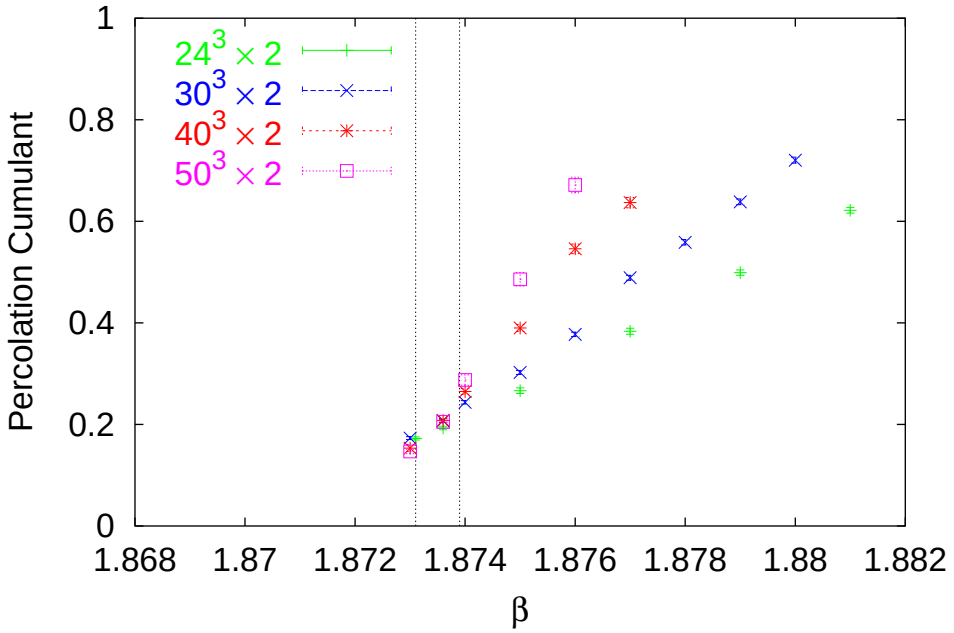

Figure 4.12: $(3+1)$-d $SU(2)$, $N_\tau = 2$. Percolation cumulant near the critical point for four lattice sizes.

The four curves cross remarkably well at the same point, within errors, in excellent agreement with the thermal threshold, indicated within one standard deviation by the dashed lines. The rescaling of the percolation cumulant curves indicates that the percolation exponent $\nu_{perc} = \nu_{Is}$ (Figs. 4.13 and 4.14).

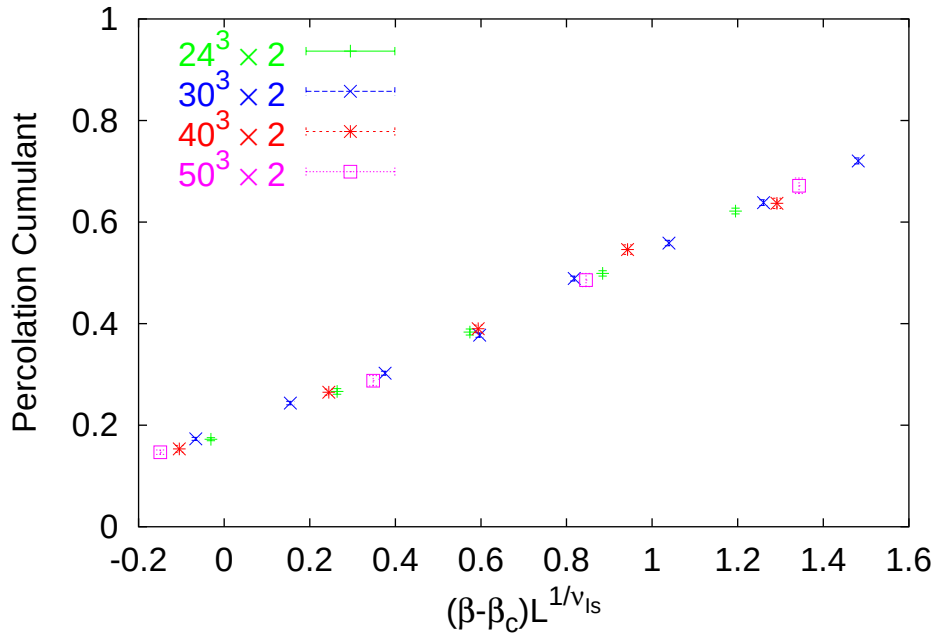

Figure 4.13: $(3+1)$-d $SU(2)$, $N_\tau = 2$. Rescaling of the percolation cumulant curves of Fig. 4.12 using $\beta_c = 1.8734$ and the 3-dimensional Ising exponent $\nu_{Is} = 0.6294$.

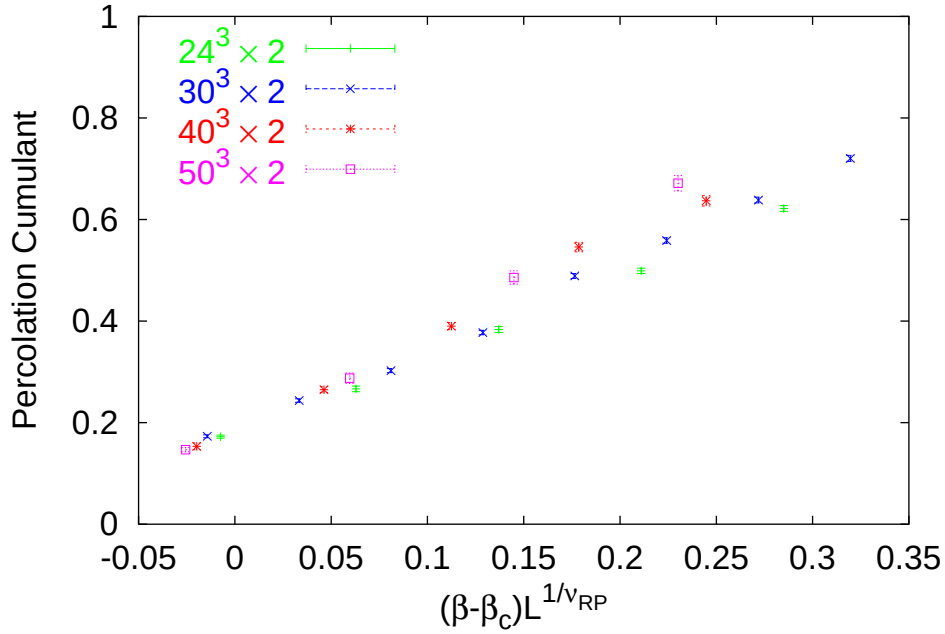

Figure 4.14: $(3+1)$-d $SU(2)$, $N_\tau = 2$. Rescaling of the percolation cumulant curves of Fig. 4.12 using $\beta_c = 1.8734$ and the 3-dimensional random percolation exponent $\nu_{RP} = 0.8765$.

To determine the exponents' ratios β/ν and γ/ν, we used the usual finite size scaling procedure, performing simulations at criticality of many different lattice sizes to improve the quality of the scaling fits (we took even values of the lattice side L between 20 and 50). Unfortunately, we could not determine β/ν, because of strong fluctuations of the percolation strength P around β_c. The value of P at criticality is, in general, quite small, and it suffers more than S the approximations involved by our procedure. Consequently, the slopes of the data points in the log-log scaling fits of P vary wildly, and the error of β/ν turns out to be too large. On the other hand, γ/ν can be evaluated with the usual accuracy ($\approx 1\%$) and its value is in agreement with the one of $SU(2)$ (Table 4.4).

	Critical point	γ/ν	ν
Percolation results	1.8734(2)	$1.977^{+0.011}_{-0.017}$	$0.628^{+0.011}_{-0.009}$
Thermal results	$1.8735^{+0.0004}_{-0.0003}$	$1.959^{+0.009}_{-0.007}$	$0.630^{+0.010}_{-0.008}$
3D Ising Model		1.963(7)	0.6294(10)

Table 4.4: Percolation critical indices for (3+1)-d $SU(2)$, $N_\tau = 2$, with the new cluster definition. We also put for comparison the thermal results determined in Section 4.5.3. and the 3D Ising values.

In conclusion, in spite of the several approximations we were forced to introduce to define the percolation picture with the second approach, for $N_\tau = 2$ the new clusters seem again to follow the behaviour of the thermal quantities. Besides, the value of the critical threshold is better than the one determined by the first approach.

4.6.3 Numerical Results for (3+1)-d SU(2), N_τ= 4

The case $N_\tau = 2$, discussed in the previous section, is important because it shows that the new percolation approach can be successfully applied and because it confirms the result obtained in Section 4.5.3, even if the two types of clusters have apparently nothing to do with each other. However, for $N_\tau = 4$, the things get more interesting, since the new method allows us to explore this case, which is instead unaccessible to the first approach.

As far as the thermal critical behaviour is concerned, we adopted as reference values the results of a recent study of Engels et al. [10]. In particular, in [10] the critical point β_c was determined with great accuracy: $\beta_c = 2.29895(10)$. We simulated (3+1)-d $SU(2)$ at $\beta = 2.29895$ and looked for the corresponding effective theory. The lattice size was $32^3 \times 4$, the number of measurements 2000; we evaluated the configurations every 60 updates to have them uncorrelated.

We tried first to use the same set of 15 operators which worked so well in the $N_\tau = 2$ case. Unfortunately, the effective theory we obtained fails in reproducing the behaviour of the magnetization. There is, in fact, a clear discrepancy between the average values. This fact is not

unexpected: it is known that, by increasing N_τ, longer range interactions come into play. We then enlarged further on the set of spin-spin operators. For 19 operators, we got the set of couplings reported in Table 4.5.

Coupling	Avg. Value	Coupling	Avg. Value
κ_1	0.08390(4)	κ_{11}	0.00082(5)
κ_2	0.01839(5)	κ_{12}	0.00055(4)
κ_3	0.00775(4)	κ_{13}	0.00035(2)
κ_4	0.00697(1)	κ_{14}	0.00030(4)
κ_5	0.00343(2)	κ_{15}	0.00013(4)
κ_6	0.00197(1)	κ_{16}	0.00020(5)
κ_7	0.00114(1)	κ_{17}	0.00018(3)
κ_8	0.00083(1)	κ_{18}	0.00017(1)
κ_9	0.00035(6)	κ_{19}	0.00017(4)
κ_{10}	0.00105(9)		

Table 4.5: Couplings of the effective theory for the Polyakov loop configurations of $(3+1)$-d $SU(2)$ ($N_\tau = 4$) at the critical coupling $\beta_c = 2.29895$.

The new 4 operators connect a point (000) to (330) (κ_{16}), (331) (κ_{17}), (332) (κ_{18}) and (333) (κ_{19}). The average value of m from the effective theory is now 0.121(3), in agreement with the $SU(2)$ value 0.128(6).

We see that all interactions are ferromagnetic. So, also for $N_\tau = 4$, there seems to be a promising effective theory that we can exploit to carry on percolation studies.

Next, $SU(2)$ simulations were performed on the following lattices: $24^3 \times 4$, $30^3 \times 4$, $40^3 \times 4$ and $50^3 \times 4$. To build the clusters we use the bond weights relative to the set of couplings of Table 4.5, for any value of the $SU(2)$ coupling β (see Section 4.6.2). We took the measurements every 10 updates for any coupling and lattice size; in this way the percolation data are uncorrelated.

Fig. 4.15 illustrates where the geometrical transition takes place: the crossing point of the percolation cumulant curves concides with the thermal threshold (dashed line) within errors. The scaling analysis of the cumulant curves can be seen in Figs. 4.16 and 4.17. Also here it turns out that $\nu_{perc} = \nu_{Is}$. The final results of the finite size scaling analysis are presented in Table 4.6. To get better scaling fits we considered again several lattice sizes close to the

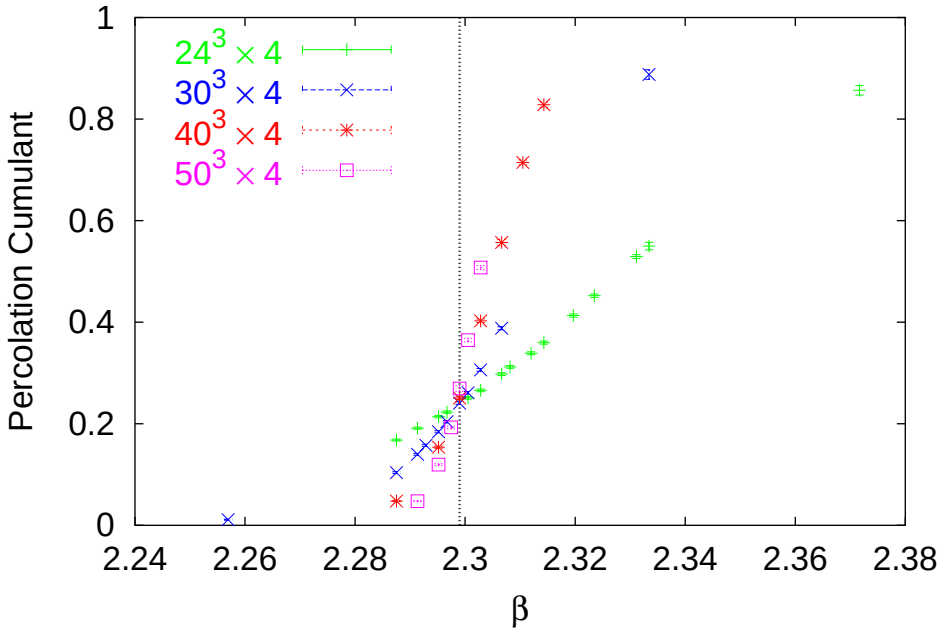

Figure 4.15: $(3+1)$-d $SU(2)$, $N_\tau = 4$. Percolation cumulant near the critical point for different lattice sizes.

critical point, taking for the lattice side L all even numbers between 20 and 50. The value of the exponents' ratio β/ν is missing for the same problem stressed in the previous section.

	Critical point	γ/ν	ν
Percolation results	2.2991(2)	$1.979^{+0.016}_{-0.014}$	$0.629^{+0.007}_{-0.011}$
Thermal results	2.29895(10)	1.944(13)	0.630(11)
3D Ising Model		1.963(7)	0.6294(10)

Table 4.6: Percolation critical indices for $(3+1)$-d $SU(2)$, $N_\tau = 4$. They are compared with the thermal results of [10] and the 3D Ising values.

We notice that γ/ν is not in accord with the corresponding $SU(2)$ estimate taken from [10]. Nevertheless, it overlaps with the 3D Ising value, although the agreement is not as good as in the $N_\tau = 2$ case. This fact indicates that, for $N_\tau = 4$, the effective theory (4.39) does not approximate $SU(2)$ so well as for $N_\tau = 2$. The main reason could be the approximation induced by the condition that the theory must contain only spin-spin operators. As a matter of fact, Okawa showed that, going from $N_\tau = 2$ to $N_\tau = 4$, multispin couplings become important [12]. Besides, for $N_\tau > 4$, we do not exclude that antiferromagnetic couplings may appear, which cannot still be handled in a percolation framework.

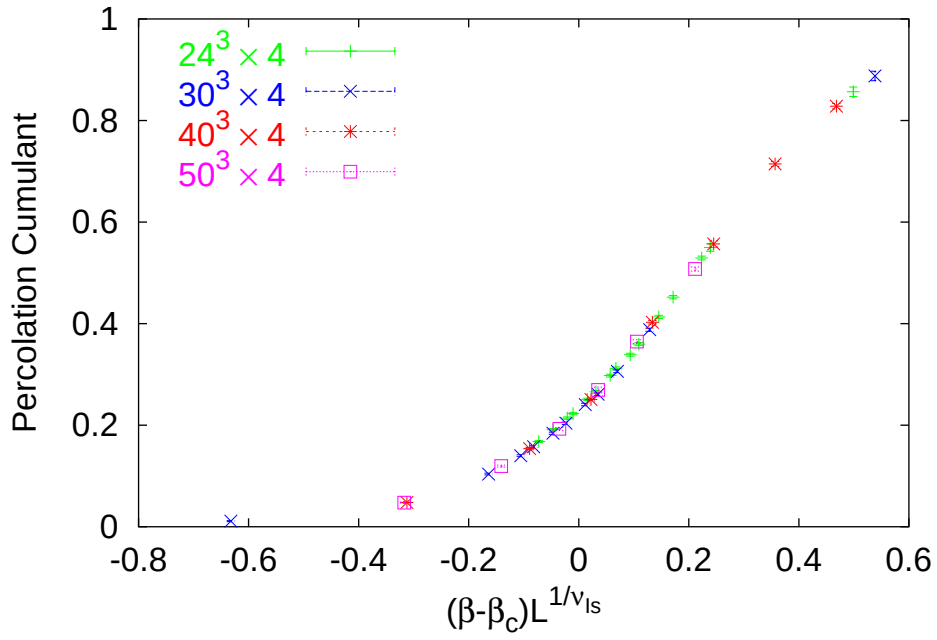

Figure 4.16: $(3+1)$-d $SU(2)$, $N_\tau = 4$. Rescaling of the percolation cumulant curves of Fig. 4.15 using $\beta_c = 2.2991$ and the 3-dimensional Ising exponent $\nu_{Is} = 0.6294$.

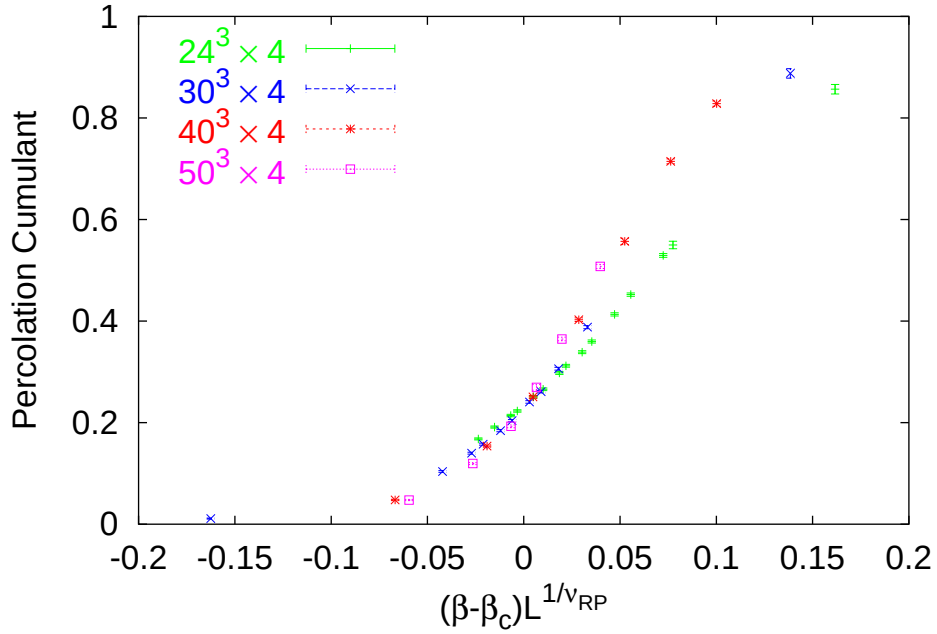

Figure 4.17: $(3+1)$-d $SU(2)$, $N_\tau = 4$. Rescaling of the percolation cumulant curves of Fig. 4.15 using $\beta_c = 2.2991$ and the 3-dimensional random percolation exponent $\nu_{RP} = 0.8765$.

We stress that our aim was to check whether it is possible to find a percolation picture for $SU(2)$ which works in the weak coupling regime as well. For $N_\tau = 4$ the cluster definition of our approach leads to a percolation transition which reproduces fairly well the thermal counterpart. The arguments we have presented above suggest that our method may fail for $N_\tau > 4$; this statement should be verified through numerical simulations.

Summary

We have seen that the Coniglio-Klein percolation picture of the paramagnetic-ferromagnetic transition of the Ising model can be used, with suitable modifications, to describe the spontaneous symmetry-breaking of a wide class of theories.

In particular, there seems to be a one-to-one correspondence between spin-spin interactions and geometrical bonds connecting the spins involved in the interactions. The probability for a bond to be active is a simple function of the associated coupling strength. We have found out that the spin variables need not be discrete like in the Ising model, but they can vary continuously in a range, and even be n-components vectors, like in $O(n)$ spin models. The only difference in the percolation picture is that the bond probability is *local*, since it depends on the values of the spin variables at the sites connected by the bond.

In the more general case of a theory characterized by more interactions, the percolation picture can be trivially extended if all interactions are spin-spin and ferromagnetic. For that, one needs just to combine together all bonds corresponding to each interaction. It is not clear whether it is possible to formulate a general percolation frame in the presence of frustration. Besides, if multispin couplings have a geometrical counterpart, more complicated objects than simple bonds (e.g. plaquettes) may be involved. This could lead to a highly non-trivial representation, which is still far from being established.

The possibility of dealing with continuous degrees of freedom opens the way, in principle, to a possible application of percolation models to field theories. We considered the case of $SU(2)$ pure gauge theory, because its critical behaviour is identical to the one of the Ising model and we hoped that such connection could simplify our task.

We stressed that no rigorous percolation picture a la Coniglio-Klein is possible as long as we do not know the exact expressions of the interactions between the Polyakov loops. This fact forced us to approximate $SU(2)$ by means of special effective theories, for which an equivalent percolation model exists. We have followed two different approaches to extract a suitable effective theory.

The first approach, based on series expansions of the $SU(2)$ lattice action, works rather well but its validity is limited to the strong coupling limit.

The second approach is more a brute force procedure, since it aims to find an Ising-like spin model, with just spin-spin interactions, which reproduces the configurations of the signs of the Polyakov loops. The new method leads to good results both in the strong coupling case we had examined with the first approach ($N_\tau = 2$) and if we move towards the weak coupling limit ($N_\tau = 4$). However, for $N_\tau = 4$ the approximation looks worse than for $N_\tau = 2$. More precisely, the value of the exponents' ratio γ/ν seems to shift slightly towards the random percolation value, even if it is still in agreement with the Ising ratio. This can mean that the procedure is not reliable for higher values of N_τ. As a matter of fact, we have to recognize that our ansatz for the Hamiltonian of the effective model is probably too restrictive, and that multispin couplings may become important for big N_τ's. Moreover, the precision of the method decreases the more spin-spin operators we introduce. In fact, if we analyze any time the same number of $SU(2)$ configurations, the errors on the final couplings of the effective theory are of the same order, no matter how many couplings we have. Consequently, the corresponding uncertainty on the model is the greater the more the couplings are. The Polyakov loop clusters, which are built by using the bond weights calculated from the couplings of the effective theory, become thus less and less defined. In order not to lose accuracy, one must lower the error on each single coupling, and that is possible only if we increase the number of $SU(2)$ configurations to analyze, which can lead to prohibitively lengthy simulations.

In conclusion, the second approach has certainly some drawbacks. Nevertheless, it allowed us to define some Polyakov loop clusters which have, with good approximation, the properties of the physical droplets of $SU(2)$ we were looking for, also in a case which approaches the weak coupling limit ($N_\tau = 4$). For this reason, the second approach is to be preferred to the first one, which strongly depends on a special lattice regularization of $SU(2)$.

From our investigations it is not possible to argue whether the critical behaviour of other field theories can be described by means of percolation. The strict relationship between $SU(N)$ gauge theories and $Z(N)$ spin models can represent a useful tool to devise suitable percolation pictures for the gauge theories starting from results known for the simpler spin models. In principle, that is exactly what we have done in our case, exploiting the analogy between $SU(2)$ and the Ising model. In practice, the task gets more complicated for $SU(N)$, when $N > 2$. For example, $SU(3)$ gauge theory is certainly the most interesting case of all, because it involves the "real" gluons. In two space dimensions, $SU(3)$ undergoes a second order phase transition, like the three states Potts model. Very recently [66] it was shown that the 2-dimensional three states Potts model admits an equivalent percolation formulation, which could thus be used for $SU(3)$. However, $SU(3)$ in two space dimensions is rather an academic model. One is surely more interested in the realistic 3-dimensional case. The fact that the $SU(3)$ phase transition in three space dimensions is first order poses an essential problem concerning the relationship between percolation and first order phase transitions.

The situation gets even more involved when one considers the case of *full QCD*, i. e. $SU(3)$ plus dynamical quarks, since the transition from confinement to deconfinement is probably a *crossover*, i.e. it takes place without any singularity in the partition function. We have seen in Section 2.6 that there are cases in which geometrical properties can change abruptly without a corresponding discontinuity in the thermal variables. This could provide a criterion to *define*

different phases and the relative transition in an extended sense [67]. Work in this direction is in progress.

We conclude our summary with some general remarks concerning the method we have chosen to study correlated percolation, i. e. Monte Carlo simulations. There is, in fact, basically no literature about this subject, as most of the known results are based on analytical proofs, and the few numerical studies rely on series expansions.

We point out the importance of the percolation cumulant, from which one can derive a precise estimate of the critical point. Besides, the scaling of the percolation cumulant curves allows to get the value of the critical exponent ν, with $4-5\,\%$ accuracy for the lattice sizes we have considered. The accuracy can be increased by analyzing larger lattices. Anyway, better estimates of ν can be obtained by using standard finite size scaling techniques, like the scaling of the pseudocritical points (see end of Section 1.5).

We remark that, for equal statistics, the errors on the percolation variables are much smaller than the errors on the corresponding thermal variables. The latter seems to be a general feature of site-bond percolation, because the clusters depend as well on the bonds' distribution. This introduces a further random element which contributes to reduce sensibly the correlation of the percolation measurements with respect to the thermal counterparts, which depend *only* on the spin configurations. We found that the data of the percolation strength P are always more correlated than the corresponding data of the average cluster size S.

For a study of the thermal transition variables like the susceptibility χ or the Binder cumulant g_r are necessary. Such quantities cannot be determined directly from measurements on the spin configurations, but are calculated by means of averages of powers of the order parameter. That usually leads to big error bars on the final results of χ and g_r. Instead, the percolation counterparts of χ and g_r, i.e. the average cluster size and the percolation cumulant, are calculated directly from the clusters' configurations, so that their errors are rather small.

Hence, in order to get the same accuracy on the average values, the thermal investigation of a model would require more CPU time than the relative percolation study. Nevertheless we have to point out that the errors on the thermal variables can be considerably reduced by means of reweighting techniques like the DSM [45], which we have often used in our studies, whereas similar interpolation methods do not exist for correlated percolation [‡]. In this work we were thus forced to use directly the data points in the finite size scaling fits. We think that the Fortuin-Kasteleyn-Swendsen-Wang model we have discussed in Section 2.4 could be used to implement an efficient method for the interpolation of Fortuin-Kasteleyn percolation data relative to the q-state Potts model.

From the finite size scaling analysis, it turns out that the scaling behaviour of the percolation variables is rather pure: that is clearly shown by the precision of the scaling of the percolation

[‡]For random percolation a reweighting method was recently proposed [68, 69]; the role of the energy is carried out by the probability of having a configuration in correspondence of a value p of the density of occupied sites (bonds).

cumulants we have performed many times in this work. In particular, in all our analyses, corrections to scaling seem negligible, and finite size effects disappear already for relatively small lattice sizes. This is quite impressive, especially when one makes comparisons with the thermal variables, which are normally strongly affected by such perturbations. Nevertheless, we have to keep in mind that the accuracy on our evaluation of the critical exponents has always been about $1 - 2\,\%$, which is good for our purposes [§] but not exceptional. Moreover, the percolation data of our $SU(2)$ studies are already affected by the approximations involved in the determination of the effective theory, which are by far more important than eventual corrections to scaling. On the other hand, if we want to obtain more accurate estimates of the results for models which admit an exact percolation formulation, like the continuous spin models of Chapter 3, corrections to scaling may become important: in high precision numerical studies of random percolation that seems indeed to be the case [23]. We remind that we have almost always adopted free boundary conditions for the cluster identification. The results on $O(n)$ spin models, however, suggest that the situation could be further on improved by using periodic boundary conditions (see Section 3.3).

[§] We remind that for the systems we investigated we had to check whether the critical exponents of the percolation transition agree with the thermal exponents of the system or rather with the ones of random percolation. The thermal exponents of all the models we have considered differ from the random percolation exponents of about $10 - 20\,\%$, so that our accuracy is good enough to distinguish the two cases.

Appendix A

Cluster Labeling

Suppose we want to perform percolation studies by means of lattice Monte Carlo simulations. We can divide the process in two phases:

- a configuration is created specifying, according to the percolation model we have chosen, which sites are occupied and which ones are empty;
- all occupied sites of the configurations are set into clusters, following the prescription of the percolation model (pure site, site-bond, etc.).

The first phase depends on the type of system we are studying. In the case of random percolation, for instance, one needs just a good *random number generator* to create the required configurations. First, one fixes the value p of the density of occupied sites. In general one associates a random number r between zero and one to a lattice site and compares it with p. If $r < p$, the site is occupied, otherwise it is empty. The procedure is repeated for all sites of the lattice. In the case of correlated percolation, the configuration is created by means of suitable Monte Carlo algorithms. For example, in the Ising model, the spin configurations can be produced by standard updates like Metropolis, heat bath, or cluster algorithms. Anyhow, such procedures will assign a value of the spin to each lattice site. Suppose we define the sites as occupied if their spins point up, then also the percolation frame will be established.

The delicate point is then represented by the second phase of the process that we have mentioned above, namely the cluster building. To identify a cluster configuration one needs essentially to associate to each site some label L, which indicates that the site belongs to some cluster. What we would like to have is an algorithm which gives all sites within the same cluster the same label, and gives different labels to sites belonging to different clusters. If this is possible, the search of an eventual percolation cluster becomes trivial. In fact, it suffices to check whether the same label is present in two opposite sides/faces of the lattice. Besides, the size s of a cluster is simply determined by counting how many times a particular label occurs in the lattice.

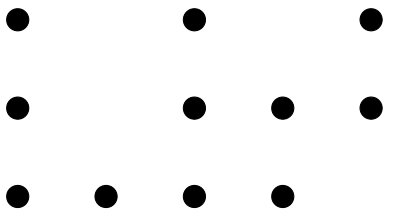

Figure A.1: Scheme of a 3×5 lattice with 11 occupied sites, which we want to set into clusters according to the pure site percolation rule.

To have an idea of the difficulties to find a suitable and efficient algorithm for the cluster labeling, we take as example the simple configuration we have sketched in Fig. A.1. The black points represent the occupied sites of the lattice, and we want to identify the relative site percolation clusters.

We can ask the computer to start from the top-left site and to proceed from left to right within each line, and then from the top to the bottom. Any time, the program will check whether the site (S) it analyzes is occupied or not. Assuming it is, one checks its left (L) and top (T) neighbours. If none of them is occupied, S takes a label which has not been used previously; on the other hand, if at least one of such neighbours is also occupied, say L, S will take the label of L (we notice that both L and T have been previously examined and therefore, if occupied, they carry some label).

Now we can start our procedure for the configuration of Fig. A.1. The top-left site is occupied, it therefore receives the label 1. The next occupied site is the third from the left: its left neighbour is empty and above there are no lattice sites, so that it gets a new label 2. The same happens for the last site of the top line, which receives the label 3. For the first line we then obtain the following labeling, where the zeros indicate the empty sites:

1 0 2 0 3

The first site of the second line is occupied, like its top neighbour, which carries the label 1. Hence the new site takes also the label 1. For the same reason the next occupied site of the second line receives the label 2, like the third one. But when we arrive to the last site of the line, we have a problem: in fact, this site is connected to both its neighbours, which carry different labels. Which label shall we then associate to it? The present situation is sketched by the scheme below

1 0 2 0 3
1 0 2 2 ?

The crucial point is that the site in question connects two clusters which were so far separated. From now on, the labels 2 and 3 mark thus one and the same cluster. We assign to our troublesome site the smaller of the two labels, but we have to keep in mind that all sites marked by 3 must be finally switched to 2. The simplest way of doing that is to ask our computer to come back to the top-left lattice site and to mark with the label 2 all encountered sites which carry the label 3. But this process would be very time consuming, since it would force the computer to scan the lattice a number of times which is of the same order of the lattice volume V. The total number of operations involved by the procedure of cluster labeling would thus grow as V^2, which makes the relative computing time prohibitively large for big lattice sizes. We would rather like to have a computing time proportional to the lattice volume.

Hoshen and Kopelman [70] found a smart way to solve the problem. One needs just to associate to each label M a number, which we indicate $N(M)$. Such number takes into account the relations between cluster labels that one finds while scanning the lattice. So, when we introduce a new label M, we set $N(M) = M$. If, at some stage, the cluster M turns out to be connected to another cluster P, with $P < M$, like in our example ($M = 3$, $P = 2$), then we reset $N(M) = P$. With this prescription let us proceed with the analysis of our configuration. The label 1 is obviously fundamental, since it is the first we have introduced, so that $N(1) = 1$. The label 2 marks a cluster which has, so far, no connections with 1, and therefore $N(2) = 2$. The same for the third label, before one examines the crucial case at which we interrupted our analysis, so $N(3) = 3$. The site we have indicated through the question mark obtains now the label 2. The fact that the clusters 2 and 3 are the same leads us to reset $N(3) = 2$. Finally, let us investigate the third and last line of the lattice. The first two sites are simple to identify: they both receive the label 1. The third one establishes a connection between the clusters 1 and 2. Because of that, the site takes the label 1 and $N(2) = 1$. We end up with the following situation

$$\begin{array}{ccccc} 1 & 0 & 2 & 0 & 3 \\ 1 & 0 & 2 & 2 & 2 \\ 1 & 1 & 1 & 1 & 0 \end{array}$$

$$N(1) = 1, \quad N(2) = 1, \quad N(3) = 2.$$

In this way we need to go through the whole lattice once and to store the connections found later in the "label of labels" array N. To finish our job, we must assign to each site the right label. For that we just have to classify all labels which have been introduced. Let us assume that we take a label M. The first thing to do is to check whether $N(M) = M$. If it is so, all sites marked with M carry the correct label. If, otherwise, $N(M) = P < M$, then one has to check whether P is a fundamental label, i.e. whether $N(P) = P$. In this case, we reset the label M to the new value P. If $N(P) = L < P$ one repeats the procedure until one finds that $N(S) = S$ for some label S, which becomes the final label of the sites initially marked with M. It is easy to check that this iterative procedure leads to the correct cluster labeling of the sample configuration of Fig. A.1.

In conclusion, the Hoshen-Kopelman algorithm is a very efficient method for the identification of the cluster configurations which is necessary to carry on numerical percolation studies on a

lattice. The algorithm requires essentially a single scan of the lattice and the label classification we have described above, which can be done by means of simple routines in the program.

Bibliography

[1] Comment of L. Onsager to the paper of C. J. Gorter, *The Two Fluid Model for Helium II*, Nuovo Cimento Supplemento **6**, 249 (1949).

[2] D. Stauffer, A. Aharony, *Introduction to Percolation Theory*, Taylor & Francis, London 1994.

[3] G. R. Grimmett, *Percolation*, Springer-Verlag, 1999.

[4] A. Coniglio, C. R. Nappi, F. Peruggi, L. Russo, *Percolation and Phase Transitions in the Ising Model*, Communications in Mathematical Physics **51**, 315 (1976).

[5] M. F. Sykes, D. S. Gaunt, *A Note on the Mean Size of Clusters in the Ising Model*, Journal of Physics A **9**, 2131 (1976).

[6] H. Müller-Krumbhaar, *The Droplet Model in Three Dimensions: Monte Carlo Calculation Results*, Physics Letters A **48**, 459 (1974).

[7] P. W. Kasteleyn, C. M. Fortuin, *Phase Transitions in Lattice Systems with Random Local Properties*, Journal of the Physical Society of Japan **26** (Suppl.), 11 (1969); C.M. Fortuin, P. W. Kasteleyn, *On the Random-Cluster Model. I. Introduction and Relation to Other Models*, Physica **57**, 536 (1972); C. M. Fortuin, *On the Random-Cluster Model. II. The Percolation Model*, Physica **58**, 393 (1972); C. M. Fortuin, *On the Random-Cluster Model. III. The Simple Random-Cluster Model*, Physica **59**, 545 (1972).

[8] A. Coniglio, W. Klein, *Clusters and Ising Critical Droplets: a Renormalization Group Approach*, Journal of Physics A **13**, 2775 (1980).

[9] B. Svetitsky, L. Yaffe, *Critical Behaviour at Finite-Temperature Confinement Transitions*, Nuclear Physics B **210** [FS6], 423 (1982); L. Yaffe, B. Svetitsky, *First-Order Phase Transition in the SU(3) Gauge Theory at Finite Temperature*, Physical Review D **26**, 963 (1982); B. Svetitsky, *Symmetry Aspects of Finite-Temperature Confinement Transitions*, Physics Reports **132**, 1 (1986).

[10] J. Engels, S. Mashkevich, T. Scheideler, G. Zinovjev, *Critical Behaviour of SU(2) Lattice Gauge Theory. A Complete Analysis with the χ^2 Method*, Physics Letters B **365** 219 (1996).

[11] F. Green, F. Karsch, *Mean Field Analysis of SU(N) Deconfining Transitions in the Presence of Dynamical Quarks*, Nuclear Physics B **238**, 297 (1984).

[12] M. Okawa, *Universality of Deconfining Phase Transitions in (3+1)-dimensional SU(2) Lattice Gauge Theory*, Physical Review Letters **60**, 1805 (1988).

[13] A. Gonzalez-Arroyo, M. Okawa, *Universality of Deconfining Phase Transitions in Finite-Temperature Lattice Gauge Theories*, Physical Review Letters **58**, 2165 (1987).

[14] P. J. Flory, *Molecular Size Distribution in Three Dimensional Gelation I-III*, Journal of the American Chemical Society **63**, 3083, 3091, 3906 (1941); W. H. Stockmayer, *Theory of Molecular Size Distribution and Gel Formation in Branched-Chain Polymers*, Journal of Chemical Physics **11**, 45 (1943).

[15] P. G. de Gennes, *La Percolation: un Concept Unificateur*, La Recherche **7**, 919 (1976); A. L. Efros, *Physics and Geometry of Disorder*, Mir, Moscow 1986.

[16] B. B. Mandelbrot, *The Fractal Geometry of Nature*, Freeman, San Francisco 1982; T. Vicsek, *Fractal Growth Phenomena*, World Scientific, Singapore 1989.

[17] H. L. Frisch, J. M. Hammersley, *Percolation Processes and Related Topics*, Journal of the Society for Industrial and Applied Mathematics **11**, 894 (1963); J. T. Cox, R. Durrett, *Limit Theorems for the Spread of Epidemics and Forest Fires*, Stochastic Processes and their Applications **30**, 171 (1988); J. van den Berg, G. R. Grimmett, R. B. Schinazi, *Dependent Random Graphs and Spatial Epidemics*, Annals of Applied Probability **8**, 317 (1998).

[18] D. Stauffer, *Percolation Models of Financial Market Dynamics*, to be published in Advances in Complex Systems.

[19] V. Ambegaokar, B. I. Halperin, J. S. Langer, *Hopping Conductivity in Disordered Systems*, Physical Review B **4**, 2612 (1971); J. P. Straley, *Non-Universal Threshold Behaviour of Random Resistor Networks with Anomalous Distributions of Conductances*, Journal of Physics C **15**, 2343 (1982); S. Feng, B. I. Halperin, P. Sen, *Transport Properties of Continuum Systems Near the Percolation Threshold*, Physical Review B **35**, 197 (1987); B. I. Halperin, *Remarks on Percolation and Transport in Networks with a Wide Range of Bond Strengths*, Physica D **38**, 179 (1989).

[20] J. W. Essam, M. E. Fisher, *Some Cluster Size and Percolation Problems*, Journal of Mathematical Physics **2**, 609 (1961); M. E. Fisher, *Critical Probabilities for Cluster Size and Percolation Problems*, Journal of Mathematical Physics **2**, 620 (1961).

[21] M. Aizenman, H. Kesten, C. M. Newman, *Uniqueness of the Infinite Cluster and Continuity of Connectivity Functions for Short- and Long-Range Percolation*, Communications in Mathematical Physics **111**, 505 (1987).

[22] M. Aizenman, *The Geometry of Critical Percolation and Conformal Invariance*, Proceedings STATPHYS 1995 (Xianmen) (H. Bai-lin, ed.), World Scientific, Singapore 1995; M. Aizenman, *On the Number of Incipient Spanning Clusters*, Nuclear Physics B **485** [FS], 551 (1997).

[23] H. G. Ballesteros, L. A. Fernández, V. Martín-Mayor, G. Parisi, J. J. Ruiz-Lorenzo, *Scaling Corrections: Site Percolation and Ising Model in Three Dimensions*, Journal of Physics A: Mathematical and General **32**, 1 (1999).

[24] K. G. Wilson, *Renormalization Group and Critical Phenomena. 1. Renormalization Group and the Kadanoff Scaling Picture*, Physical Review B **4**, 3174 (1971); K. G. Wilson, *Renormalization Group and Critical Phenomena. 2. Phase Space Cell Analysis of Critical Behaviour*, Physical Review B **4**, 3184 (1971).

[25] P. J. Reynolds, H. E. Stanley, W. Klein, *A Real-Space Renormalization Group for Site and Bond Percolation*, Journal of Physics C **10**, L 167 (1977).

[26] P. J. Reynolds, H. E. Stanley, W. Klein, *Large-Cell Monte Carlo Renormalization Group for Percolation*, Physical Review B **21**, 1223 (1980).

[27] H. Kesten, *The Critical Probability of Bond Percolation on the Square Lattice Equals* $\frac{1}{2}$, Communications in Mathematical Physics **74**, 41 (1980).

[28] K. Binder, D. W. Heermann, *Monte Carlo Simulations in Statistical Physics, An Introduction*, Springer-Verlag, 40-41 (1988).

[29] K. G. Wilson, J. Kogut, *The Renormalization Group and the* ϵ *Expansion*, Physics Reports **12**, 75 (1974).

[30] M. E. Fisher, *The Theory of Condensation and the Critical point*, Physics **3**, 255 (1967).

[31] L. Onsager, *Crystal Statistics. I. A Two-dimensional Model with an Order-Disorder Transition*, Physical Review **65**, 117 (1944).

[32] R. G. Edwards, A. D. Sokal, *Generalization of the Fortuin-Kasteleyn-Swendsen-Wang Representation and Monte Carlo Algorithm*, Physical Review D **38**, 2009 (1988).

[33] R. H. Swendsen, J. S. Wang, *Nonuniversal Critical Dynamics in Monte Carlo Simulations*, Physical Review Letters **58**, 86 (1987).

[34] C. N. Yang, T. D. Lee, *Statistical Theory of Equations of State and Phase Transitions. I. Theory of Condensation*, Physical Review **87**, 404 (1952).

[35] J. Kertész, *Existence of Weak Singularities when Going Around the Liquid-Gas Critical Point*, Physica A **161**, 58 (1989).

[36] R. H. Swendsen, J. S. Wang, *Cluster Monte Carlo Algorithms*, Physica A **167**, 565 (1990).

[37] J. Adler, D. Stauffer, *Search for Liquid-Gas Transition Above the Critical Temperature*, Physica A **175**, 222 (1991).

[38] R. B. Griffiths, *Rigorous Results for Ising Ferromagnets of Arbitrary Spin*, Journal of Mathematical Physics **10**, 1559 (1969).

[39] U. Wolff, *Collective Monte Carlo Updating for Spin Systems*, Physical Review Letters **62**, 361 (1989).

[40] U. Wolff, *Collective Monte Carlo Updating in a High Precision Study of the X-Y Model*, Nuclear Physics B **322**, 759 (1989).

[41] T. E. Harris, *A Lower Bound for the Critical Probability in a Certain Percolation Process*, Proceedings of the Cambridge Philosophical Society **56**, 13 (1960).

[42] L. Chayes, J. Machta, *Graphical Representations and Cluster Algorithms. I. Discrete Spin Systems*, Physica A **239**, 542 (1997).

[43] L. Chayes, J. Machta, *Graphical Representations and Cluster Algorithms II*, Physica A **254**, 477 (1998).

[44] H. L. Gray, W. R. Schucany, *The Generalized Jackknife Statistics*, Dekker, New York 1972.

[45] M. Falcioni, E. Marinari, M. L. Paciello, G. Parisi, B. Taglienti, *Complex Zeros in the Partition Function of the Four-dimensional SU(2) Lattice Gauge Model*, Physics Letters B **108**, 331 (1982); E. Marinari, *Complex Zeroes of the d=3 Ising Model: Finite-Size Scaling and Critical Amplitudes*, Nuclear Physics B **235**, 123 (1984); G. Bhanot, S. Black, P. Carter, R. Salvador, *A New Method for the Partition Function of Discrete Systems with Application to the 3D Ising Model*, Physics Letters B **183**, 331 (1986); A. M. Ferrenberg, R. H. Swendsen, *New Monte Carlo Technique for Studying Phase Transitions*, Physical Review Letters **61**, 2635 (1988); A. M. Ferrenberg, R. H. Swendsen, *Optimized Monte Carlo Data Analysis*, Physical Review Letters **63**, 1195 (1989).

[46] R. S. Ellis, J. L. Monroe, C. M. Newman, *The GHS and Other Correlation Inequalities for a Class of Even Ferromagnets*, Communications in Mathematical Physics **46**, 167 (1976).

[47] M. Creutz, *Monte Carlo Study of Quantized SU(2) Gauge Theory*, Physical Review D **21**, 2308 (1980).

[48] E. Manoussakis, R. Salvador, *Equivalence between the Nonlinear σ Model and the Spin-$\frac{1}{2}$ Antiferromagnetic Heisenberg Model: Spin Correlations in La_2CuO_4*, Physical Review B **40**, 2205 (1989).

[49] R. Pisarski, F. Wilczek, *Remarks on the Chiral Phase Transition in Chromodynamics*, Physical Review D **29**, 338 (1984); F. Wilczek, *Application of the Renormalization Group to a Second-Order QCD Phase Transition*, International Journal of Modern Physics A **7**, 3911 (1992); K. Rajagopal, F. Wilczek, *Static and Dynamic Critical Phenomena at a Second Order QCD phase Transition*, Nuclear Physics B **399**, 395 (1993).

[50] L. Chayes, *Discontinuity of the Spin-Wave Stiffness in the Two-Dimensional XY Model*, Communications in Mathematical Physics **197**, 623 (1998).

[51] M. Campbell, L. Chayes, *The Isotropic O(3) Model and the Wolff Representation*, Journal of Physics A **31**, L255 (1998).

[52] M. Hasenbusch, T. Török, *High-Precision Monte Carlo Study of the 3D XY-Universality Class*, Journal of Physics A **32**, 6361 (1999).

[53] M. Oevers, *Kritisches Verhalten in O(4)-symmetrischen Spinmodellen und 2-flavour QCD*, Diploma thesis, Bielefeld University (1996).

[54] K. Kanaya, S. Kaya, *Critical Exponents of a Three-dimensional O(4) Spin Model*, Physical Review D **51**, 2404 (1995).

[55] J. Engels, T. Mendes, *Goldstone Mode Effects and Scaling Function for the Three-dimensional O(4) Model*, Nuclear Physics B **572**, 289 (2000); J. Engels, S. Holtmann, T. Mendes, T. Schulze, *Equation of State and Goldstone Mode Effects of the Three-dimensional O(2) Model*, Physics Letters B **492**, 1 (2000).

[56] G. 't Hooft, M. Veltman, *Regularization and Renormalization of Gauge Fields*, Nuclear Physics B **44**, 189 (1972).

[57] K. Wilson, *Confinement of Quarks*, Physical Review D **10** 2445 (1974).

[58] O. Kaczmarek, *Korrelationsfunktionen und Potentiale mit Verbesserten Wirkungen*, Diploma Thesis, Bielefeld University (1997).

[59] A. M. Polyakov, *Thermal Properties of Gauge Fields and Quark Liberation*, Physics Letters B **72**, 477 (1978).

[60] L. Susskind, *Dynamics of Spontaneous Symmetry Breaking in the Weinberg-Salam Theory*, Physical Review D **20**, 2619 (1979).

[61] F. Green, *Strong Coupling Expansions for the String Tension at Finite Temperature*, Nuclear Physics B **215**, 83 (1983).

[62] M. Teper, *The Finite-Temperature Phase Transition of SU(2) Gauge Fields in 2+1 Dimensions*, Physics Letters B **313**, 417 (1993).

[63] R. H. Swendsen, *Monte Carlo Calculation of Renormalized Coupling Parameters. II. d=3 Ising Model*, Physical Review B **30**, 3875 (1984).

[64] A. Gonzalez-Arroyo, M. Okawa, *Renormalized Coupling Constants by Monte Carlo Methods*, Physical Review D **35**, 672 (1987).

[65] J. Deckert, S. Wansleben, J. G. Zabolitzky, *Monte Carlo Calculation for the Effective Couplings of Polyakov Loops*, Physical Review D **35**, 683 (1987).

[66] P. Blanchard, L. Chayes, D. Gandolfo, *The Random Cluster Representation for the Infinite-Spin Ising Model: Application to QCD Pure Gauge Theory*, Nuclear Physics B **588**, 229 (2000).

[67] H. Satz, *Phase Transitions in QCD*, Proceedings of the 3^{rd} Catania Relativistic Ion Studies (*CRIS 2000*), Acicastello (Italy).

[68] G. Harris, *Percolation on Strings and the Cover-Up of the c=1 Disaster*, Nuclear Physics B **418**, 278 (1994).

[69] H. G. Ballesteros, L. A. Fernández, V. Martín-Mayor, A. Muñoz Sudupe, G. Parisi, J. J. Ruiz-Lorenzo, *Measures of Critical Exponents in the Four-Dimensional Site Percolation*, Physics Letters B **400**, 346 (1997).

[70] J. Hoshen, R. Kopelman, *Percolation and Cluster Distribution. I. Cluster Multiple Labeling Technique and Critical Concentration Algorithm*, Physical Review B **14**, 3438 (1976).

Publications

The investigations related to the original work done in this thesis are exposed in a number of papers and have been presented to the physics community at various conferences. Below we enclose the complete list of publications.

- S. Fortunato, H. Huang, H. Satz,
  Deconfinement and Percolation in $SU(2)$ Gauge Theory.
  Poster at Quark Matter '99, Torino (Italy).

- S. Fortunato, H. Satz,
  Percolation and Deconfinement in $SU(2)$ Gauge Theory.
  Talk given at the 17th International Symposium on Lattice Field Theory (LATTICE '99), Pisa (Italy).
  Published in Nuclear Physics B Proceedings Supplement **83**, 452 (2000).
  E-Print Archive: hep-lat/9908033.

- S. Fortunato, H. Satz,
  Polyakov Loop Percolation and Deconfinement in $SU(2)$ Gauge Theory,
  Physics Letters B **475**, 311 (2000).
  E-Print Archive: hep-lat/9911020.

- P. Bialas, P. Blanchard, S. Fortunato, D. Gandolfo, H. Satz,
  Percolation and Magnetization in the Continuous Spin Ising Model,
  Nuclear Physics B **583**, 368 (2000).
  E-Print Archive: hep-lat/0003014.

- S. Fortunato, H. Satz,
  Percolation and Magnetization for Generalized Continuous Spin Models.
  Submitted to Nuclear Physics B.
  E-Print Archive: hep-lat/0007005.

- S. Fortunato, H. Satz,
  Percolation and Deconfinement in $SU(2)$ Gauge Theory.
  Talk given at the 3^{rd} Catania Relativistic Ion Studies (CRIS 2000), Acicastello (Italy).
  To be published in Nuclear Physics A Proceedings.
  E-Print Archive: hep-lat/0007012.

- P. Blanchard, S. Digal, S. Fortunato, D. Gandolfo, T. Mendes, H. Satz,
  Cluster Percolation in $O(n)$ Spin Models,
  Journal of Physics A: Math. Gen. **33**, 8603 (2000).
  E-Print Archive: hep-lat/0007035.

- S. Fortunato, F. Karsch, P. Petreczky, H. Satz,
  Percolation and Critical Behaviour in $SU(2)$ Gauge Theory.
  Talk given at the 18th International Symposium on Lattice Field Theory (LATTICE 2000), Bangalore (India).
  To be published in Nuclear Physics B Proceedings.
  E-Print Archive: hep-lat/0010026

- S. Fortunato, F. Karsch, P. Petreczky, H. Satz,
  Effective $Z(2)$ Spin Models of Deconfinement and Percolation in $SU(2)$ Gauge Theory.
  Submitted to Physics Letters B.
  E-Print Archive: hep-lat/0011084.

Declaration

This thesis has been composed, wholly and solely, by myself and contains my own work, except where indicated. I have not used other sources apart from those given in the bibliography and additional textbooks.

The program for the Monte Carlo update of $SU(2)$ was written by J. Engels and T. Scheideler; for the Ferrenberg-Swenden interpolation I adopted a program of J. Engels; the program to determine the effective theory of $SU(2)$ starting from the Polyakov loop configurations was written by P. Petreczky; the $O(n)$ programs were derived by an $O(4)$ version written by M. Oevers. All other programs used in my calculations have been written by myself.

Santo Fortunato